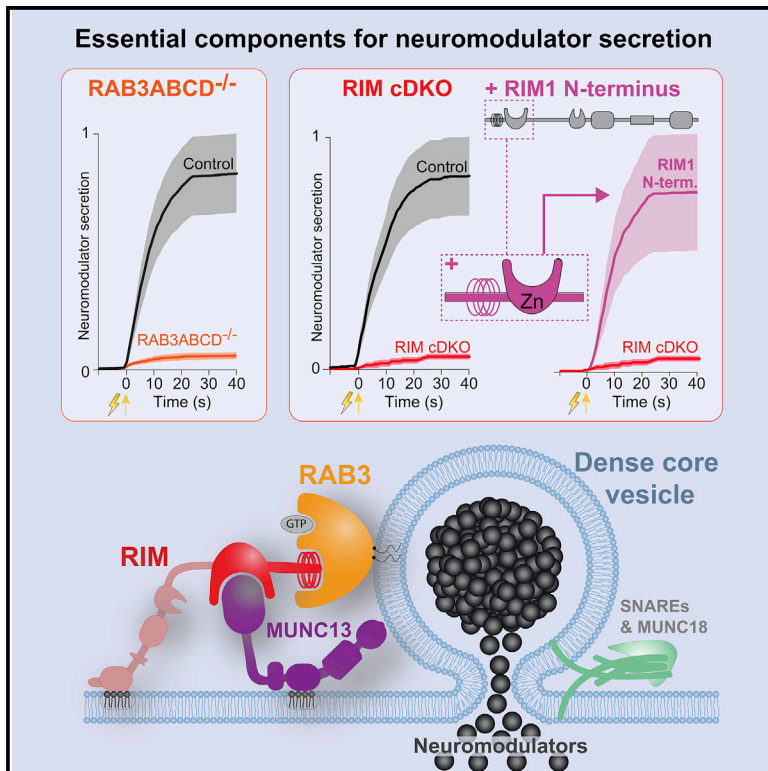


# The RAB3-RIM Pathway Is Essential for the Release of Neuromodulators

## Graphical Abstract



## Authors

Claudia M. Persoon,  
Rein I. Hoogstraaten, Joris P. Nassal,  
Jan R.T. van Weering,  
Pascal S. Kaeser, Ruud F. Toonen,  
Matthijs Verhage

## Correspondence

ruud.toonen@cncr.vu.nl (R.F.T.),  
matthijs@cncr.vu.nl (M.V.)

## In Brief

Neurons secrete neuromodulators/ neuropeptides from dense-core vesicles (DCVs) by a largely unknown mechanism. Persoon et al. identify RAB3 and RIM1/2 as essential factors. RAB3's indispensable role is the first distinct feature of DCV secretion as compared to synaptic vesicle secretion.

## Highlights

- RAB3 and RIM1/2 are essential for neuromodulator release from dense-core vesicles
- RIM's N-terminal RAB3- and MUNC13-binding domains are sufficient to support release
- The indispensable role of RAB3 marks a main difference between secretory pathways
- RIM/MUNC13 may provide a mammalian substitute for the yeast exocyst complex



# The RAB3-RIM Pathway Is Essential for the Release of Neuromodulators

Claudia M. Persoon,<sup>1</sup> Rein I. Hoogstraaten,<sup>2</sup> Joris P. Nassal,<sup>1</sup> Jan R.T. van Weering,<sup>1</sup> Pascal S. Kaeser,<sup>3</sup> Ruud F. Toonen,<sup>2,\*</sup> and Matthijs Verhage<sup>1,2,4,\*</sup>

<sup>1</sup>Department of Clinical Genetics, UMC Amsterdam, the Netherlands

<sup>2</sup>Department of Functional Genomics, Center for Neurogenomics and Cognitive Research (CNCR), Vrije Universiteit (VU) Amsterdam, de Boelelaan 1087, 1081 HV Amsterdam, the Netherlands

<sup>3</sup>Department of Neurobiology, Harvard Medical School, Boston, USA

<sup>4</sup>Lead Contact

\*Correspondence: [ruud.toonen@cncr.vu.nl](mailto:ruud.toonen@cncr.vu.nl) (R.F.T.), [matthijs@cncr.vu.nl](mailto:matthijs@cncr.vu.nl) (M.V.)

<https://doi.org/10.1016/j.neuron.2019.09.015>

## SUMMARY

Secretion principles are conserved from yeast to humans, and many yeast orthologs have established roles in synaptic vesicle exocytosis in the mammalian brain. Surprisingly, SEC4 orthologs and their effectors, the exocyst, are dispensable for synaptic vesicle exocytosis. Here, we identify the SEC4 ortholog RAB3 and its neuronal effector, RIM1, as essential molecules for neuropeptide and neurotrophin release from dense-core vesicles (DCVs) in mammalian neurons. Inactivation of all four RAB3 genes nearly ablated DCV exocytosis, and re-expression of RAB3A restored this deficit. In RIM1/2-deficient neurons, DCV exocytosis was undetectable. Full-length RIM1, but not mutants that lack RAB3 or MUNC13 binding, restored release. Strikingly, a short N-terminal RIM1 fragment only harboring RAB3- and MUNC13-interacting domains was sufficient to support DCV exocytosis. We propose that RIM and MUNC13 emerged as mammalian alternatives to the yeast exocyst complex as essential RAB3/SEC4 effectors and organizers of DCV fusion sites by recruiting DCVs via RAB3.

## INTRODUCTION

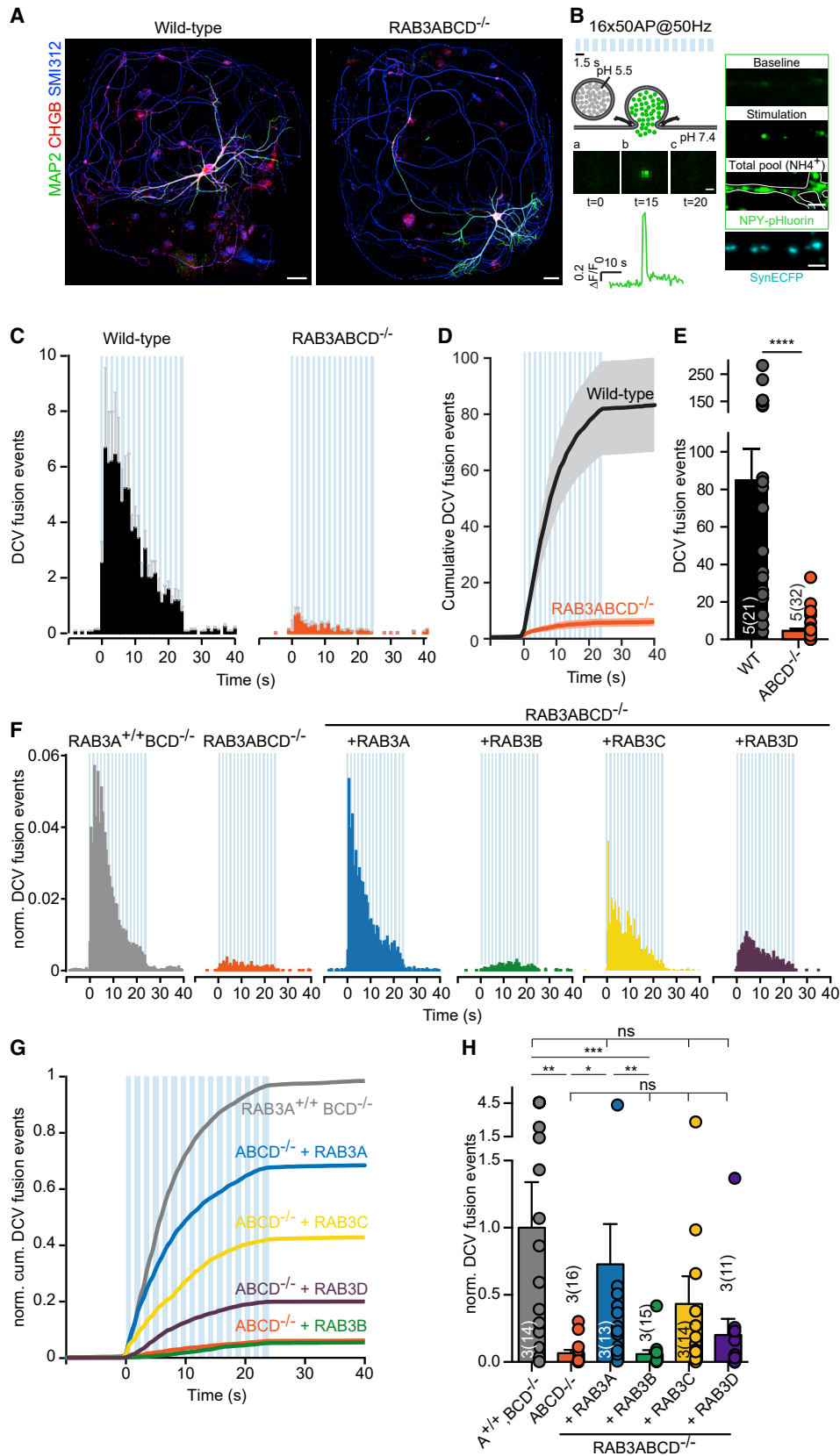
Secretion mechanisms are highly conserved across species and rely on ancient principles. In yeast *Saccharomyces cerevisiae*, 23 proteins were initially identified to drive the secretory pathway (Novick et al., 1980, 1981; Novick and Schekman, 1979), of which ten, SEC1–6, 8–10, and 15, act in the last steps of secretion (Novick et al., 1981), together with SNC1/2 (Protopopov et al., 1993) and SSO1/2 (Aalto et al., 1993). Subsequent research revealed that orthologs for many of these proteins drive regulated secretion of synaptic vesicles (SVs) in mammalian neurons (Jahn and Scheller, 2006; Kaeser and Regehr, 2014; Südhof, 2013; Südhof and Rothman, 2009). Strikingly, among the ten SEC genes that act in the last steps, only two have estab-

lished roles in mammalian SV fusion, SEC1 (MUNC18) and SEC9 (SNAP25). Orthologs of the other eight—encoding the GTPase SEC4 and its effectors; SEC2, a guanine exchange factor for SEC4 (Walch-Solimena et al., 1997); and 6 subunits of the SEC4 effector complex called the exocyst complex, SEC3, 5, 6, 8, 10, and 15 (Bowser et al., 1992; Guo et al., 1999; TerBush et al., 1996; TerBush and Novick, 1995)—are largely dispensable for SV fusion (Mehta et al., 2005; Murthy et al., 2003; Schlüter et al., 2004, 2006; Schwenger and Kuner, 2010). The role of these orthologs in regulated secretion in mammalian neurons remains poorly understood.

RAB3 proteins, orthologs of yeast SEC4p (Zahraoui et al., 1989), are highly expressed in brain (Fischer von Mollard et al., 1990; Schlüter et al., 2002) and dynamically associate with SVs (Fischer von Mollard et al., 1990; Takamori et al., 2006). Null mutant mice, lacking all four mammalian RAB3 paralogs (RAB3A–D, RAB3 QKO from hereon), show perinatal lethality but only subtle changes in synaptic transmission (Schlüter et al., 2004, 2006), in contrast to the essential function of SEC4p in vesicle secretion in yeast (Novick et al., 1980; Salminen and Novick, 1987). RAB3A null mice, which are homozygous viable and have minor changes in synaptic transmission (Geppert et al., 1997), show several altered behaviors, including circadian rhythmicity (Kapfhamer et al., 2002), reversal learning and exploration (D'Adamo et al., 2004), memory precision (Ruediger et al., 2011), and ethanol responses (Kapfhamer et al., 2002), although other mnemonic capabilities were normal (Hensbroek et al., 2003). These data suggest important, as yet unidentified, roles of mammalian RAB3 proteins.

Neuropeptides, neurotrophins, and other signaling molecules, together referred to as neuromodulators, are secreted by dense-core vesicles (DCVs) and control diverse physiological functions such as brain development, synaptic plasticity, circadian rhythm, and many behaviors and emotions (Cheng et al., 2011; Malva et al., 2012; Mertens et al., 2007; Meyer-Lindenberg et al., 2011; Pang et al., 2004). Defects in neuromodulator signaling are associated with psychiatric disorders, obesity, and diabetes (Meyer-Lindenberg et al., 2011; Vähätalo et al., 2015). While SV fusion principles are well characterized, many fundamental questions remain unanswered for neuromodulator secretion.





Here, we identify SEC4-ortholog RAB3 and its mammalian effector, RIM, as essential molecules for regulated secretion of neuromodulators from DCVs in mammalian neurons. We used hippocampal excitatory neurons to describe essential components of the DCV secretory pathway. We show that, unlike the previously reported (mild) effects on SV fusion (Schlüter et al., 2006), DCV fusion was reduced by >90% in RAB3 QKO neurons. Furthermore, in RIM-deficient conditional double-knockout (cDKO) neurons, DCV fusion was completely lost. N-terminal RAB3- and MUNC13-interacting domains of RIM co-trafficked with DCVs in a RAB3-dependent manner and were sufficient to fully restore DCV fusion. We propose that RIMs and MUNC13 emerged as mammalian alternatives to the yeast exocyst complex as essential RAB3/SEC4 effectors and organizers of DCV fusion sites by positioning MUNC13 and recruiting DCVs via RAB3.

## RESULTS

### Deletion of All RAB3 Proteins Severely Impairs DCV Fusion

The involvement of mammalian RAB3 proteins in release of neuromodulators was assessed by recording DCV fusion in single hippocampal neurons on glia micro-islands from RAB3 QKO and wild-type mice at days *in vitro* 14 (DIV 14; Figure 1A). Expression of neuropeptide Y (NPY) fused to pH-sensitive EGFP (pHluorin) using lentivirus targets this reporter to virtually all DCVs, with >90% overlap with endogenous neurotrophin BDNF and neuropeptide co-factors chromogranins A/B and without altering the total number of DCVs per neuron (Dominguez et al., 2018; Persoon et al., 2018). Hence, this reporter labels DCVs irrespective of their endogenous neuropeptide and neurotrophin content and can be used to study their general secretion principles applicable to many cargo types. The NPY-pHluorin reporter detects single DCV fusion events by an instant increase of fluorescence due to rapid deacidification of the vesicle's interior when the fusion pores open (Figure 1B; Arora et al., 2017; Emperador Melero et al., 2017; Farina et al., 2015; Persoon et al., 2018; van Keimpema et al., 2017). Upon calcium influx induced by action potential trains (16 bursts of 50 action potentials [APs] at 50 Hz; Balkowiec and Katz, 2002; de Wit et al., 2009; Gärtner and Staiger, 2002; Hartmann

et al., 2001; Matsuda et al., 2009; van de Bospoort et al., 2012), DCV fusion in RAB3 QKO neurons was almost absent (Figures 1C–1E), showing an ~20-fold reduction as compared to wild-type neurons (Figures 1C–1E). The loss of DCV fusion in RAB3 QKO neurons was confirmed using BDNF as an independent reporter for neuromodulator release (Figures S1A–S1E). Taken together, these data indicate that RAB3 is a key factor in neuromodulator release from DCVs.

We excluded several potentially confounding factors that could, in principle, contribute to this major reduction in DCV fusion: (1) the number of NPY-pHluorin-labeled DCVs per neuron was similar between genotypes (Figure S1F); (2) the temporal distribution of fusion before and during stimulation (Figures S1G and S1H) and (3) calcium dynamics (Figure S1I) were also similar; (4) the location of fusion events, synaptic or extra-synaptic, did not differ between wild-type and RAB3 QKO neurons (Figures S1K and S2A–S2C); (5) the number of synapses and the total dendritic length of wild-type, RAB3A<sup>+/+</sup>, BCD<sup>-/-</sup> (RAB3 triple knockout [TKO]), and RAB3 QKO neurons were similar (Figures S2D–S2G), as observed before (Schlüter et al., 2006); (6) the fluorescence intensity of VGLUT1 (Figure S2H) at synapses was not altered in RAB3 QKO neurons; and (7) the number and distribution of puncta labeled with the endogenous DCV marker chromogranin B (CHGB) was similar between genotypes (Figures S2I–S2L and S2O). While the number of CHGB puncta and total CHGB protein levels (Figure S2N) was similar between RAB3 QKO and control neurons, the intensity of CHGB puncta (Figure S2M) and intensity of individual DCV fusion events (Figure S1J) were slightly, but significantly, reduced (<20%), indicating a possible mild impairment in DCV loading. Together, these data exclude several potentially confounding effects and strengthen the conclusion that RAB3 proteins are important regulators of DCV fusion.

To test for functional redundancy between RAB3A–D (Schlüter et al., 2002), we expressed each paralog in RAB3 QKO neurons and analyzed DCV fusion events (Figures 1F–1H). Re-expression of RAB3A, RAB3C, and RAB3D, but not RAB3B, restored the number of DCV fusion events to levels that were not significantly different from RAB3 TKO neurons (Figures 1F–1H). However, only re-expression of RAB3A significantly increased DCV fusion, compared to RAB3 QKO

### Figure 1. RAB3 Deletion Impairs DCV Fusion

(A) Representative composite confocal image of single cultured hippocampal neurons from wild-type (left) or RAB3ABCD<sup>-/-</sup> (right) mice. Dendrites (MAP2, green), axons (SMI312, blue), and DCVs (CHGB, red) were labeled. Scale bars: 40  $\mu$ m.

(B) NPY-pHluorin as optical reporter for DCV fusion. Repetitive electrical stimulation (16 trains of 50 APs at 50 Hz) is represented by blue bars. Middle panels a–c show a single DCV fusion event reported by NPY-pHluorin, with  $\Delta F/F_0$  (inset below). Scale bar: 1  $\mu$ m. NPY-pHluorin is quenched in the acidic environment of the DCV lumen (a). Upon depolarization-induced Ca<sup>2+</sup>-influx, the DCV fusion pore opens indicated by a rapid increase in fluorescence (b), followed by a rapid decline upon cargo release or fusion pore closure and vesicle reacidification (c). Right panels: DCV fusion events during stimulation (Stimulation), total number of DCVs upon NH<sub>4</sub> superfusion (Total pool), Synapsin-ECFP labeled synapses (SynECFP; Figures S2A–S2C). Scale bar: 5  $\mu$ m.

(C–H) DCV fusion analysis using NPY-pHluorin in single wild-type or RAB3ABCD<sup>-/-</sup> hippocampal neurons. (C) Histograms, (D) cumulative plot, and (E) summary graph of DCV fusion events per cell. Mann-Whitney U test: \*\*\*\*p < 0.0001. (F) Histograms, (G) cumulative plot, and (H) summary graph of DCV fusion events per cell for RAB3A<sup>+/+</sup>BCD<sup>-/-</sup>, RAB3ABCD<sup>-/-</sup>, or RAB3ABCD<sup>-/-</sup> expressing RAB3A, -B, -C, or -D neurons, normalized to RAB3A<sup>+/+</sup>BCD<sup>-/-</sup>. Kruskal-Wallis with Dunn's correction: \*p < 0.05, \*\*p < 0.01, \*\*\*p < 0.001. ns = non-significant, p > 0.05.

See also Figures S1 and S2.

In all figures: repetitive electrical stimulation (16 trains of 50 APs at 50 Hz) is represented by blue bars. All data shown as mean  $\pm$  SEM. N represents number of experiments and number of single neuron observations in brackets. Individual neurons are represented as dots. Detailed information (average, SEM, n, and detailed statistics) is shown in STAR Methods.

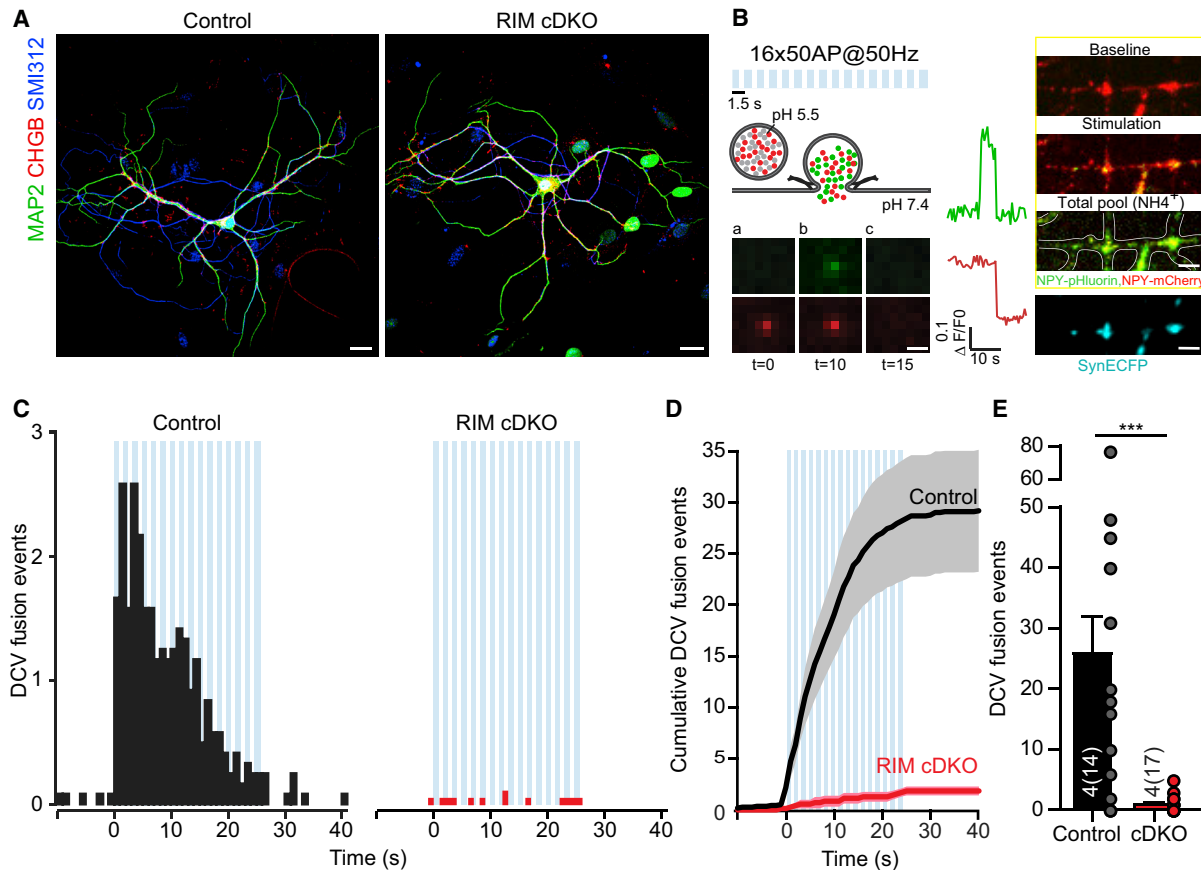


### Figure 2. RIM Depletion Blocks DCV Fusion

(A) Representative composite confocal image of single hippocampal control (left) or RIM 1/2 cDKO (right) neurons. Dendrites (MAP2, green), axons (SMI312, blue), and DCVs (CHGB, red) were labeled. Scale bars: 20  $\mu$ m.

(B) NPY-pHluorin and NPY-mCherry as dual-color optical reporters for DCV fusion. Lower panels a–c show a single DCV fusion event reported by NPY-pHluorin and NPY-mCherry, with  $\Delta F/F_0$  traces (green, NPY-pHluorin; red, NPY-mCherry). Right panels: DCV fusion events during stimulation (Stimulation), total number of DCVs upon NH<sub>4</sub> superfusion (Total pool), and Synapsin-ECFP labeled synapses (SynECFP). Scale bar (left): 1  $\mu$ m; scale bar (right): 5  $\mu$ m.

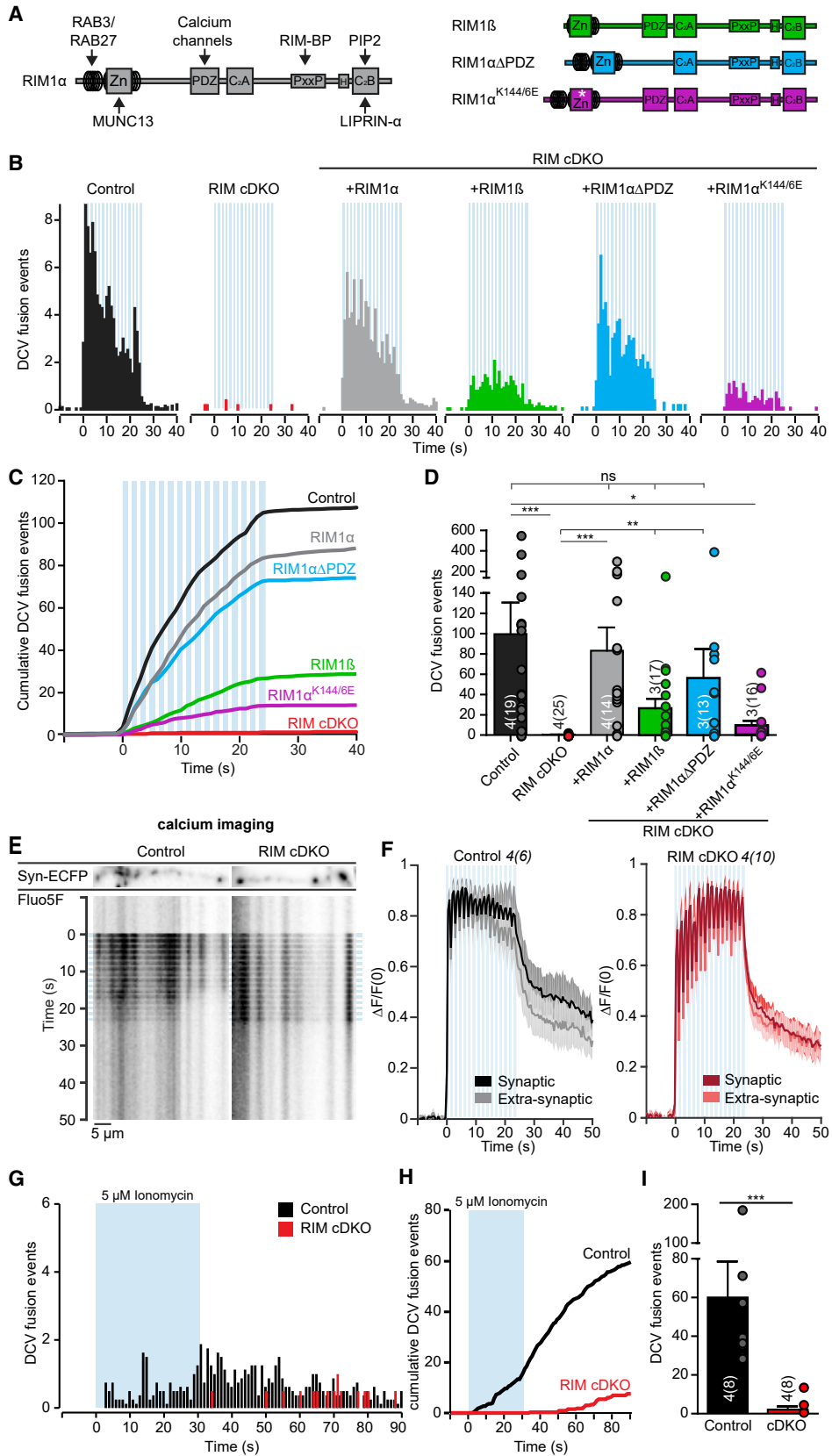
(C–E) DCV fusion analysis using NPY-pHluorin and NPY-mCherry in single hippocampal control (black) or RIM1/2 cDKO (red) neurons. (C) Histograms, (D) cumulative plot, and (E) summary graph of DCV fusion events per cell. Mann-Whitney U test: \*\*\* $p \leq 0.0002$ . See also Figures S3–S6.

neurons (Figures 1F–1H). The expression levels of rescue constructs (Figures S1L and S1M) and number of NPY-pHluorin-labeled DCVs per neuron (Figure S1N) were similar between each condition. Together, these data suggest that RAB3C and RAB3D partially restore DCV release but less efficiently than RAB3A, while RAB3B does not rescue DCV release.

### RIM1 Is Essential for DCV Fusion

RIM1/2 proteins, multi-domain scaffolding proteins enriched at presynaptic active zones, are established mammalian RAB3A/C effectors at the target membrane (Wang et al., 1997). To test if RIM1/2 are important in DCV fusion, we used single isolated hippocampal neurons from conditional RIM1/RIM2 DKO mice in which Cre-recombinase deletes expression of all RIM 1 ( $\alpha$  and  $\beta$ ) and RIM 2 ( $\alpha$ ,  $\beta$ , and  $\gamma$ ) isoforms (Kaeser et al., 2011). Hippocampal neurons (Figure 2A) were infected at DIV 0 with lentiviral constructs expressing active, EGFP-tagged Cre-recombinase (RIM cDKO),

resulting in the absence of RIM protein expression from DIV 8 (Figure S3A), or inactive, EGFP-tagged mutant Cre-recombinase (control). To test if RIMs function in neuromodulator release, DCVs were co-labeled with NPY-pHluorin and NPY fused to red fluorescent mCherry (NPY-mCherry), which, upon DCV fusion, shows a rapid decrease in fluorescence due to cargo diffusion (Figure 2B). NPY-mCherry allows for analysis of DCV transport and behavior prior to fusion, as mCherry does not quench in the low pH of the DCV lumen (Figure 2B). RIM cDKO neurons showed a more than 95% reduction in NPY-mCherry-labeled DCV fusion events upon stimulation, compared to controls (Figures 2C–2E; Figure S3B). The few remaining events in RIM cDKO neurons occurred mostly outside synapses (Figure S3C), of which the fluorescence disappeared within 1 s (Figures S3D and S3E), and were not detected as NPY-pHluorin-labeled fusion events (Figures S3F and S3G). The total number of NPY-mCherry puncta was not altered (Figure S3H). The loss of DCV fusion



(legend on next page)

in RIM cDKO neurons was confirmed using BDNF-pHluorin as an independent reporter for neuromodulator release (Figures S3J–S3L).

Morphological characterization at DIV 14 showed a modestly reduced number of synapses and MUNC13 intensity when Cre-recombinase was expressed at DIV 0 (Figures S4A–S4G). No differences were found in the number or intensity of CHGB puncta (Figures S4A and S4H–S4L). CHGB puncta co-localized slightly more with VGLUT1-positive synapses compared to control (Figures S4M and S4N), and synaptic electron micrograph sections showed a trend toward accumulation of DCVs at the presynapse (Figures S4O and S4P). DCVs are actively transported throughout the neuron by microtubule-based motor proteins (Lo et al., 2011; Stucchi et al., 2018; Zahn et al., 2004), but DCV transport parameters (speed, distance moved) were not altered in RIM cDKO neurons (Figures S5A–S5H). Hence, RIM cDKO neurons have fewer synapses when Cre-infected at DIV 0 with a trend for DCV accumulation but have a normal DCV population, indicating that RIMs are not required for DCV biogenesis, loading, or transport.

To test if reduced synapse numbers could explain the DCV fusion phenotype, we expressed Cre-recombinase at DIV 5 instead of DIV 0, which does not affect synapse numbers (Figures S5I–S5L), and observed a similar block in DCV fusion in RIM-deficient neurons at DIV 18 (Figures S5M–S5O), showing that changes in synapse number do not correlate with a reduction in DCV fusion in RIM-deficient neurons. Cre-recombinase expression in wild-type neurons did not negatively affect DCV fusion (Figures S5P–S5R). Together, we conclude that RIMs are essential for DCV fusion.

To study whether RIM1 or RIM2 is required for DCV fusion, single hippocampal neurons from RIM1 cKO mice or RIM2 cKO mice were infected with Cre-recombinase or control virus at DIV 0. Upon stimulation, RIM2-deficient neurons (RIM1<sup>+/+</sup>, RIM2<sup>-/-</sup>) showed a similar number of DCV fusion events compared to controls, while DCV fusion was strongly reduced in RIM1-deficient neurons (RIM1<sup>-/-</sup>, RIM2<sup>+/+</sup> and RIM1<sup>-/-</sup>, RIM2<sup>+/-</sup>) and RIM2-deficient neurons heterozygous for RIM1 (Figures S6A–S6F). Multiple bursts of APs were required to trigger DCV fusion in RIM1-deficient neurons (Figures S6B and S6C). Total DCV numbers were similar in all genotypes (Figure S6E). These data show that RIM1 is required for efficient DCV fusion and, in absence of RIM1, RIM2-dependent DCV fusion is strongly reduced and delayed.

### N-Terminal Interactions of RIMs with RAB3 and MUNC13 Regulate DCV Fusion

RIMs regulate synaptic vesicle fusion through interactions with MUNC13, voltage-gated calcium channels, and PIP2 (Figure 3A [left]; de Jong et al., 2018; Deng et al., 2011; Han et al., 2011; Kaeser et al., 2011). To study if these interactions are required for DCV fusion, we expressed multiple RIM-rescue constructs (Figure 3A) in RIM cDKO neurons from DIV 0, which were expressed at similar levels and all localized to synaptic regions at DIV 14 (Figures S6G and S6H), as reported before (Kaeser et al., 2011). Upon stimulation, full-length RIM1 $\alpha$  rescued DCV fusion to control levels (Figures 3B–3D). RIM1 $\beta$  lacks interaction with RAB3 (Kaeser et al., 2008), which binds RIM1 $\alpha$  through the N-terminal  $\alpha$  helix (Figure 3A; Wang et al., 1997). DCV fusion in RIM1 $\beta$ -expressing RIM cDKO neurons was reduced by almost 75% compared to controls (Figures 3B–3D). RIM1 $\alpha$ - $\Delta$ PDZ, lacking the PDZ domain that binds to voltage-gated calcium channels (Figure 3A; Kaeser et al., 2011), almost completely rescued DCV fusion in RIM cDKO neurons (Figures 3B–3D). MUNC13 binds to the N-terminal zinc finger of RIM (Betz et al., 2001; Dulubova et al., 2005; Schoch et al., 2002), and mutating two lysine residues (K144 and K146) of RIM to glutamates (RIM1 $\alpha$ -K144/6E, Figure 3A) results in a loss of MUNC13 binding (Deng et al., 2011; Dulubova et al., 2005; Lu et al., 2006). Expression of RIM1 $\alpha$ -K144/6E in RIM cDKO neurons did not restore DCV fusion (Figures 3B–3D). Neither the onset of fusion nor the total pool was altered (Figures S6I and S6J), but the percentage of synaptic fusion events was increased in the different rescue conditions (Figure S6K), in line with their synaptic expression (Figures S6G and S6H). These data show that the N-terminal interactions of RIMs with RAB3 and MUNC13 are essential for efficient DCV fusion.

To confirm that RIM interaction with voltage-gated calcium channels is not essential for DCV fusion, we first measured calcium influx using Fluo5-AM in synaptic and extra-synaptic regions. Both RIM cDKO neurons and control neurons showed a calcium influx profile corresponding with the bursts of repetitive stimulation (Figures 3E and 3F). In RIM cDKO neurons, multiple bursts of activity were required to reach maximum fluorescence (Figures 3E and 3F). Next, we applied the calcium ionophore ionomycin to increase intracellular calcium levels independently of voltage-gated calcium channels. Ionomycin (5  $\mu$ M) elicited robust DCV fusion in control but not in RIM cDKO neurons (Figures 3G–3I, S6L, and S6M). From these data, we conclude that a defect in calcium entry or location of

#### Figure 3. N Terminus Interactions of RIM1/2 Regulate DCV Fusion

(A) Domain structure of full-length RIM1 $\alpha$  (left) with key interactions. Diagram of RIM1 $\beta$ , RIM1 $\alpha$ - $\Delta$ PDZ, and RIM1 $\alpha$ -K144/6E rescue proteins expressed in RIM cDKO neurons (right). Zn, zinc-finger domain with surrounding  $\alpha$ -helical regions; PxxP, proline-rich region; H, location of a human influenza hemagglutinin (HA)-tag; asterisk, K144/6E substitution.

(B–D) DCV fusion analysis using NPY-pHluorin in single control or RIM cDKO hippocampal neurons without or with rescue constructs (RIM cDKO + rescue). (B) Histograms, (C) cumulative plot, and (D) summary graph of DCV fusion events per cell. Kruskal-Wallis with Dunn's correction: \* $p < 0.05$ , \*\* $p < 0.01$ , \*\*\* $p < 0.001$ . ns,  $p > 0.05$ .

(E) Kymograph and (F) average normalized  $\Delta F/F_0$  traces of intracellular calcium (Fluo5-AM) levels upon repetitive electrical stimulation (blue bars) in control or RIM cDKO neurons at synaptic (labeled by Synapsin-ECFP) or extra-synaptic regions.

(G–I) DCV fusion analysis using NPY-pHluorin in single control or RIM cDKO hippocampal neurons upon 30 s application of 5  $\mu$ M ionomycin (blue bar). (G) Histograms, (H) cumulative plot, and (I) summary graph of DCV fusion events per cell. Mann-Whitney U test: \*\*\* $p = < 0.0007$ .

See also Figure S6.

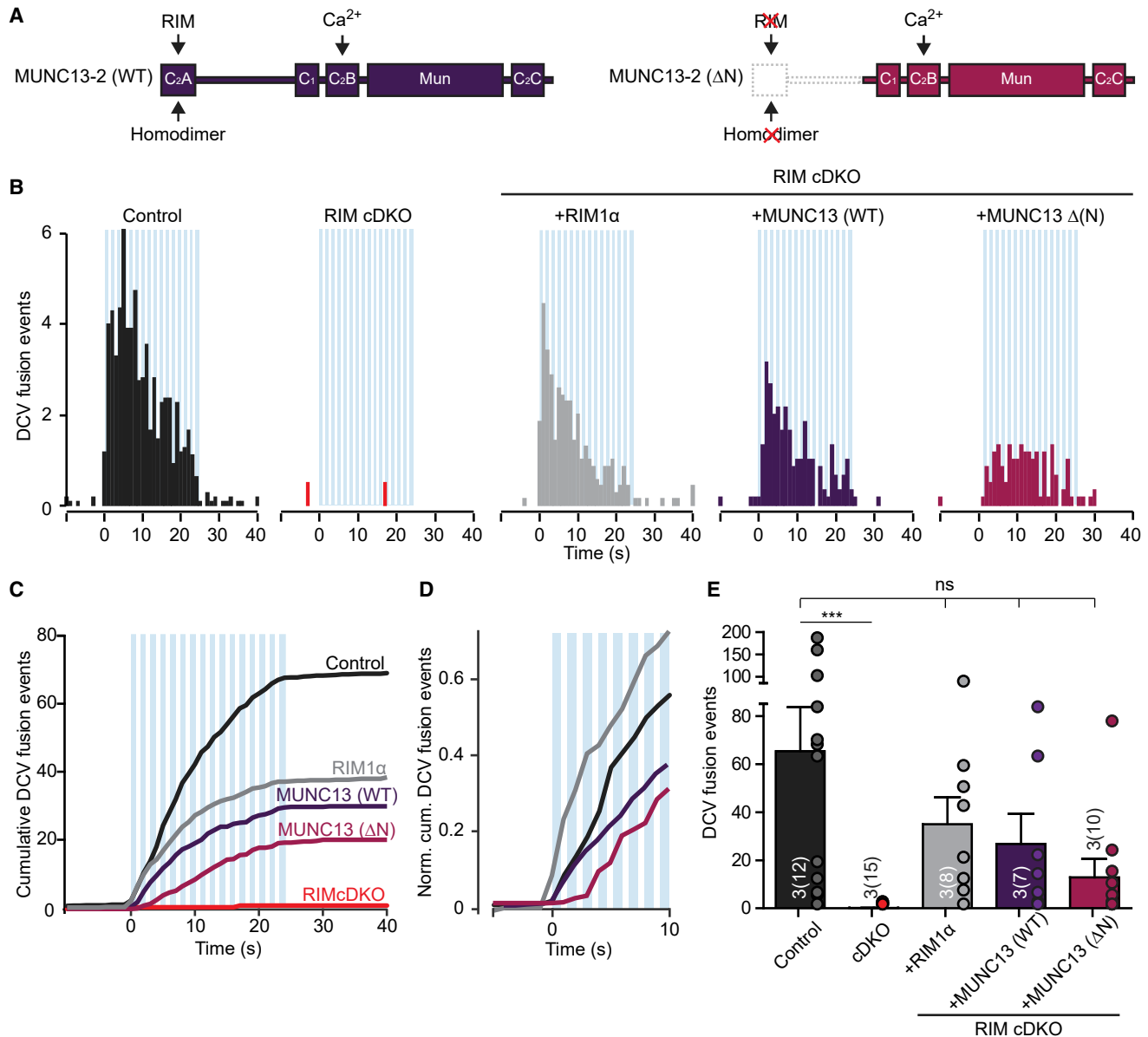


**Figure 4. Expression of MUNC13 Rescues DCV Fusion in RIM cDKO Neurons**

(A) Diagram of MUNC13-2 wild-type (WT) and MUNC13-2 (ΔN) rescue proteins expressed in RIM cDKO neurons. Key domains and interactions are indicated. Constructs were labeled at the C terminus with mCherry to visualize expression (not indicated).

(B–E) DCV fusion analysis using NPY-pHluorin in single control or RIM cDKO hippocampal neurons without or with expression of full-length RIM1α (gray), MUNC13-2 WT (purple), or MUNC13-2 (ΔN) (magenta). (B) Histograms, (C) cumulative plot, (D) normalized cumulative plot of first 10 s of stimulation, and (E) summary graph of DCV fusion events per cell. Kruskal-Wallis with Dunn's correction: \*\*\*p < 0.001. ns, p > 0.05. See also Figure S7.

voltage-gated calcium channels cannot explain the lack of DCV fusion in RIM cDKO neurons.

#### Overexpression of MUNC13 Rescues DCV Fusion in RIM cDKO Neurons

RIMs prime synaptic vesicle fusion by converting an autoinhibitory MUNC13 homodimer into an activated heterodimer by interaction of the RIM Zn<sup>2+</sup> finger with the C2A domain of

MUNC13 (Camacho et al., 2017). To test whether activation of MUNC13 is required for DCV fusion, we expressed wild-type ubMUNC13-2 (Figure 4A, left) or N-terminally truncated ubMUNC13-2 (Figure 4A, right; MUNC13-2 ΔN), which does not interact with RIM1α or form homodimers (Deng et al., 2011), in RIM cDKO neurons. Overexpression of MUNC13-2 (WT) or MUNC13-2 (ΔN) restored DCV fusion (Figures 4B–4E and S7A–S7D), although RIM-deficient cDKO neurons expressing



MUNC13-2 ( $\Delta$ N) required multiple bursts of stimulation before DCV fusion to peak (Figure 4D). These results show that overexpression of MUNC13-2 rescues DCV fusion in RIM cDKO neurons and that the N-terminal C2A domain of MUNC13-2 is not required for DCV fusion. Furthermore, the data suggest that MUNC13 supports DCV fusion independent of RIM when overexpressed.

### N-Terminal Domain of RIM1 $\alpha$ Is Sufficient to Support DCV Fusion

To test if the N-terminal interactions of RIMs are sufficient to support DCV fusion, we expressed different N-terminal RIM1 fragments in RIM cDKO neurons (Figure 5A; Deng et al., 2011). Rescue with the N-terminal RIM1 $\alpha$  fragment containing RAB3- and MUNC13-binding sequences (RIM1 $\alpha$ -RZ) fully restored DCV fusion (Figures 5B–5D and S7E–S7I). Expression of RIM1 $\beta$ -Z, which lacks RAB3 binding but still binds MUNC13, rescued DCV fusion in RIM cDKO neurons but significantly lower compared to control (Figures 5B–5D and S7E–S7I, similar to full-length RIM1 $\beta$ , Figure 3D). Both the N-terminal RIM1 $\alpha$  and RIM1 $\beta$  fragments containing the Zn<sup>2+</sup>-finger mutations eliminating MUNC13 binding (RIM1 $\alpha$ -RZ-K144/6E and RIM1 $\beta$ -Z-K144/6E) did not restore DCV fusion in RIM cDKO neurons (Figures 5B–D and S7E–S7I). Together, these data show that the N-terminal fragment of RIM is sufficient to support DCV fusion, and it does so with more efficiency than for synaptic vesicle fusion (Deng et al., 2011). Furthermore, interactions with both RAB3 and MUNC13 are important.

### N Terminus of RIM Interacts with DCVs through RAB3A

RAB3 binds to SVs (Fischer von Mollard et al., 1990) and to secretogranin II-positive secretory granules in PC12 cells (Handley et al., 2007). To assess whether RAB3A is present on DCVs in hippocampal neurons, colocalization experiments were performed in RAB3 QKO neurons expressing RAB3A-mCherry and NPY-pHluorin (Figure 6A). RAB3A-mCherry was found in stationary deposits at synapses (Figure 6A), co-transported with NPY-pHluorin (Figure 6A; yellow lines) or transported without colocalizing with NPY-pHluorin (Figure 6A). Also, moving NPY-pHluorin puncta negative for RAB3A-mCherry were found (Figure 6A; green lines). These data suggest that RAB3A is transported on a subset of DCVs.

RIMs are expressed at the presynaptic active zone (Wong et al., 2018). To investigate if RIMs also interact with DCVs, we infected neurons with full-length mCherry-tagged RIM1 but did not obtain sufficient expression. However, the mCherry-tagged, N-terminal RIM rescue construct (RIM1 $\alpha$ -RZ-mCherry) did express well enough to study transport of RIM1 $\alpha$ -RZ-mCherry and NPY-pHluorin in RIM cDKO neurons (Figure 6B). RIM1 $\alpha$ -RZ-mCherry was predominantly located at synapses (Figure 6B) but also co-transported with a subset of NPY-pHluorin-labeled vesicles outside synapses (Figure 6B; yellow lines). We hypothesized that the interaction between DCVs and the N terminus of RIM1 $\alpha$  is mediated by RAB3A. To test this, the percentage of moving NPY-pHluorin-labeled DCVs positive for RIM1 $\alpha$ -RZ-mCherry was quantified in RAB3 QKO neurons and RIM cDKO neurons (Figures 6C and 6D). In RIM cDKO neurons, approximately 33% of moving NPY-pHluorin puncta co-transported RIM1 $\alpha$ -RZ-mCherry

(Figure 6D; black), while in RAB3 QKO neurons only 11.5% of moving NPY-pHluorin puncta were positive for RIM1 $\alpha$ -RZ-mCherry (Figure 6D; gray). Hence, in RAB3 QKO neurons, the interaction of DCVs with the N terminus of RIMs is partly lost, suggesting RIMs interact with DCVs mainly through RAB3.

To test if RAB3A and RIMs are transported together on DCVs, NPY-pHluorin, RIM1 $\alpha$ -RZ-ECFP, and RAB3A-mCherry were co-expressed in RAB3 QKO neurons (Figure 6E) or wild-type neurons (Figure S8A). Moving NPY-pHluorin puncta colocalized with RIM1 $\alpha$ -RZ (Figures 6E and S8A; white), with RAB3A (Figures 6E and S8A; yellow), and co-transport of NPY with RAB3A and RIM1 $\alpha$ -RZ (Figures 6E and S8A; magenta). These data suggest that RAB3A and RIM1 $\alpha$ -RZ are transported together on a subset of DCVs.

To test if MUNC13 and RIMs are transported together on DCVs, NPY-pHluorin, RIM1 $\alpha$ -RZ-ECFP, and MUNC13-2-mCherry were co-expressed in wild-type neurons (Figure S8B). Endogenous MUNC13 localizes predominantly to synapses, with little immunoreactivity colocalizing with an endogenous DCV marker outside synaptic regions (Figures S8C–S8E). However, MUNC13-mCherry colocalizes with moving NPY-pHluorin puncta positive for RIM1 $\alpha$ -RZ (Figure S8B; magenta). This co-trafficking of MUNC13 and RIM1 $\alpha$  with DCVs suggests that MUNC13 and RIMs may form heterodimers on DCVs, and RIM activates MUNC13 already while traveling through the axon. However, the limited evidence for colocalization of endogenous MUNC13 and DCVs and the fact that live imaging of full-length RIM was not feasible prevents strong conclusions.

## DISCUSSION

In this study, we identify essential roles for RAB3 and RIM1/2 in neuromodulator release in mammalian CNS neurons. RAB3 QKO neurons showed a 20-fold decrease in DCV fusion and RIM1/2 cDKO neurons a 100-fold decrease. DCV fusion in RIM cDKO neurons was rescued by expression of wild-type RIM1 $\alpha$  but not RAB3- or MUNC13-binding-deficient RIM1 mutants. The N-terminal fragment of RIM1 that interacts with RAB3 and MUNC13 was sufficient to fully restore DCV fusion. This N-terminal fragment also co-trafficked with DCVs via RAB3. We conclude that RIMs are essential RAB3 effectors for mammalian neuromodulator release and organize DCV fusion by positioning/activating MUNC13 and recruiting DCVs through RAB3 interactions (Figure 7), in analogy to the exocyst complex in yeast.

To our knowledge, the RIM1/2 null DCV fusion phenotype is stronger than any other null mutation studied so far: in MUNC13-1/2 DKO neurons, 40% of DCV fusion events remain (van de Bospoort et al., 2012), 10%–40% remain in the CAPS1/2 DKO (Farina et al., 2015; van Keimpema et al., 2017), and 10%–20% remain upon deletion of SNAREs, i.e., SNAP25 knockout/down or TeTx expression (Arora et al., 2017; Shimojo et al., 2015). RIM-deficient neurons showed a 100-fold reduction in evoked DCV fusion (approximately 0.75 fusion events per cell [72 events in 96 cells], compared to approximately 70 events per cell in controls [5,063 events in 72 cells]). Hence, RIMs are required for neuromodulator release in hippocampal neurons, and no redundant pathways exist. Furthermore, it is evident that SNAREs are not sufficient for DCV fusion in living neurons.

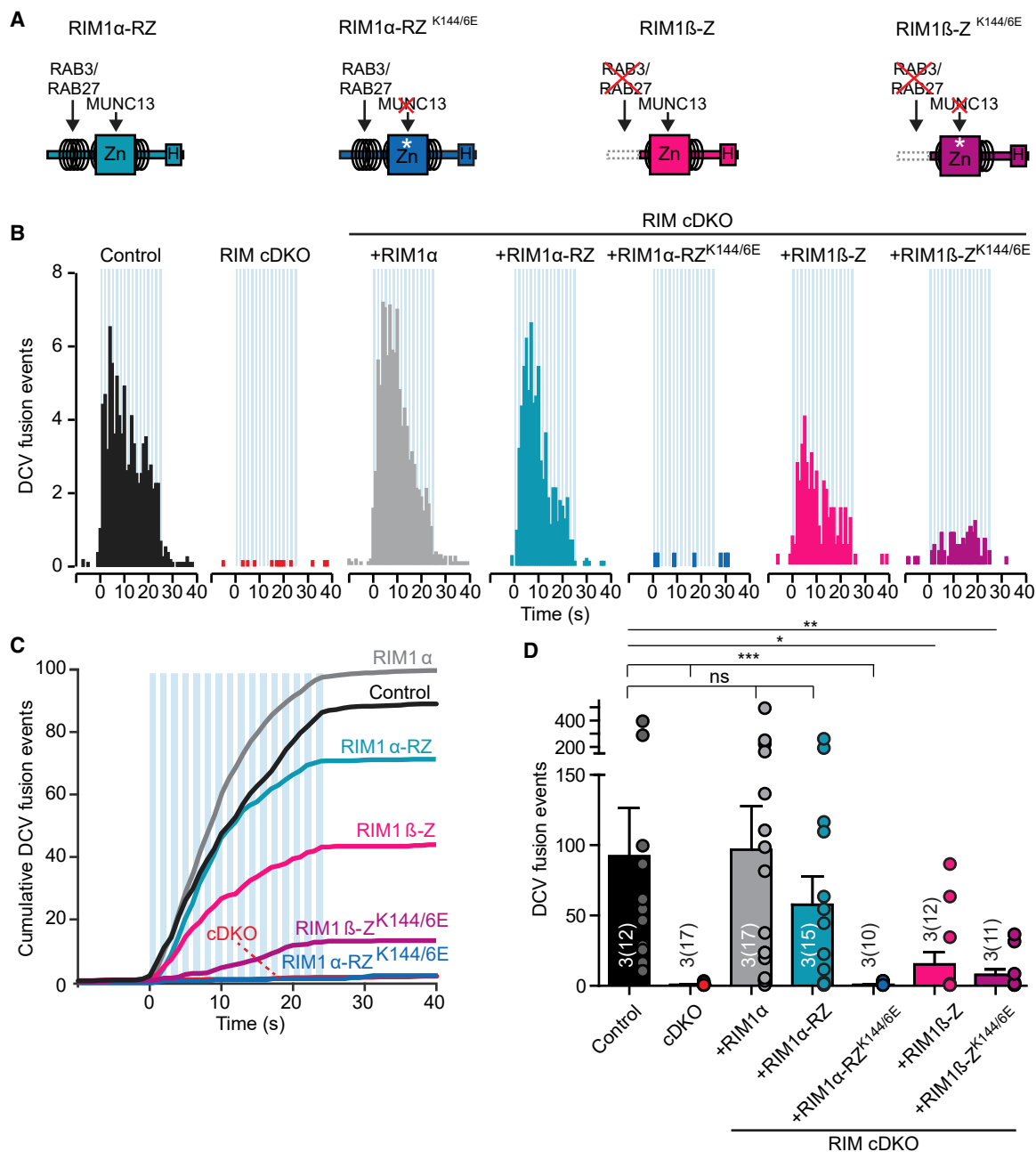


**Figure 5. RIM1 $\alpha$  N-Terminal Domain Is Sufficient to Restore DCV Fusion in RIM cDKO Neurons**

(A) Diagram of N-terminal wild-type and mutant RIM rescue domains expressed in RIM cDKO neurons. Key domains and interactions are indicated. Zn, zinc-finger domain with surrounding  $\alpha$ -helical regions; H, location of a HA-tag; asterisk, K144/6E substitution.

(B–D) DCV fusion analysis using NPY-pHluorin in single control or RIM cDKO hippocampal neurons without or with expression of full-length RIM1 $\alpha$  (gray) or N-terminal rescue constructs (RIM cDKO + rescue). (B) Histogram, (C) cumulative plot, and (D) summary graph of DCV fusion events per cell. Kruskal-Wallis with Dunn's correction: \* $p < 0.05$ , \*\* $p < 0.01$ , \*\*\* $p < 0.001$ . ns,  $p > 0.05$ .

See also Figure S7.

Finally, the almost complete loss of NPY-pHluorin or BDNF-pHluorin events in the absence of RIM1/2 also confirms the specificity of the DCV-fusion reporters, because synaptic vesicle exocytosis is less strongly impaired in RIM1/2 cDKO neurons (de Jong et al., 2018; Kaeser et al., 2011).

### RAB3A Regulates the Mammalian DCV Secretory Pathway at a Late Step, Analogous to SEC4p in Yeast

Since the original discovery that the ras-like, GTP-binding protein SEC4p is one of the essential components in the last step of the secretory pathway in yeast (Goud et al., 1988), members

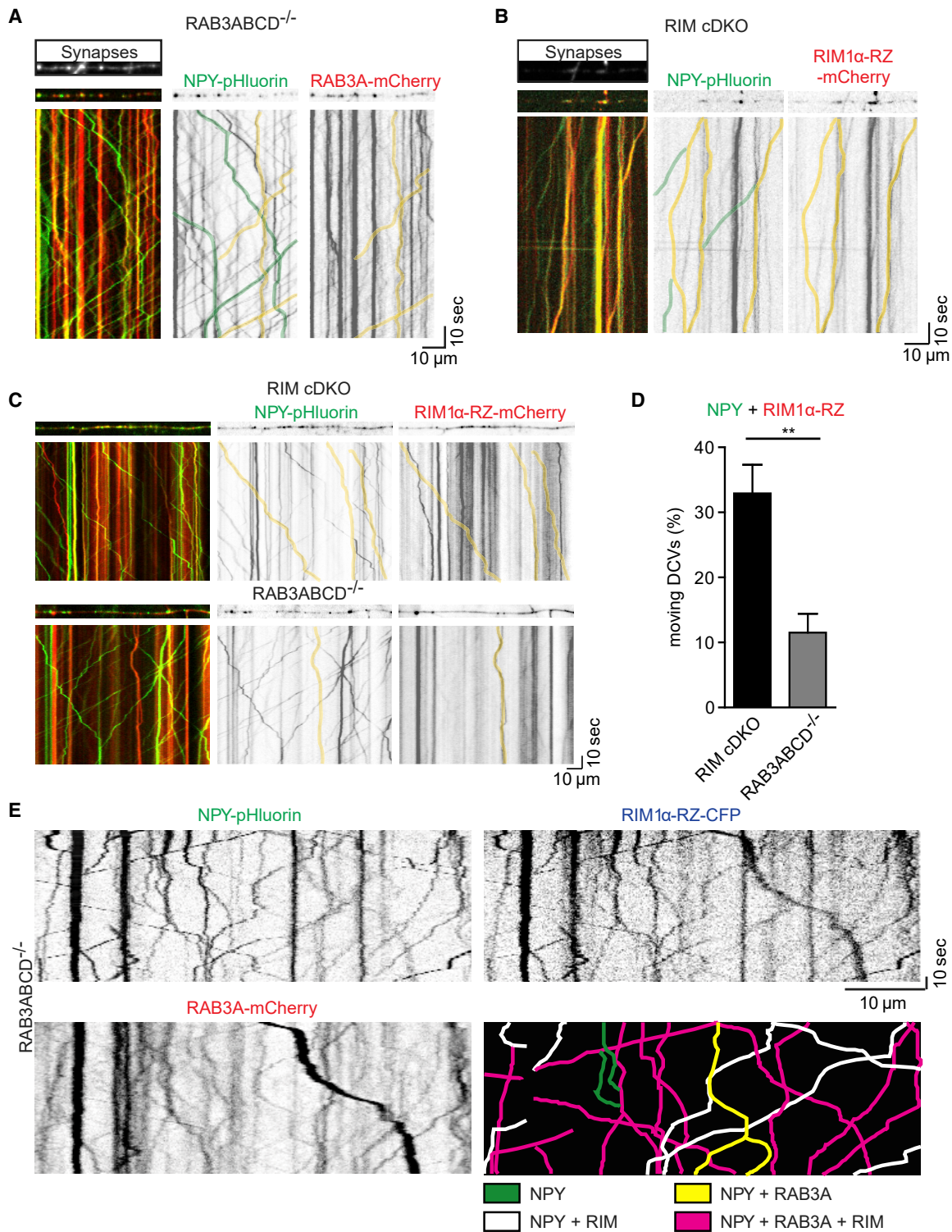


**Figure 6. RIM N Terminus Interaction with DCVs Is Reduced in RAB3-Deficient Neurons**

(A) Representative kymograph showing trajectories of DCVs (NPY-pHluorin, green) and RAB3A-mCherry (red) in RAB3ABCD<sup>-/-</sup> neurons. Synapsin-ECFP labels synapses (above kymograph). NPY-only transport (green) and co-transport of NPY and RAB3A (yellow) is indicated by overlays.

(B) Representative kymograph showing trajectories of DCVs (NPY-pHluorin, green) and N-terminal fragment RIM1 $\alpha$ -RZ-mCherry (red) in RIM cDKO neurons. Synapsin-ECFP labels synapses (above kymograph). NPY-only transport (green) and co-transport of NPY and RIM1 $\alpha$ -RZ-mCherry (yellow) is indicated by overlays.

(legend continued on next page)

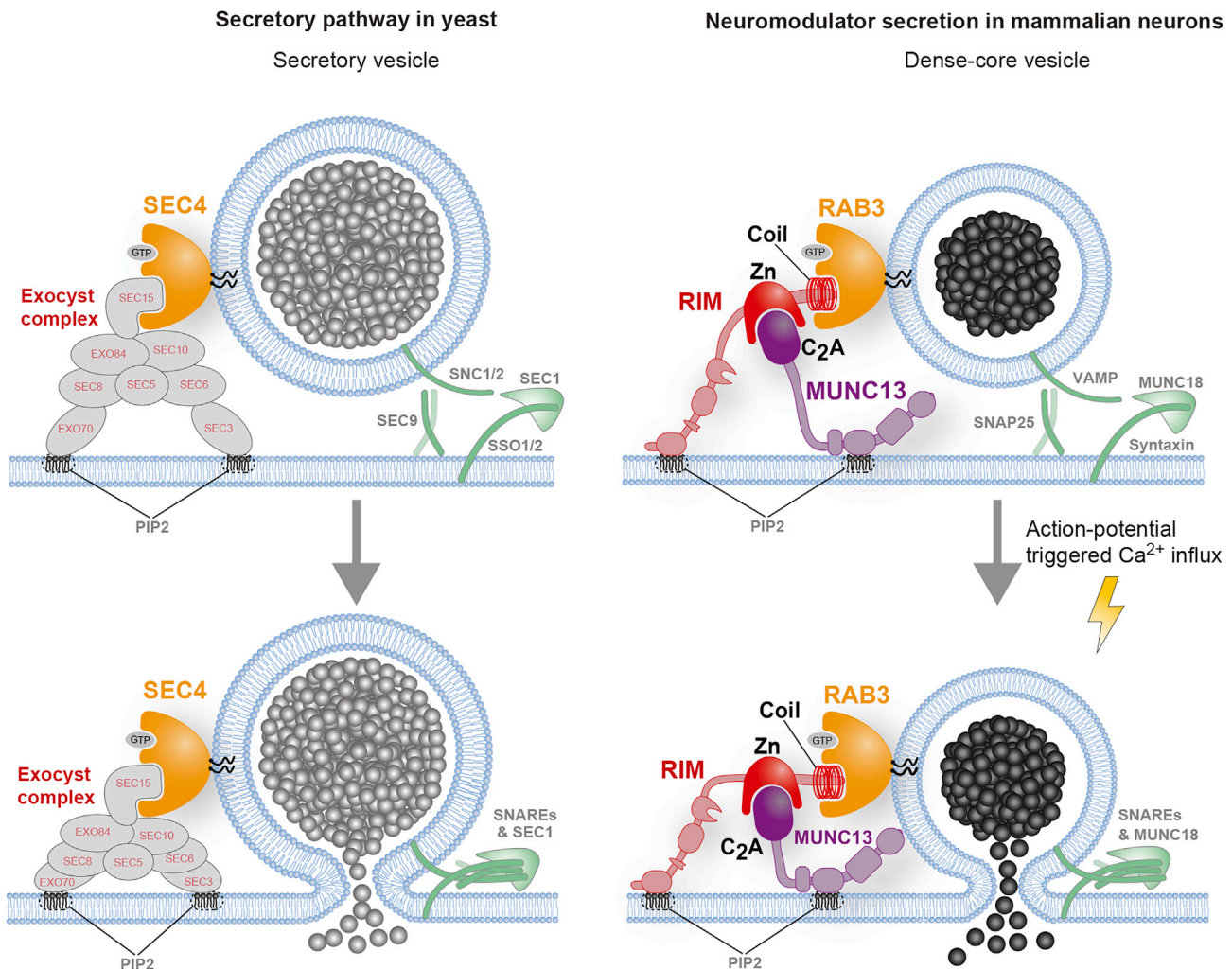


**Figure 7. Function of RAB3, RIM, and MUNC13 in DCV Fusion**

In yeast (left), secretory vesicle binding to the plasma membrane (top, left) relies on the interaction between SEC4 (RAB3) and the Exocyst complex before SNARE-mediated fusion (bottom, left). In mammalian neurons (right), RAB3, RIM, and MUNC13 regulate the late steps in DCV fusion. Through N-terminal interactions, RIMs position MUNC13 and recruit DCVs via RAB3, which is located on the vesicle (top, right). After this step, action potential-triggered, SNARE-mediated fusion can occur (bottom, right). These interactions are essential for the organization of DCV fusion sites, in analogy to the exocyst complex in yeast. Zn, zinc-finger domain.

of the RAB protein family have been found to regulate many intracellular fusion reactions (see for a review: Galvez et al., 2012). RAB3A has been considered to serve a similar role as SEC4p in the mammalian brain due to the high homology to SEC4p, high expression levels in brain, and dynamic association to synaptic vesicles (Fischer von Mollard et al., 1990; Takamori

et al., 2006; Zahraoui et al., 1989). Furthermore, RAB3A regulates secretory granule fusion in pancreatic beta cells (Yaekura et al., 2003), PC12 cells (Tsuboi and Fukuda, 2006), and sperm (Bustos et al., 2012), but synaptic transmission in RAB3A-knockout mice is only mildly affected (Geppert et al., 1997), and deficiency for all four RAB3 paralogs hardly affects synaptic

(C) Example kymographs of NPY-pHluorin and RIM1 $\alpha$ -RZ-mCherry transport in RIM cDKO (top) and RAB3 QKO (bottom) neurons. Co-transport is indicated by yellow lines.

(D) Quantification of co-transport of NPY-pHluorin with RIM1 $\alpha$ -RZ-mCherry in RIM cDKO (black) and RAB3 QKO (gray) neurons. A subset of moving NPY puncta per cell were quantified for trafficking with or without RIM1 $\alpha$ -RZ-mCherry. Percentage of moving NPY co-trafficking with RIM1 $\alpha$ -RZ-mCherry per cell is shown.

(E) Example kymograph of co-transport of NPY-pHluorin with RIM1 $\alpha$ -RZ-ECFP and RAB3A-mCherry in RAB3 QKO neurons. Graphical overlay (bottom right) indicates transport of NPY (green), co-transport of NPY with RAB3A (yellow), NPY with RIM1 $\alpha$ -RZ (white), or NPY with RAB3A and RIM1 $\alpha$ -RZ (magenta).

Neurons were imaged in the presence of Tyrode's solution containing 50 mM NH<sub>4</sub>Cl to visualize all DCVs.

See also Figure S8.

transmission (Schlüter et al., 2006). Also, in *C. elegans* neurons and mouse chromaffin cells, RAB3 deficiency produces partial effects on membrane fusion, largely/partially explained by other defects (impaired vesicle biogenesis; Nonet et al., 1997; Schönn et al., 2010). The current data indicate that although RAB3s may not be the (only) unequivocal SEC4p ortholog for synaptic vesicle fusion, RAB3s are crucial in a late step of the DCV secretory pathway, analogous to its ortholog SEC4p.

To our knowledge, the current study describes the first major phenotype for RAB3 deficiency in the mammalian brain. Whereas synaptic vesicle fusion is hardly affected (Schlüter et al., 2006), DCV fusion is reduced 20-fold, while the number of DCVs and their transport were unaffected. RAB3 function may have become redundant for synaptic transmission altogether, or robust regulation of synaptic vesicle fusion is secured by emergence of additional paralogs, such as RAB27A/B (Mahoney et al., 2006). For DCV fusion and neuromodulator release, no other (RAB) proteins endogenously expressed in hippocampal neurons compensate for the loss of RAB3 expression.

Interestingly, while synaptic transmission was largely intact, several behaviors were altered in RAB3A null mice, including circadian rhythmicity (Kapfhamer et al., 2002), reversal learning and exploration (D'Adamo et al., 2004), memory precision (Ruediger et al., 2011), and ethanol responses (Kapfhamer et al., 2002), although other mnemonic capabilities were normal (Hensbroek et al., 2003). While such effects have been interpreted in the context of synaptic deficits, for example the loss of mossy fiber LTP in RAB3A KO (Castillo et al., 1997), they are equally consistent with loss of neuromodulator signaling.

### RIM1 Is an Essential RAB3 Effector in and outside Synapses

The absence of RIM1/2 resulted in a 100-fold reduction in DCV fusion, which was rescued by RIM1 $\alpha$ -RZ, harboring only the RAB3- and MUNC13-binding domains. Conversely, DCV fusion was not rescued by re-expression of RIM1 $\beta$ , which binds all known RIM1 binding partners, except RAB3. Hence, RIM1 is an essential RAB3A effector for neuromodulator release in hippocampal neurons. The selective loss of RIM2 (i.e., in the presence of 1 or 2 intact RIM1 alleles) tended to increase DCV fusion compared to control (Figure S6), suggesting that RIM2 may not have the same role in neuromodulator release as RIM1 in the neurons studied here.

The essential role of RIM1 for all neuromodulator release is unexpected because many DCV fusion events occur outside synapses, albeit with a low release probability (de Wit et al., 2009; Persoon et al., 2018; van de Bospoort et al., 2012), whereas RIM1 is an active zone protein. Fusion events that occur outside synapses or at dendrites were also absent in RIM1/2-deficient neurons. Hence, a small number of RIM molecules may be present at non-synaptic sites to support non-synaptic DCV fusion. However, despite detailed sub-cellular localization studies (Tang et al., 2016; Wong et al., 2018), there is no evidence for such non-synaptic localization of RIM1/2. Therefore, the possibility that RIM1/2 travels on DCVs, probably via RAB3 interaction (Figure 6), and provides on-board support for DCV fusion is an alternative and possible scenario. While expression of full-length RIM1 produced cellular levels too low to detect

unequivocal co-trafficking, the co-trafficking of the N-terminal fragment with DCVs was evident (Figure 6), and the efficient rescue of DCV fusion with this construct (Figure 5) supports such a scenario. The fact that labeled RIM1 zinc-finger constructs travel with a 3-fold larger fraction of DCVs in RIM1/2-deficient neurons than in RAB3 QKO neurons is also consistent with the idea that endogenous RIM1/2 associates and travels with DCVs by binding RAB3.

Despite substantial co-trafficking, most DCVs appear to travel without detectable RIM1 $\alpha$ -RZ (Figure 6). However, non-synaptic DCV fusion is relatively rare (40%) and requires extreme stimulation intensity/frequency (Persoon et al., 2018; van de Bospoort et al., 2012). The number of RIM1-containing DCVs seems enough to explain these sparse events. DCV fusion depends on the t-SNARE SNAP25 (Arora et al., 2017; Shimojo et al., 2015) and most likely on syntaxins, which are known to be abundantly expressed in axons, also outside synapses (Garcia et al., 1995). Taken together, these considerations suggest that some DCVs fuse at non-synaptic sites with a low probability using RAB3A and possibly RIM1 on the DCV, requiring only cytosolic molecules and the t-SNAREs at the target membrane, while most DCVs fuse at synapses exploiting the local enrichment of RIM1 and t-SNAREs at the target membrane.

### The RIM1-MUNC13 Interaction Is Essential for DCV Fusion and Neuromodulator Release

In RIM1/2-deficient neurons, the loss of neuromodulator release is effectively rescued with full-length RIM1, but not a RIM1 mutant with two amino acid mutations that prevent MUNC13-1 binding (Figure 3). Moreover, a small N-terminal RIM1 fragment, containing only the RAB3 and MUNC13-1 binding sites, also rescues release, but not when the same fragment contains the same two mutations (Figure 5). These four observations suggest that in addition to the essential role of the RAB3-RIM interaction, the interaction between RIM1 and MUNC13-1 is also essential for neuromodulator release.

MUNC13-1 levels are from 35% (Figure S4G) to 67% (Deng et al., 2011) decreased in RIM1/2-deficient hippocampal neurons. The remaining endogenous MUNC13-1 levels apparently are not sufficient to support neuromodulator release in the absence of RIMs, and the interaction between the two molecules is required, as recently proposed, for synaptic vesicle fusion (Camacho et al., 2017). RIM1 is considered to disinhibit MUNC13s by competitive binding to their N-terminal homodimerization domain (Camacho et al., 2017; Deng et al., 2011; Dulubova et al., 2005). The fact that full-length MUNC13 is even more efficient in rescuing neuromodulator release in the absence of RIM1/2 compared to a MUNC13 mutant lacking this homodimerization domain (Figure 4) suggests that, under physiological conditions, the interaction between RIM1 and MUNC13 and the disinhibition of MUNC13 may not be essential for neuromodulator release. Alternatively, other factors that monomerize MUNC13 could be present for DCV but not synaptic vesicles, or, more trivially, overexpression may have strong gain-of-function effects on DCV fusion independent of the presence of RIM. While MUNC13 effectively rescued DCV fusion in RIM-deficient neurons, the onset of evoked DCV fusion was slow (Figure 4D). This may be explained by delayed calcium influx, as calcium

responsiveness is not restored by expression of MUNC13 in RIM-deficient neurons (Deng et al., 2011).

MUNC13 is proposed to tether synaptic vesicles by bridging between vesicle and plasma membrane via its C2C domain and C1/C2B domains, respectively (Liu et al., 2016; Rizo, 2018). Such a mechanism may explain why MUNC13 overexpression rescues neuromodulator release in the absence of RIMs: high cellular MUNC13 levels may also bridge between DCV and plasma membrane and partially compensate for the loss of the dominant native RIM-RAB3 tethering mechanism for DCVs. Recruitment of MUNC13 to release sites and MUNC13 activation may both contribute to the essential role of RIM1 in DCV fusion.

### RAB3/RIM1 Functions Define Diverging Aspects among CNS-Regulated Secretory Pathways

Secretion of neurotransmitters from synaptic vesicles, of neuromodulators from DCVs, and other forms of regulated secretion most likely emerged from a common ancestral mechanism. This study reveals several robust molecular differences between synaptic vesicle and DCV secretory pathways. First, while deficiency for all four RAB3s produces only a mild effect on synaptic vesicle fusion, DCV fusion is affected by >90%. Second, the role of RIM's PDZ domain and its known role in organizing/clustering Ca<sup>2+</sup> channels (Kaesler et al., 2011) is important for synaptic vesicle, but not DCV, fusion. This is likely because DCV fusion does not require tight coupling of Ca<sup>2+</sup> channels to DCVs before fusion and is consistent with the observation that DCV fusion relies on Ca<sup>2+</sup> buildup during long AP trains, and bypassing Ca<sup>2+</sup> channels using ionomycin still produced a >95% reduction of DCV fusion in RIM1/2 null neurons. Third, RIM's disinhibition of MUNC13 is important for synaptic vesicle, but not DCV, fusion (see above). Fourth, while RIM1's C2B domain is essential for RIM's role in synaptic vesicle fusion by interaction with phosphatidylinositol 4,5-bisphosphate (de Jong et al., 2018), this domain, as well as 80% of RIM1 sequence downstream of the zinc-finger domain, which also interacts with ELKS, RIM-binding proteins, and  $\alpha$ -liprins (Hibino et al., 2002; Schoch et al., 2002; Wang et al., 2002), is dispensable for efficient neuromodulator release. These functional differences suggest that RIM's two N-terminal domains are the core domains essential for ancestral secretion principles and that the rest of the protein contains evolutionary adaptations that specifically support the ultra-fast, synchronous fusion of synaptic vesicles in synapses.

In yeast, the six exocyst complex subunits SEC3, 5, 6, 8, 10, and 15 are essential effectors of SEC4/RAB3 in the last steps in the secretory pathway, but their orthologs appear not to be important for regulated secretion in neurons, although available information is still scarce (Schwenger and Kuner, 2010). In invertebrates, the exocyst complex appears to be dispensable for synaptic transmission (Mehta et al., 2005; Murthy et al., 2003), but the RIM orthologs *unc10*/dRIM are not (Koushika et al., 2001; Liu et al., 2011), similar to vertebrate synapses and striatal dopamine varicosities (Deng et al., 2011; Kaesler et al., 2011; Liu et al., 2018). One possible scenario is that RIMs and MUNC13 have emerged in evolution, between unicellular organisms and nematodes/flyes, as an alternative SEC4/RAB3 effector to the exocyst complex in regulated secretion. Consistent with this

idea is that the exocyst complex is ubiquitously expressed in multicellular organisms, but RAB3 and RIM are strongly enriched in cells that specialize in regulated secretion.

In conclusion, our data show that RAB3A and its effector, RIM1, are responsible for the regulated secretion of chemical signals from DCVs in mammalian hippocampal neurons. RIM1 organizes neuromodulator vesicle fusion, also outside synapses, by positioning or activating MUNC13 and recruiting DCVs via RAB3s.

### STAR★METHODS

Detailed methods are provided in the online version of this paper and include the following:

- KEY RESOURCES TABLE
- LEAD CONTACT AND MATERIALS AVAILABILITY
- EXPERIMENTAL MODEL AND SUBJECT DETAILS
  - Animals
- METHOD DETAILS
  - Primary neuronal cultures
  - Constructs
  - Lentiviral Infection
  - Protein quantitation
  - ELISA
  - Immunocytochemistry
  - Electron Microscopy
  - Live imaging
  - Imaging analysis
- QUANTIFICATION AND STATISTICAL ANALYSIS
- DATA AND CODE AVAILABILITY

### SUPPLEMENTAL INFORMATION

Supplemental Information can be found online at <https://doi.org/10.1016/j.neuron.2019.09.015>.

### ACKNOWLEDGMENTS

The authors thank Tobias Moser (University Medical Center Goettingen) for providing the conditional RIM1/2 mouse line; Robbert Zalm for cloning and producing viral particles; Frank den Oudsten and Desiree Schut for producing glia feeders and primary culture assistance; Joke Wortel for animal breeding and electron microscopy; Frank den Oudsten, Erik Ceelen, and Joost Hoetjes for genotyping; Ingrid Saarloos for protein chemistry; and members of the CNCR DCV project team for fruitful discussions. EM analysis was performed at the VU/Umc EM facility (ZonMW 91111009). This work is supported by an ERC Advanced Grant (322966) of the European Union (to M.V.) and by the NIH (R01MH113349 and R01NS103484 to P.S.K.).

### AUTHOR CONTRIBUTIONS

C.M.P., P.S.K., R.F.T., and M.V. designed the experiments. C.M.P. performed immunostainings, protein quantification, and live-cell imaging experiments and analyzed the data. R.I.H. performed live-cell imaging of RAB3 rescue experiments and co-transport of NPY, RAB3A, and RIM1 $\alpha$ -RZ. J.P.N. performed BDNF ELISA experiments. J.R.T.v.W. provided electron microscopy data. C.M.P., R.I.H., P.S.K., R.F.T., and M.V. designed figures and wrote the manuscript with input from all authors.

### DECLARATION OF INTERESTS

The authors declare that they have no conflicts of interest.

Received: March 15, 2019  
 Revised: August 1, 2019  
 Accepted: September 10, 2019  
 Published: October 31, 2019

## REFERENCES

- Aalto, M.K., Ronne, H., and Keränen, S. (1993). Yeast syntaxins Sso1p and Sso2p belong to a family of related membrane proteins that function in vesicular transport. *EMBO J.* *12*, 4095–4104.
- Arora, S., Saarloos, I., Kooistra, R., van de Bospoort, R., Verhage, M., and Toonen, R.F. (2017). SNAP-25 gene family members differentially support secretory vesicle fusion. *J. Cell Sci.* *130*, 1877–1889.
- Balkowiec, A., and Katz, D.M. (2002). Cellular mechanisms regulating activity-dependent release of native brain-derived neurotrophic factor from hippocampal neurons. *J. Neurosci.* *22*, 10399–10407.
- Betz, A., Thakur, P., Junge, H.J., Ashery, U., Rhee, J.S., Scheuss, V., Rosenmund, C., Rettig, J., and Brose, N. (2001). Functional interaction of the active zone proteins Munc13-1 and RIM1 in synaptic vesicle priming. *Neuron* *30*, 183–196.
- Bowser, R., Müller, H., Govindan, B., and Novick, P. (1992). Sec8p and Sec15p are components of a plasma membrane-associated 19.5S particle that may function downstream of Sec4p to control exocytosis. *J. Cell Biol.* *118*, 1041–1056.
- Bustos, M.A., Lucchesi, O., Ruete, M.C., Mayorga, L.S., and Tomes, C.N. (2012). Rab27 and Rab3 sequentially regulate human sperm dense-core granule exocytosis. *Proc. Natl. Acad. Sci. USA* *109*, E2057–E2066.
- Camacho, M., Basu, J., Trimbuch, T., Chang, S., Pulido-Lozano, C., Chang, S.S., Duluvova, I., Abo-Rady, M., Rizo, J., and Rosenmund, C. (2017). Heterodimerization of Munc13 C<sub>2</sub>A domain with RIM regulates synaptic vesicle docking and priming. *Nat. Commun.* *8*, 15293.
- Castillo, P.E., Janz, R., Südhof, T.C., Tzounopoulos, T., Malenka, R.C., and Nicoll, R.A. (1997). Rab3A is essential for mossy fibre long-term potentiation in the hippocampus. *Nature* *388*, 590–593.
- Cheng, P.L., Song, A.H., Wong, Y.H., Wang, S., Zhang, X., and Poo, M.M. (2011). Self-amplifying autocrine actions of BDNF in axon development. *Proc. Natl. Acad. Sci. USA* *108*, 18430–18435.
- D'Adamo, P., Wolfer, D.P., Kopp, C., Tobler, I., Toniolo, D., and Lipp, H.P. (2004). Mice deficient for the synaptic vesicle protein Rab3a show impaired spatial reversal learning and increased explorative activity but none of the behavioral changes shown by mice deficient for the Rab3a regulator Gdi1. *Eur. J. Neurosci.* *19*, 1895–1905.
- de Jong, A.P.H., Roggero, C.M., Ho, M.R., Wong, M.Y., Brautigam, C.A., Rizo, J., and Kaeser, P.S. (2018). RIM C2B Domains Target Presynaptic Active Zone Functions to PIP2-Containing Membranes. *Neuron* *98*, 335–349.e7.
- de Wit, J., Toonen, R.F., and Verhage, M. (2009). Matrix-dependent local retention of secretory vesicle cargo in cortical neurons. *J. Neurosci.* *29*, 23–37.
- Deng, L., Kaeser, P.S., Xu, W., and Südhof, T.C. (2011). RIM proteins activate vesicle priming by reversing autoinhibitory homodimerization of Munc13. *Neuron* *69*, 317–331.
- Dominguez, N., van Weering, J.R.T., Borges, R., Toonen, R.F.G., and Verhage, M. (2018). Dense-core vesicle biogenesis and exocytosis in neurons lacking chromogranins A and B. *J. Neurochem.* *144*, 241–254.
- Dulubova, I., Lou, X., Lu, J., Huryeva, I., Alam, A., Schneggenburger, R., Südhof, T.C., and Rizo, J. (2005). A Munc13/RIM/Rab3 tripartite complex: from priming to plasticity? *EMBO J.* *24*, 2839–2850.
- Emperador Melero, J., Nadadhur, A.G., Schut, D., Weering, J.V., Heine, V.M., Toonen, R.F., and Verhage, M. (2017). Differential Maturation of the Two Regulated Secretory Pathways in Human iPSC-Derived Neurons. *Stem Cell Reports* *8*, 659–672.
- Farina, M., van de Bospoort, R., He, E., Persoon, C.M., van Weering, J.R., Broeke, J.H., Verhage, M., and Toonen, R.F. (2015). CAPS-1 promotes fusion competence of stationary dense-core vesicles in presynaptic terminals of mammalian neurons. *eLife*. Published online February 26, 2015. <https://doi.org/10.7554/eLife.05438>.
- Fischer von Mollard, G., Mignery, G.A., Baumert, M., Perin, M.S., Hanson, T.J., Burger, P.M., Jahn, R., and Südhof, T.C. (1990). rab3 is a small GTP-binding protein exclusively localized to synaptic vesicles. *Proc. Natl. Acad. Sci. USA* *87*, 1988–1992.
- Galvez, T., Gilleron, J., Zerial, M., and O'Sullivan, G.A. (2012). SnapShot: Mammalian Rab proteins in endocytic trafficking. *Cell* *151*, 234–234.e2.
- Garcia, E.P., McPherson, P.S., Chilcote, T.J., Takei, K., and De Camilli, P. (1995). rbSec1A and B colocalize with syntaxin 1 and SNAP-25 throughout the axon, but are not in a stable complex with syntaxin. *J. Cell Biol.* *129*, 105–120.
- Gärtner, A., and Staiger, V. (2002). Neurotrophin secretion from hippocampal neurons evoked by long-term-potential-inducing electrical stimulation patterns. *Proc. Natl. Acad. Sci. USA* *99*, 6386–6391.
- Geppert, M., Goda, Y., Stevens, C.F., and Südhof, T.C. (1997). The small GTP-binding protein Rab3A regulates a late step in synaptic vesicle fusion. *Nature* *387*, 810–814.
- Goud, B., Salminen, A., Walworth, N.C., and Novick, P.J. (1988). A GTP-binding protein required for secretion rapidly associates with secretory vesicles and the plasma membrane in yeast. *Cell* *53*, 753–768.
- Guo, W., Roth, D., Walch-Solimena, C., and Novick, P. (1999). The exocyst is an effector for Sec4p, targeting secretory vesicles to sites of exocytosis. *EMBO J.* *18*, 1071–1080.
- Han, Y., Kaeser, P.S., Südhof, T.C., and Schneggenburger, R. (2011). RIM determines Ca<sup>2+</sup> channel density and vesicle docking at the presynaptic active zone. *Neuron* *69*, 304–316.
- Handley, M.T., Haynes, L.P., and Burgoyne, R.D. (2007). Differential dynamics of Rab3A and Rab27A on secretory granules. *J. Cell Sci.* *120*, 973–984.
- Hartmann, M., Heumann, R., and Lessmann, V. (2001). Synaptic secretion of BDNF after high-frequency stimulation of glutamatergic synapses. *EMBO J.* *20*, 5887–5897.
- Hensbroek, R.A., Kamal, A., Baars, A.M., Verhage, M., and Spruijt, B.M. (2003). Spatial, contextual and working memory are not affected by the absence of mossy fiber long-term potentiation and depression. *Behav. Brain Res.* *138*, 215–223.
- Hibino, H., Pironkova, R., Onwumere, O., Vologodskaja, M., Hudspeth, A.J., and Lesage, F. (2002). RIM binding proteins (RBPs) couple Rab3-interacting molecules (RIMs) to voltage-gated Ca(2+) channels. *Neuron* *34*, 411–423.
- Jahn, R., and Scheller, R.H. (2006). SNAREs—engines for membrane fusion. *Nat. Rev. Mol. Cell Biol.* *7*, 631–643.
- Kaeser, P.S., and Regehr, W.G. (2014). Molecular mechanisms for synchronous, asynchronous, and spontaneous neurotransmitter release. *Annu. Rev. Physiol.* *76*, 333–363.
- Kaeser, P.S., Kwon, H.B., Chiu, C.Q., Deng, L., Castillo, P.E., and Südhof, T.C. (2008). RIM1alpha and RIM1beta are synthesized from distinct promoters of the RIM1 gene to mediate differential but overlapping synaptic functions. *J. Neurosci.* *28*, 13435–13447.
- Kaeser, P.S., Deng, L., Wang, Y., Dulubova, I., Liu, X., Rizo, J., and Südhof, T.C. (2011). RIM proteins tether Ca<sup>2+</sup> channels to presynaptic active zones via a direct PDZ-domain interaction. *Cell* *144*, 282–295.
- Kapfhamer, D., Valladares, O., Sun, Y., Nolan, P.M., Rux, J.J., Arnold, S.E., Veasey, S.C., and Bućan, M. (2002). Mutations in Rab3a alter circadian period and homeostatic response to sleep loss in the mouse. *Nat. Genet.* *32*, 290–295.
- Koushika, S.P., Richmond, J.E., Hadwiger, G., Weimer, R.M., Jorgensen, E.M., and Nonet, M.L. (2001). A post-docking role for active zone protein Rim. *Nat. Neurosci.* *4*, 997–1005.
- Liu, K.S., Siebert, M., Mertel, S., Knoche, E., Wegener, S., Wichmann, C., Matkovic, T., Muhammad, K., Depner, H., Mettke, C., et al. (2011). RIM-binding protein, a central part of the active zone, is essential for neurotransmitter release. *Science* *334*, 1565–1569.

- Liu, X., Seven, A.B., Camacho, M., Esser, V., Xu, J., Trimbuch, T., Quade, B., Su, L., Ma, C., Rosenmund, C., and Rizo, J. (2016). Functional synergy between the Munc13 C-terminal C1 and C2 domains. *eLife* 5, e13696.
- Liu, C., Kershberg, L., Wang, J., Schneeberger, S., and Kaeser, P.S. (2018). Dopamine Secretion Is Mediated by Sparse Active Zone-like Release Sites. *Cell* 172, 706–718.e15.
- Lo, K.Y., Kuzmin, A., Unger, S.M., Petersen, J.D., and Silverman, M.A. (2011). KIF1A is the primary anterograde motor protein required for the axonal transport of dense-core vesicles in cultured hippocampal neurons. *Neurosci. Lett.* 491, 168–173.
- Lu, J., Machius, M., Dulubova, I., Dai, H., Südhof, T.C., Tomchick, D.R., and Rizo, J. (2006). Structural basis for a Munc13-1 homodimer to Munc13-1/RIM heterodimer switch. *PLoS Biol.* 4, e192.
- Mahoney, T.R., Liu, Q., Itoh, T., Luo, S., Hadwiger, G., Vincent, R., Wang, Z.W., Fukuda, M., and Nonet, M.L. (2006). Regulation of synaptic transmission by RAB-3 and RAB-27 in *Caenorhabditis elegans*. *Mol. Biol. Cell* 17, 2617–2625.
- Malva, J.O., Xapelli, S., Baptista, S., Valero, J., Agasse, F., Ferreira, R., and Silva, A.P. (2012). Multifaces of neuropeptide Y in the brain—neuroprotection, neurogenesis and neuroinflammation. *Neuropeptides* 46, 299–308.
- Matsuda, N., Lu, H., Fukata, Y., Noritake, J., Gao, H., Mukherjee, S., Nemoto, T., Fukata, M., and Poo, M.M. (2009). Differential activity-dependent secretion of brain-derived neurotrophic factor from axon and dendrite. *J. Neurosci.* 29, 14185–14198.
- Mehta, S.Q., Hiesinger, P.R., Beronja, S., Zhai, R.G., Schulze, K.L., Verstreken, P., Cao, Y., Zhou, Y., Tepass, U., Crair, M.C., and Bellen, H.J. (2005). Mutations in *Drosophila* sec15 reveal a function in neuronal targeting for a subset of exocyst components. *Neuron* 46, 219–232.
- Meijer, M., Burkhardt, P., de Wit, H., Toonen, R.F., Fasshauer, D., and Verhage, M. (2012). Munc18-1 mutations that strongly impair SNARE-complex binding support normal synaptic transmission. *EMBO J.* 31, 2156–2168.
- Mertens, I., Husson, S.J., Janssen, T., Lindemans, M., and Schoofs, L. (2007). PACAP and PDF signaling in the regulation of mammalian and insect circadian rhythms. *Peptides* 28, 1775–1783.
- Meyer-Lindenberg, A., Domes, G., Kirsch, P., and Heinrichs, M. (2011). Oxytocin and vasopressin in the human brain: social neuropeptides for translational medicine. *Nat. Rev. Neurosci.* 12, 524–538.
- Murthy, M., Garza, D., Scheller, R.H., and Schwarz, T.L. (2003). Mutations in the exocyst component Sec5 disrupt neuronal membrane traffic, but neurotransmitter release persists. *Neuron* 37, 433–447.
- Nonet, M.L., Staunton, J.E., Kilgard, M.P., Fergestad, T., Hartweg, E., Horvitz, H.R., Jorgensen, E.M., and Meyer, B.J. (1997). *Caenorhabditis elegans* rab-3 mutant synapses exhibit impaired function and are partially depleted of vesicles. *J. Neurosci.* 17, 8061–8073.
- Novick, P., and Schekman, R. (1979). Secretion and cell-surface growth are blocked in a temperature-sensitive mutant of *Saccharomyces cerevisiae*. *Proc. Natl. Acad. Sci. USA* 76, 1858–1862.
- Novick, P., Field, C., and Schekman, R. (1980). Identification of 23 complementation groups required for post-translational events in the yeast secretory pathway. *Cell* 21, 205–215.
- Novick, P., Ferro, S., and Schekman, R. (1981). Order of events in the yeast secretory pathway. *Cell* 25, 461–469.
- Pang, P.T., Teng, H.K., Zaitsev, E., Woo, N.T., Sakata, K., Zhen, S., Teng, K.K., Yung, W.H., Hempstead, B.L., and Lu, B. (2004). Cleavage of proBDNF by tPA/plasmin is essential for long-term hippocampal plasticity. *Science* 306, 487–491.
- Persoon, C.M., Moro, A., Nassal, J.P., Farina, M., Broeke, J.H., Arora, S., Dominguez, N., van Weering, J.R., Toonen, R.F., and Verhage, M. (2018). Pool size estimations for dense-core vesicles in mammalian CNS neurons. *EMBO J.* 37, e99672.
- Protopopov, V., Govindan, B., Novick, P., and Gerst, J.E. (1993). Homologs of the synaptobrevin/VAMP family of synaptic vesicle proteins function on the late secretory pathway in *S. cerevisiae*. *Cell* 74, 855–861.
- Rizo, J. (2018). Mechanism of neurotransmitter release coming into focus. *Protein Sci.* 27, 1364–1391.
- Ruediger, S., Vittori, C., Bednarek, E., Genoud, C., Strata, P., Sacchetti, B., and Caroni, P. (2011). Learning-related feedforward inhibitory connectivity growth required for memory precision. *Nature* 473, 514–518.
- Salminen, A., and Novick, P.J. (1987). A ras-like protein is required for a post-Golgi event in yeast secretion. *Cell* 49, 527–538.
- Schlüter, O.M., Khvotchev, M., Jahn, R., and Südhof, T.C. (2002). Localization versus function of Rab3 proteins. Evidence for a common regulatory role in controlling fusion. *J. Biol. Chem.* 277, 40919–40929.
- Schlüter, O.M., Schmitz, F., Jahn, R., Rosenmund, C., and Südhof, T.C. (2004). A complete genetic analysis of neuronal Rab3 function. *J. Neurosci.* 24, 6629–6637.
- Schlüter, O.M., Basu, J., Südhof, T.C., and Rosenmund, C. (2006). Rab3 superprimed synaptic vesicles for release: implications for short-term synaptic plasticity. *J. Neurosci.* 26, 1239–1246.
- Schmitz, S.K., Hjorth, J.J., Joemai, R.M., Wijntjes, R., Eijgenraam, S., de Bruijn, P., Georgiou, C., de Jong, A.P., van Ooyen, A., Verhage, M., et al. (2011). Automated analysis of neuronal morphology, synapse number and synaptic recruitment. *J. Neurosci. Methods* 195, 185–193.
- Schoch, S., Castillo, P.E., Jo, T., Mukherjee, K., Geppert, M., Wang, Y., Schmitz, F., Malenka, R.C., and Südhof, T.C. (2002). RIM1alpha forms a protein scaffold for regulating neurotransmitter release at the active zone. *Nature* 415, 321–326.
- Schonn, J.S., van Weering, J.R., Mohrmann, R., Schlüter, O.M., Südhof, T.C., de Wit, H., Verhage, M., and Sørensen, J.B. (2010). Rab3 proteins involved in vesicle biogenesis and priming in embryonic mouse chromaffin cells. *Traffic* 11, 1415–1428.
- Schwenger, D.B., and Kuner, T. (2010). Acute genetic perturbation of exocyst function in the rat calyx of Held impedes structural maturation, but spares synaptic transmission. *Eur. J. Neurosci.* 32, 974–984.
- Shimojo, M., Courchet, J., Pieraut, S., Torabi-Rander, N., Sando, R., 3rd, Polleux, F., and Maximov, A. (2015). SNAREs Controlling Vesicular Release of BDNF and Development of Callosal Axons. *Cell Rep.* 11, 1054–1066.
- Stucchi, R., Plucińska, G., Hummel, J.J.A., Zahavi, E.E., Guerra San Juan, I., Klykov, O., Scheltema, R.A., Altelaar, A.F.M., and Hoogenraad, C.C. (2018). Regulation of KIF1A-Driven Dense Core Vesicle Transport: Ca<sup>2+</sup>/CaM Controls DCV Binding and Liprin- $\alpha$ /TANC2 Recruits DCVs to Postsynaptic Sites. *Cell Rep.* 24, 685–700.
- Südhof, T.C. (2013). Neurotransmitter release: the last millisecond in the life of a synaptic vesicle. *Neuron* 80, 675–690.
- Südhof, T.C., and Rothman, J.E. (2009). Membrane fusion: grappling with SNARE and SM proteins. *Science* 323, 474–477.
- Takamori, S., Holt, M., Stenius, K., Lemke, E.A., Grønborg, M., Riedel, D., Urlaub, H., Schenck, S., Brügger, B., Ringler, P., et al. (2006). Molecular anatomy of a trafficking organelle. *Cell* 127, 831–846.
- Tang, A.H., Chen, H., Li, T.P., Metzbowler, S.R., MacGillavry, H.D., and Blanpied, T.A. (2016). A trans-synaptic nanocolumn aligns neurotransmitter release to receptors. *Nature* 536, 210–214.
- TerBush, D.R., and Novick, P. (1995). Sec6, Sec8, and Sec15 are components of a multisubunit complex which localizes to small bud tips in *Saccharomyces cerevisiae*. *J. Cell Biol.* 130, 299–312.
- TerBush, D.R., Maurice, T., Roth, D., and Novick, P. (1996). The Exocyst is a multiprotein complex required for exocytosis in *Saccharomyces cerevisiae*. *EMBO J.* 15, 6483–6494.
- Tsuboi, T., and Fukuda, M. (2006). Rab3A and Rab27A cooperatively regulate the docking step of dense-core vesicle exocytosis in PC12 cells. *J. Cell Sci.* 119, 2196–2203.
- Vähätalo, L.H., Ruohonen, S.T., Mäkelä, S., Kovalainen, M., Huotari, A., Mäkelä, K.A., Määttä, J.A., Miinalainen, I., Gilsbach, R., Hein, L., et al. (2015). Neuropeptide Y in the noradrenergic neurons induces obesity and inhibits sympathetic tone in mice. *Acta Physiol. (Oxf.)* 213, 902–919.



- van de Bospoort, R., Farina, M., Schmitz, S.K., de Jong, A., de Wit, H., Verhage, M., and Toonen, R.F. (2012). Munc13 controls the location and efficiency of dense-core vesicle release in neurons. *J. Cell Biol.* *199*, 883–891.
- van Keimpema, L., Kooistra, R., Toonen, R.F., and Verhage, M. (2017). CAPS-1 requires its C2, PH, MHD1 and DCV domains for dense core vesicle exocytosis in mammalian CNS neurons. *Sci. Rep.* *7*, 10817.
- Walch-Solimena, C., Collins, R.N., and Novick, P.J. (1997). Sec2p mediates nucleotide exchange on Sec4p and is involved in polarized delivery of post-Golgi vesicles. *J. Cell Biol.* *137*, 1495–1509.
- Wang, Y., Okamoto, M., Schmitz, F., Hofmann, K., and Südhof, T.C. (1997). Rim is a putative Rab3 effector in regulating synaptic-vesicle fusion. *Nature* *388*, 593–598.
- Wang, Y., Liu, X., Biederer, T., and Südhof, T.C. (2002). A family of RIM-binding proteins regulated by alternative splicing: Implications for the genesis of synaptic active zones. *Proc. Natl. Acad. Sci. USA* *99*, 14464–14469.
- Wong, M.Y., Liu, C., Wang, S.S.H., Roquas, A.C.F., Fowler, S.C., and Kaeser, P.S. (2018). Liprin- $\alpha$ 3 controls vesicle docking and exocytosis at the active zone of hippocampal synapses. *Proc. Natl. Acad. Sci. USA* *115*, 2234–2239.
- Yaekura, K., Julyan, R., Wicksteed, B.L., Hays, L.B., Alarcon, C., Sommers, S., Poitout, V., Baskin, D.G., Wang, Y., Philipson, L.H., and Rhodes, C.J. (2003). Insulin secretory deficiency and glucose intolerance in Rab3A null mice. *J. Biol. Chem.* *278*, 9715–9721.
- Zahn, T.R., Angleson, J.K., MacMorris, M.A., Domke, E., Hutton, J.F., Schwartz, C., and Hutton, J.C. (2004). Dense core vesicle dynamics in *Caenorhabditis elegans* neurons and the role of kinesin UNC-104. *Traffic* *5*, 544–559.
- Zahraoui, A., Touchot, N., Chardin, P., and Tavitian, A. (1989). The human Rab genes encode a family of GTP-binding proteins related to yeast YPT1 and SEC4 products involved in secretion. *J. Biol. Chem.* *264*, 12394–12401.

## STAR★METHODS

## KEY RESOURCES TABLE

| REAGENT or RESOURCE  | SOURCE         | IDENTIFIER   |
|--|----------------|--|
| <b>Antibodies</b>  |                |  |
| Monoclonal mouse Homer1  | SYSY           | Cat#160011;<br>RRID:AB_2120992   |
| Monoclonal mouse anti-Pan-Axonal Neurofilament marker (SMI-312R) | Covance        | Cat# SMI-312R; RRID:AB_2314906   |
| Monoclonal mouse $\beta$ 3-tubulin                               | Cell Signaling | Cat# 4466; RRID:AB_1904176   |
| Monoclonal mouse Actin   | Chemicon       | Cat# MAB1501;<br>RRID:AB_2223041   |
| Monoclonal mouse HA (12CA5)                                      | Roche          | Cat#11583816001;<br>RRID:AB_514505   |
| Monoclonal mouse MUNC13-1  | SYSY           | Cat# 126111;<br>RRID:AB_887735   |
| Monoclonal mouse PSD95   | Abcam          | Cat# ab2723;<br>RRID:AB_303248   |
| Polyclonal chicken MAP2  | Abcam          | Cat# Ab5392; RRID:AB_2138153   |
| Polyclonal guinea pig Synaptophysin1                             | SYSY           | Cat# 101 004; RRID:AB_1210382  |
| Polyclonal guinea pig VGLUT1                                     | Millipore      | Cat# AB5905;<br>RRID:AB_2301751  |
| Polyclonal rabbit RIM1/2 ZN-finger                               | SYSY           | Cat# 140 203; RRID:AB_887775   |
| Polyclonal rabbit Chromogranin B                                 | SYSY           | Cat# 259103;<br>RRID:AB_2619973  |
| Alexa Fluor conjugated secondary antibodies                      | Invitrogen     | Cat# A21244, A11001, A21450 A11040,<br>A11010, A11003;<br>RRID:AB_141663, AB_2534069,<br>AB_141882, AB_1500590, AB_2534077,<br>AB_141370 |
| anti-rabbit or anti-mouse IRDye secondary antibodies             | LI-COR         | Cat# LI 925-32210, 926-68073;<br>RRID:AB_2687825, AB_10954442  |
| alkaline phosphatase-conjugated secondary antibodies             | Jackson        | Cat#111-055-003, 115-055-003;<br>RRID:AB_2337947, AB_2338528   |
| <b>Chemicals, Peptides, and Recombinant Proteins</b>             |                |  |
| Agarose type II-A  | Sigma          | Cat# A9918; CAS: 9012-36-6   |
| Laminin  | Sigma          | Cat# L2020   |
| Poly-D-lysine  | Sigma          | Cat# P6407   |
| Rat tail collagen  | BD Biosciences | Cat# 354236  |
| B-27   | GIBCO          | Cat# 17504-044   |
| poly-L-ornithine   | Sigma          | Cat# P4957   |
| normal goat serum  | GIBCO          | Cat# 16210-072   |
| Mowiol 4-88  | Sigma          | Cat# 81381   |
| Glutaraldehyde   | Merck          | Cat# 1042390250  |
| Cacodylate   | Merck          | Cat# 820670  |
| OsO4   | EMS            | Cat# 19172   |
| K4Ru(CN)6  | Sigma          | Cat# 378232.2  |
| Glycid Ether (Epon)  | Serva          | Cat# 21045.02  |
| Dodecenyl succinic anhydride (Epon)                              | Serva          | Cat# 20755.02  |
| Methyl nadic anhydride (Epon)                                    | Serva          | Cat# 29452.03  |
| benzyltrimethylamine (Epon)                                      | EMS            | Cat# 1140025   |

(Continued on next page)

**Continued**

| REAGENT or RESOURCE                        | SOURCE  | IDENTIFIER  |
|--|---|---|
| Uranyl acetate                             | Polyscience   | Cat# 21447  |
| Lead nitrate (lead citrate)                | Merck   | Cat# 1.07398.0100   |
| Sodium citrate (lead citrate)              | VWR   | Cat# 27831.297  |
| Ionomycin                                  | Fisher BioReagent   | Cat# 10429883   |
| Fluo-5F-AM                                 | Molecular Probes  | Cat# F14222   |
| Critical Commercial Assays                 |   |   |
| Mouse BDNF ELISA                           | Biosensis   | Cat# BEK-2003   |
| Experimental Models: Organisms/Strains     |   |   |
| Mouse: <i>Rab3ABCD</i> null                | Schlüter et al., 2004   | N/A   |
| Mouse: <i>Rim1/2</i> conditional knock-out | Kaesler et al., 2008, 2011  | N/A   |
| Rat: Wistar (CrI:WI)                       | Charles River   | Strain code: 003  |
| Recombinant DNA                            |   |   |
| pFSW nclcre                                | Kaesler et al., 2011  | N/A   |
| pFSW nclDeltacre                           |   |   |
| pSyn(pr) hNPYpHluorin-N1                   | van de Bospoort et al., 2012  | N/A   |
| pSyn(pr) hNPYmCherry                       |   |   |
| pSyn(pr) rBDNFpHluorin                     | de Wit et al., 2009   | N/A   |
| pSyn(pr) Synapsin-1ECFP                    | Modified gift from:<br>Dr A. Jeromin (Allen Brain<br>Institute, Seattle, USA) | N/A   |
| pSyn(pr) RIM1alfa-HA                       | Modified from:  | N/A   |
| pSyn(pr) RIM1alfa-K144-6E-HA               | Deng et al., 2011   |   |
| pSyn(pr) RIM1alfa-dPDZ-HA                  | Kaesler et al., 2011  |   |
| pSyn(pr) RIM1beta-HA                       |   |   |
| pSyn(pr) RIM1alfa-Zn-HA                    | Modified from:  | N/A   |
| pSyn(pr) RIM1alfa-Zn-K144-6E-HA            | Deng et al., 2011   |   |
| pSyn(pr) RIM1beta-Zn-HA                    | Kaesler et al., 2011  |   |
| pSyn(pr) RIM1beta-ZN-HA(K144/6E)           |   |   |
| pSyn(pr) RIM1alfa-Zn-HA-ECFP               | Modified from:  | N/A   |
| pSyn(pr) RIM1alfa-Zn-HA-mCherry            | Deng et al., 2011<br>Kaesler et al., 2011                                     |   |
| pSIN-TRE-rUnc-13 (WT)mCherryN1-Syn-rtTA2   | Modified from:  | N/A   |
| pSyn(pr) rUnc-13 (delta N term)mCherry     | Deng et al., 2011   |   |
| pSyn(pr) mCherry-RAB3A(mus)                | Created in this study   | N/A   |
| pSyn(pr) RAB3B(mus)mCherry                 |   |   |
| pSyn(pr) RAB3C(mus)mCherry                 |   |   |
| pSyn(pr) RAB3D(mus)mCherry                 |   |   |
| Software and Algorithms                    |   |   |
| MATLAB R2018a                              | MathWorks   | <a href="https://www.mathworks.com">https://www.mathworks.com</a>   |
| SynD – Synapse and neurite detection       | Schmitz et al., 2011  | <a href="https://www.johanneshjorth.se/SynD/SynD.html">https://www.johanneshjorth.se/SynD/SynD.html</a>   |
| ImageJ                                     |   | <a href="https://imagej.net/Welcome">https://imagej.net/Welcome</a><br>RRID:SCR_003070  |
| GraphPad Prism                             | GraphPad Software   | <a href="https://www.graphpad.com/RRID:SCR_002798">https://www.graphpad.com/RRID:SCR_002798</a>   |
| NIS-Elements                               | Nikon Instruments   | <a href="https://www.microscope.healthcare.nikon.com/products/software">https://www.microscope.healthcare.nikon.com/products/software</a> RRID:SCR_014329 |

**LEAD CONTACT AND MATERIALS AVAILABILITY**

Further information and requests for resources and reagents should be directed to and will be fulfilled by the Lead Contact, Matthijs Verhage ([matthijs@cncr.vu.nl](mailto:matthijs@cncr.vu.nl)). All unique plasmids generated in this study are available from the Lead Contact without restriction. No other unique reagents were generated in this study.

## EXPERIMENTAL MODEL AND SUBJECT DETAILS

### Animals

Homozygous double conditional RIM1 $\alpha$  $\beta$ /RIM2 $\alpha$  $\beta$  $\gamma$  mutant mice described previously (Kaeser et al., 2011; Kaeser et al., 2008) were used for timed mating of homozygous cDKO mice. All newborn (P1) RIM cDKO mice used for experiments were genotyped by PCR (Kaeser et al., 2011). RAB3ABCD KO mice have been described previously (Schlüter et al., 2004). As RAB3ABCD<sup>-/-</sup> embryos die shortly after birth, embryonic day 18.5 embryos were obtained by caesarean section of pregnant females from timed matings of RAB3A<sup>+/-</sup>, BCD<sup>-/-</sup> mice and genotyped by PCR as described previously (Schlüter et al., 2004). C57BL/6 mice were used for wild-type cultures. For glia preparations newborn pups from female Wistar rats were used. Animals were housed and bred according to institutional and Dutch governmental guidelines (DEC-FGA 11-03 and AVD112002017824).

## METHOD DETAILS

### Primary neuronal cultures

Dissociated hippocampal neuron cultures were prepared from newborn (P1) RIM cDKO mice, E18.5 C57BL/6 (wild-type) or RAB3A<sup>+/-</sup>, BCD<sup>-/-</sup> littermate mouse embryos. Cerebral cortices were dissected free of meninges in Hanks' balanced salt solution (Sigma, H9394) supplemented with 10 mM HEPES (GIBCO, 15630-056). The hippocampi were isolated from the tissue and digested with 0.25% Trypsin (GIBCO, 15090-046) in Hanks-HEPES for 20 min. at 37°C. Hippocampi were washed three times with Hanks-HEPES and triturated with fire-polished glass pipettes. Dissociated neurons were counted and plated in neurobasal medium (GIBCO, 21103-049) supplemented with 2% B-27 (GIBCO, 17504-044), 1.8% HEPES, 0.25% glutamax (GIBCO, 35050-038) and 0.1% Penicillin-Streptomycin (GIBCO, 15140-122). To obtain single neuron cultures, hippocampal neurons were plated in 12-well plates at a density of 1100-1400 cells/well on 18 mm glass coverslips containing micro-islands of rat glia. Micro-islands were generated as described previously (Meijer et al., 2012) by plating 8000/well rat glia on UV-sterilized agarose (Type II-A; Sigma, A9918)-coated etched glass coverslips stamped with a mixture of 0.1 mg/mL poly-D-lysine (Sigma, P6407), 0.7 mg/mL rat tail collagen (BD Biosciences, 354236) and 10 mM acetic acid (Sigma, 45731). High-density dissociated neuron cultures for protein quantitation and secretion measurements were prepared from cortex tissue and plated on plastic 12-wells or 6-wells plates coated with 0.01% poly-L-ornithine (Sigma, P4957) and 2.5  $\mu$ g/mL laminin (Sigma, L2020) diluted in Dulbecco's phosphate-buffered saline (DPBS; GIBCO, 14190-250) overnight at RT.

### Constructs

EGFP-Cre and EGFP-control (mutant Cre) constructs were created previously (Kaeser et al., 2011) and contained an additional nuclear localization sequence of nucleoplasmin in the N terminus of EGFP to ensure complete nuclear localization of EGFP. NPY-pHluorin or NPY-mCherry were generated by replacing Venus in NPY-Venus with super-ecliptic pHluorin or red fluorescent mCherry (van de Bospoort et al., 2012). Generation of BDNF-pHluorin was described previously (de Wit et al., 2009). Synapsin-mCherry was a kind gift of Dr A. Jeromin (Allen Brain Institute, Seattle, USA) and synapsin-ECFP was obtained by replacing mCherry with ECFP. The RIM1 rescue constructs RIM1 $\alpha$ , RIM1 $\beta$ , RIM1 $\alpha$ - $\Delta$ PDZ, RIM1 $\alpha$ -K144/6E, RIM1 $\alpha$ -RZ, RIM1 $\alpha$ -RZ-K144/6E, RIM1 $\beta$ -Z, RIM1 $\beta$ -Z-K144/6E were described previously (Deng et al., 2011; Kaeser et al., 2011). They were generated from a rat RIM1 $\alpha$  or RIM1 $\beta$  expression plasmid and contained an HA tag. RIM1 $\alpha$ -RZ-mCherry or RIM1 $\alpha$ -RZ-ECFP were created by adding mCherry or ECFP to the C terminus. The MUNC13-2(WT) and MUNC13-2( $\Delta$ N) constructs were described previously (Deng et al., 2011) and contained mCherry at the C terminus. RAB3A, B, C and D constructs were obtained from a mouse cDNA library by PCR and labeled with mCherry at the C terminus. All constructs were cloned to synapsin-promoter driven constructs, sequenced verified and subcloned into pLenti vectors and viral particles were produced. Titration of lentiviral particle batches was performed by assessment of number of fluorescent cells upon infection to ensure 100% infection efficiency.

### Lentiviral Infection

Neuronal RIM cultures were infected with EGFP-Cre or EGFP-control lentiviral particles at DIV 0 or DIV 5. To visualize DCV fusion and transport (Figures 2, S3B–S3I, S5B–S5H, and S5M–S5O) cultures were infected with lentiviral particles encoding for NPY-pHluorin, NPY-mCherry and Syn-ECFP at DIV 9-10. For other DCV fusion experiments cultures were infected at DIV 9-10 with Syn-ECFP and the DCV reporter NPY-pHluorin or BDNF-pHluorin, allowing single color live cell imaging of DCV fusion and/or the addition of other constructs. For rescue experiments cultures were infected with the corresponding rescue construct at DIV 0. Neurons were post hoc fixed and immunostained for the HA-tag present on all rescue constructs to validate expression of rescue constructs in individual neurons.

### Protein quantitation

To characterize protein expression levels of RIM1/2 upon Cre-recombinase expression, high-density dissociated cortical cultures of RIM cDKO mice were infected at DIV 0 with Cre or control virus. At indicated time-points neurons were washed in cold PBS and homogenized in Laemmli sample buffer consisting of 2% SDS (VWR chemicals, M107), 10% glycerol (Merck, 818709), 0.26 M  $\beta$ -mercaptoethanol (Sigma, M3148), 60 mM Tris-HCl (Serva, 37180) pH 6.8, and 0.01% Bromophenol blue (Applichem, A3640). To measure

chromogranin B (CHGB) levels in RAB3 KO neurons, cortex tissue of RAB3A<sup>+/+</sup>, <sup>+/−</sup> or <sup>−/−</sup>, BCD<sup>−/−</sup> animals was homogenized in Laemmli sample buffer. Samples were separated on 7% SDS-polyacrylamide gels with 2,2,2-Trichloroethanol using standard SDS-PAGE technique and scanned in a Gel Doc EZ imager (Bio-Rad). Proteins were transferred to membrane O/N at 150 mA, 4°C. Blots were incubated in 2% BSA (Acros Organics, 268131000) - PBS containing 0.1% Tween-20 (Sigma, P2287) for 1 h at 4°C. Subsequently blots were incubated with primary antibodies in 2% BSA-PBS-0.1% Tween20 for 4 h at RT. Primary antibodies included polyclonal rabbit RIM1/2 ZN-finger (1:1000; SySy, 140203), monoclonal mouse  $\beta$ 3-Tubulin (1:1000; Cell Signaling, 4466), polyclonal rabbit Chromogranin B (1:500; SySy 259103) and monoclonal mouse Actin (1:10,000; Chemicon, MAB1501). After washing with PBS-0.1%Tween-20, blots were incubated with secondary antibodies (anti-rabbit or anti-mouse IRDye secondary antibodies (1:10,000; LI-COR) or alkaline phosphatase-conjugated secondary antibodies (1:10,000; Jackson) in 2% BSA-PBS-0.1% Tween20 for 45 min. at 4°C. After washing blots were scanned with Odyssey FC dual-mode imaging system (LI-COR) for 2 min in each channel (700 and 800 nm laser). When labeled with alkaline phosphatase-conjugated secondary antibodies, blots were incubated with AttoPhos substrate for 5 min, and scanned on a Fujifilm FLA-5000 Reader.

### ELISA

High-density cultures (DIV 8) were washed ones with Tyrode's solution (119 mM NaCl, 2.5 mM KCl, 2 mM CaCl<sub>2</sub>\*2H<sub>2</sub>O, 2 mM MgCl<sub>2</sub>\*6H<sub>2</sub>O, 25 mM HEPES and 30 mM Glucose\*H<sub>2</sub>O, pH 7.4, mOsmol 280) containing protease inhibitor cocktail (Sigma, S8830), and subsequently incubated for 1 min. with 200  $\mu$ l Tyrode's solution and supernatant was collected. Cultures were then incubated for 1 min. with 200  $\mu$ l Tyrode's solution containing 60 mM KCl, which replaced NaCl on an equimolar basis in the solution, and supernatant was collected. Mouse BDNF ELISA (Biosensis, BEK-2003) was used according to the manufacturer's instructions and measured with a Spectramax I3 plate reader (Molecular Devices) to quantify BDNF levels in supernatant samples.

### Immunocytochemistry

Hippocampal cultures were fixed in 3.7% formaldehyde (Electron Microscopies Sciences, 15680) in PBS, pH 7.4, for 20 min at RT. After several washing steps with PBS, cells were permeabilized for 5 min with 0.5% Triton X-100 (Fisher Chemical, T/3751/08)-PBS and subsequently incubated for 30 min. with PBS containing 2% normal goat serum (GIBCO, 16210-072) and 0.1% Triton X-100 to block nonspecific binding. Incubations with primary and secondary antibodies were performed for 1 h at RT with PBS washing steps in between. Primary antibodies used were: Polyclonal rabbit Chromogranin B (1:500; SySy 259103), polyclonal chicken MAP2 (1:10,000; Abcam ab5392), monoclonal mouse SMI-312 (1:5000; Covance), polyclonal guinea pig VGLUT1 (1:5000; Millipore AB5905), monoclonal mouse HA (12CA5, 1:500; Roche 11583816001), monoclonal mouse MUNC13-1 (1:1000; SySy 126111), polyclonal guinea pig Synaptophysin1 (1:500; SySy 101004), monoclonal mouse Homer1 (1:500; SySy 160011), monoclonal mouse PSD95 (1:200; Abcam ab2723). Alexa Fluor conjugated secondary antibodies were from Invitrogen (1:1000). Coverslips were washed again and mounted with Mowiol 4-88 (Sigma, 81381) and examined on a confocal A1R microscope (Nikon) with LU4A laser unit using a 40x oil immersion objective (NA = 1.3). Images were acquired at 1024x1024 pixels as z stacks (5 steps of 0.5  $\mu$ m) and resulting maximum projection images were used for analysis. A 60x oil immersion objective (NA 1.4) was used for zooms. Confocal settings were kept constant for all scans within an experiment.

### Electron Microscopy

Hippocampal single cultured RIM cDKO neurons (Cre and control infected) were fixed for 60 min. at room temperature with 2.5% glutaraldehyde in 0.1 M cacodylate buffer (pH 7.4), post-fixed for 1 h at room temperature with 1% OsO<sub>4</sub>/1% K<sub>4</sub>Ru(CN)<sub>6</sub> in double distilled water. Following dehydration through a series of increasing ethanol concentrations, cells were embedded in Epon and polymerized for 24 h at 65°C. After polymerization of the Epon, the coverslip was removed by alternately dipping in liquid nitrogen and hot water. Cells were selected by observing the Epon embedded culture under the light microscope, and mounted on pre-polymerized Epon blocks for thin sectioning. Ultrathin sections (approximately 70nm) were cut parallel to the cell monolayer and collected on single-slot, formvar-coated copper grids, and stained in uranyl acetate and lead citrate.

Synapses were selected at low magnification using a JEOL 1010 electron microscope. All analyses were performed on single ultrathin sections of randomly selected synapses. Digital images of synapses were taken at 80,000x magnification using iTEM software (EMSIS, Germany). For all morphological analyses, we selected only synapses with intact synaptic plasma membranes with a recognizable pre- and postsynaptic density and clear synaptic vesicle membranes. DCVs were recognized as an electron dense core surrounded by a vesicular membrane.

### Live imaging

Live imaging experiments were performed on a Nikon Ti-E Eclipse inverted microscope system fitted with a Confocal A1R (LU4A Laser) unit and an EMCCD camera (Andor DU-897). The inverted microscope together with the EMCCD were used for live imaging using the LU4A laser unit with a 40x oil objective lens (NA 1.3) and appropriate filter sets. NIS elements software (version 4.30) controlled the microscope and image acquisition. Coverslips were placed in an imaging chamber and perfused with Tyrode's solution (119 mM NaCl, 2.5 mM KCl, 2 mM CaCl<sub>2</sub>\*2H<sub>2</sub>O, 2 mM MgCl<sub>2</sub>\*6H<sub>2</sub>O, 25 mM HEPES and 30 mM Glucose\*H<sub>2</sub>O, pH 7.4, mOsmol 280). Isolated single neurons on glial-islands were selected for acquisition and Synapsin-ECFP signal was recorded (z stack, 5 steps of 0.5 $\mu$ m). Time-lapse (2Hz, exposure time dual-color imaging: 80ms per channel, single color imaging: 150 ms) recordings consisted

of 30 s baseline recordings followed by stimulation. Electrical field stimulation was applied through parallel platinum electrodes powered by a stimulus isolator (WPI A385) delivering 30-mA, 1-ms pulses, regulated by a Master-8 pulse generator (A.M.P.I.) providing 16 trains of 50 action potentials (APs) at 50 Hz with a 0.5 s interval. Chemical stimulation of 5  $\mu$ M Ionomycin, (Fisher BioReagent) dissolved in normal Tyrode's solution, was applied through glass capillaries placed in close proximity to the cell by gravity flow. To visualize the total pool of NPY-pHluorin, intracellular pH was neutralized by barrel application of normal Tyrode's solution containing 50 mM NH<sub>4</sub>Cl, which replaced NaCl on an equimolar basis in the solution. To define calcium influx profiles upon stimulation, neurons were incubated for 15 min with 1  $\mu$ M Fluo-5F-AM (Molecular Probes, F14222; stock in DMSO). Co-trafficking experiments with NPY-pHluorin were conducted in the presence of normal Tyrode's solution containing 50 mM NH<sub>4</sub>Cl, to visualize the total pool of NPY-pHluorin during the recording. All experiments were performed at RT (20–24°C). To ensure expression of HA-tagged rescue constructs, coverslips were fixed in 4% PFA-PBS after imaging for immunocytochemistry.

### Imaging analysis

#### Synapse number, DCV poolsize, neuronal morphology

Neuronal morphology and synapse or DCV numbers were analyzed using automated image analysis software synD (Schmitz et al., 2011). Synapse detection settings were optimized to measure VGLUT1, CHGB puncta or NPY-pHluorin signal and kept constant for the corresponding dataset. For co-localization analysis of different markers, morphological masks were drawn using SynD and imported in ImageJ to remove background fluorescence. Co-localization was measured in ImageJ with JACoP. Thresholds were set manually to correct for background.

#### DCV fusion

DCV fusion events were analyzed in stacks of time-lapse recordings (2 Hz, 512x512 pixels). In ImageJ DCV fusion events were manually selected and fluorescent traces were measured in a circular 4x4 pixel ROI (1.56x1.56  $\mu$ m). NPY-pHluorin or BDNF-pHluorin events were defined by a sudden increase in fluorescence, NPY-mCherry events as a sudden decrease in fluorescence. Resulting fluorescent traces were loaded in a custom-built MATLAB plugin where the traces were expressed as fluorescence change ( $\Delta F$ ) compared to initial fluorescence ( $F_0$ ) obtained by averaging the first 10 frames of the time-lapse recording. Fusion events were automatically detected and included when fluorescence showed a sudden increase (NPY-pHluorin/BDNF-pHluorin) or a sudden decrease (NPY-mCherry) two standard deviations above or below  $F_0$ . Start of a fusion event was defined as the first frame above/below 2xSD of  $F_0$  and end of the fusion event as the first frame below this threshold. Total pool measurements were performed in SynD on recordings of NPY-pHluorin after application of 50 mM NH<sub>4</sub>Cl containing Tyrode's solution to neutralize the intracellular pH and defined as the number of NPY-pHluorin puncta. For normalization of cumulative number of DCV fusion events over time, each condition was normalized to 1. The number of DCV fusion events in RAB3 QKO neurons rescued with RAB3A,B,C or D (Figures 1F–1H) was normalized by dividing the number of fusion events by the cumulative average of RAB3 TKO as control. Co-localization of the area of a fusion event with synapsin-ECFP (z stacks) was defined as a synaptic event, remaining events were classified as extra-synaptic events. Using ImageJ software binary images of maximum projections of the z stacks were created and events were defined synaptic if the fluorescent region of the fusion event co-localized with Synapsin-ECFP signal. Immunostainings with a panel of endogenous pre- and post-synaptic markers (Synaptophysin, VGLUT1 and Homer, PSD95, respectively) on neurons expressing Synapsin-ECFP (Figure S2A) were used to quantify co-localization of Synapsin-ECFP with these markers, which showed 90% colocalization with pre-synaptic, and 80% with post-synaptic markers (Figures S2B and S2C).

#### Calcium imaging

Calcium measurements were performed in ImageJ. Maximum projections of Synapsin-ECFP were used to define synaptic and extra-synaptic regions. Five neurite-located ROIs (4x4 pixels) and a background ROI were measured per neuron. Normalized  $\Delta F/F_0$  data was calculated per cell after background subtraction.

#### DCV transport

Transport of DCVs in RIM cDKO neurons and controls was measured in time-lapse recordings (2Hz) consisting of 30 s baseline imaging, 24 s stimulation (16x50AP at 50 Hz) and 30 s imaging after stimulation. Stacks were divided in 20x20 regions (ImageJ, Grid) and transport was measured in three random regions (coordinates generated by random number generation in MATLAB). NPY-mCherry labeled vesicles were manually tracked and vesicle trajectories were obtained using the imageJ plugin MtrackJ. If no vesicles were present in a selected region, the closest region containing DCVs was analyzed. Resulting velocity and distance measurements were analyzed. A vesicle was regarded as moving when the minimum distance between two consecutive frames was 400 nm (1 pixel) or more and if the total distance moved from start was at least 800 nm (2 pixels). Kymographs were created in ImageJ (MultipleKymograph, line width 3) to assess colocalization of NPY-pHluorin and RAB3A-mCherry or RIM1 $\alpha$ -RZ-mCherry. Colocalization was only measured in moving NPY-pHluorin puncta. The soma was always excluded from analysis.

## QUANTIFICATION AND STATISTICAL ANALYSIS

Shapiro-Wilk test was used to assess distribution normality. When assumptions of normality or homogeneity of variances were met, parametric tests were used: Student's t test or one-way ANOVA (Tukey as post hoc test). Otherwise, non-parametric tests used were: Mann-Whitney U-test for 2 independent groups, or Kruskal-Wallis with Dunn's correction for multiple groups. Data are plotted as

mean with standard error of the mean; N represents number of independent experiments, n the number of cells and are indicated in figures and/or figure legends. Detailed information per dataset (average, SEM, n and detailed statistics) is shown in table below.

| Dataset   | Condition                                 | Value<br>(mean ± SEMs) | n <sup>a</sup> | p value   | Statistical test                      |
|---|---|------------------------|----------------|---|---------------------------------------|
| <b>RAB3ABCD: DCV fusion experiments</b>                             |   |                        |                |   |                                       |
| DCV fusion events (#) – NPY<br><a href="#">Figure 1E</a>            | Wild-type                                 | 84.76 ± 16.88          | 5(21)          | **** p < 0.0001   | Mann-Whitney U test                   |
|   | RAB3ABCD <sup>-/-</sup>                   | 4.56 ± 1.22            | 5(32)          |   |                                       |
| Total DCV pool (#)<br><a href="#">Figure S1F</a>                    | Wild-type                                 | 1260 ± 103.5           | 5(21)          | ns <sup>b</sup> , p = 0.1049  | Student's t test                      |
|   | RAB3ABCD <sup>-/-</sup>                   | 1079 ± 57.31           | 5(32)          |   |                                       |
| Spontaneous DCV fusion (#/30 s)<br><a href="#">Figure S1G</a>       | Wild-type                                 | 0.67 ± 0.24            | 5(21)          | ns, p = 0.1783  | Mann-Whitney U test                   |
|   | RAB3ABCD <sup>-/-</sup>                   | 0.28 ± 0.10            | 5(32)          |   |                                       |
| Peak fusion intensity (F/F0)<br><a href="#">Figure S1J</a>          | Wild-type                                 | 1.809 ± 0.01           | 5(1780)        | **** p < 0.0001   | Mann-Whitney U test                   |
|   | RAB3ABCD <sup>-/-</sup>                   | 1.599 ± 0.04           | 5(146)         |   |                                       |
| DCV fusion events (#) – NPY<br><a href="#">Figure 1H (Raw data)</a> | (1) A <sup>+/+</sup> , BCD <sup>-/-</sup> | 427.4 ± 145.4          | 3(14)          | ns, p > 0.05: 1 versus 3, 1 versus 5, 1 versus 6, 2 versus 4, 2 versus 5, 3 versus 6, 4 versus 5, 4 versus 6, 5 versus 6<br>* p < 0.05: 2 versus 3<br>** p < 0.01: 1 versus 2, 3 versus 4<br>***p < 0.001: 1 versus 4                         | Kruskal-Wallis with Dunn's correction |
|   | (2) ABCD <sup>-/-</sup>                   | 26.56 ± 9.65           | 3(16)          |   |                                       |
|   | (3) ABCD <sup>-/-</sup> + RAB3A           | 294.5 ± 142.0          | 3(13)          |   |                                       |
|   | (4) ABCD <sup>-/-</sup> + RAB3B           | 23.80 ± 11.70          | 3(15)          |   |                                       |
|   | (5) ABCD <sup>-/-</sup> + RAB3C           | 185.0 ± 88.13          | 3(14)          |   |                                       |
|   | (6) ABCD <sup>-/-</sup> + RAB3D           | 85.82 ± 51.64          | 3(11)          |   |                                       |
| Normalized DCV fusion events (#)<br><a href="#">Figure 1H</a>       | (1) A <sup>+/+</sup> , BCD <sup>-/-</sup> | 1.00 ± 0.34            | 3(14)          | ns, p > 0.05: 1 versus 3, 1 versus 5, 1 versus 6, 2 versus 4, 2 versus 5, 2 versus 6, 3 versus 5, 3 versus 6, 4 versus 5, 4 versus 6, 5 versus 6<br>* p < 0.05: 2 versus 3<br>** p < 0.01: 1 versus 2, 3 versus 4<br>***p < 0.001: 1 versus 4 | Kruskal-Wallis with Dunn's correction |
|   | (2) ABCD <sup>-/-</sup>                   | 0.06 ± 0.02            | 3(16)          |   |                                       |
|   | (3) ABCD <sup>-/-</sup> + RAB3A           | 0.69 ± 0.33            | 3(13)          |   |                                       |
|   | (4) ABCD <sup>-/-</sup> + RAB3B           | 0.06 ± 0.03            | 3(15)          |   |                                       |
|   | (5) ABCD <sup>-/-</sup> + RAB3C           | 0.43 ± 0.21            | 3(14)          |   |                                       |
|   | (6) ABCD <sup>-/-</sup> + RAB3D           | 0.20 ± 0.12            | 3(11)          |   |                                       |
| Total DCV pool (#)<br><a href="#">Figure S1N</a>                    | (1) A <sup>+/+</sup> , BCD <sup>-/-</sup> | 4441 ± 372.0           | 3(14)          | ns, p > 0.05  | One-way ANOVA                         |
|   | (2) ABCD <sup>-/-</sup>                   | 4377 ± 543.1           | 3(16)          |   |                                       |
|   | (3) ABCD <sup>-/-</sup> + RAB3A           | 4611 ± 521.3           | 3(13)          |   |                                       |
|   | (4) ABCD <sup>-/-</sup> + RAB3B           | 4867 ± 551.5           | 3(15)          |   |                                       |
|   | (5) ABCD <sup>-/-</sup> + RAB3C           | 4456 ± 459.6           | 3(14)          |   |                                       |
|   | (6) ABCD <sup>-/-</sup> + RAB3D           | 4276 ± 686.4           | 3(11)          |   |                                       |
| Spontaneous DCV fusion (#/30 s)<br><a href="#">Figure S1O</a>       | (1) A <sup>+/+</sup> , BCD <sup>-/-</sup> | 4.29 ± 1.91            | 3(14)          | ns, p > 0.05: 1 versus 2, 1 versus 3, 1 versus 4, 1 versus 5, 1 versus 6, 2 versus 4, 2 versus 5, 2 versus 6, 3 versus 5, 4 versus 5, 4 versus 6, 5 versus 6<br>* p < 0.05: 2 versus 3, 3 versus 4, 3 versus 6                                | Kruskal-Wallis with Dunn's correction |
|   | (2) ABCD <sup>-/-</sup>                   | 0.75 ± 0.40            | 3(16)          |   |                                       |
|   | (3) ABCD <sup>-/-</sup> + RAB3A           | 3.23 ± 1.10            | 3(13)          |   |                                       |
|   | (4) ABCD <sup>-/-</sup> + RAB3B           | 0.67 ± 0.32            | 3(15)          |   |                                       |
|   | (5) ABCD <sup>-/-</sup> + RAB3C           | 1.14 ± 0.40            | 3(14)          |   |                                       |
|   | (6) ABCD <sup>-/-</sup> + RAB3D           | 0.55 ± 0.39            | 3(11)          |   |                                       |

(Continued on next page)

## Continued

| Dataset   | Condition   | Value<br>(mean ± SEMs)   | n <sup>a</sup>                   | p value   | Statistical test  |
|---|---|--|----------------------------------|---|---|
| Fluorescent intensity<br>RAB3A–D constructs<br>Figure S1M   | (1) Endogenous RAB3A -<br>synaptic, extra-synaptic  | 0.86 ± 0.08  | 15                               | 1: synaptic versus extra-<br>synaptic: **** p < 0.0001<br>2: synaptic versus extra-<br>synaptic:<br>**** p < 0.0001<br>3: synaptic versus extra-<br>synaptic:<br>**** p < 0.0001<br>4: synaptic versus extra-<br>synaptic:<br>**** p < 0.0001<br>5: synaptic versus extra-<br>synaptic:<br>*** p < 0.0010 | 1+4: Mann-Whitney<br>U test<br>2,3,5: Student's<br>t test |
|   | (2) ABCD <sup>-/-</sup> + RAB3A-<br>synaptic, extra-synaptic  | 1.99 ± 1.76  | 15                               |   |   |
|   | (3) ABCD <sup>-/-</sup> + RAB3B-<br>synaptic, extra-synaptic  | 3.71 ± 0.08  | 15                               |   |   |
|   | (4) ABCD <sup>-/-</sup> + RAB3C-<br>synaptic, extra-synaptic  | 0.38 ± 0.07  | 15                               |   |   |
|   | (5) ABCD <sup>-/-</sup> + RAB3D-<br>synaptic, extra-synaptic  | 2.02 ± 0.23  | 15                               |   |   |
|   |   |  | 0.59 ± 0.14                      |   |   |
|   |   | 1.77 ± 0.16  | 21                               |   |   |
|   |   | 0.58 ± 0.14  | 21                               |   |   |
|   |   | 3.06 ± 0.21  | 21                               |   |   |
|   |   | 1.84 ± 0.27  | 21                               |   |   |
| DCV fusion events (#) –<br>BDNF<br>Figure S1C               | Wild-type<br>RAB3ABCD <sup>-/-</sup>  | 59.85 ± 13.97<br>17.40 ± 4.86                                  | 5(20)<br>5(25)                   | ** p < 0.0054   | Mann-Whitney<br>U test                                    |
| ELISA – BDNF<br>Figure S1D                                  | (1) A+/+, BCD <sup>-/-</sup> ; control<br>(2) A+/+, BCD <sup>-/-</sup> ;<br>stimulation<br>(3) ABCD <sup>-/-</sup> ; control<br>(4) ABCD <sup>-/-</sup> ; stimulation | 21.92 ± 6.17<br>36.81 ± 20.89<br>27.21 ± 11.91<br>21.33 ± 5.99 | 6(12)<br>6(12)<br>6(12)<br>6(12) | ns, p > 0.05  | Kruskal-Wallis with<br>Dunn's correction                  |
| ELISA – (corrected for<br>baseline secretion)<br>Figure S1E | A+/+, BCD <sup>-/-</sup><br>ABCD <sup>-/-</sup>   | 10.84 ± 14.01<br>–5.16 ± 6.33                                  | 6(12)<br>6(12)                   | ns, p > 0.05  | Mann-Whitney<br>U test                                    |
| Pearson's correlation<br>Synapsin/ECFP<br>Figure S2B        | (1) SynECFP::SYP<br>(2) SynECFP::Homer<br>(3) SynECFP::VGLUT1<br>(4) SynECFP::PSD95   | 0.853 ± 0.02<br>0.835 ± 0.02<br>0.628 ± 0.05<br>0.653 ± 0.04   | 1(10)<br>1(10)<br>1(5)<br>1(5)   | ns, p > 0.05: 1 versus 2,<br>3 versus 4   | Mann-Whitney<br>U test                                    |
| Manders' coefficients<br>Figure S2C                         | (1) M1; SynECFP::SYP<br>(2) M1; SynECFP::Homer<br>(3) M1; SynECFP::VGLUT1<br>(4) M1; SynECFP::PSD95   | 0.916 ± 0.02<br>0.758 ± 0.04<br>0.877 ± 0.04<br>0.784 ± 0.06   | 1(10)<br>1(10)<br>1(5)<br>1(5)   | ns, p > 0.05: 3 versus 4<br>**p < 0.0073: 1 versus 2  | Mann-Whitney<br>U test                                    |
| RAB3ABCD: morphological and protein level analysis          |   |  |                                  |   |   |
| Synapse number<br>Figure S2E                                | (1) Wild-type<br>(2) RAB3A <sup>+/+</sup> , BCD <sup>-/-</sup><br>(3) RAB3ABCD <sup>-/-</sup>   | 710.2 ± 58.41<br>655.1 ± 43.65<br>694.0 ± 39.42                | 3(28)<br>4(51)<br>4(54)          | ns, p > 0.05  | Kruskal-Wallis with<br>Dunn's correction                  |
| Dendritic length (mm)<br>Figure S2F                         | (1) Wild-type<br>(2) RAB3A <sup>+/+</sup> , BCD <sup>-/-</sup><br>(3) RAB3ABCD <sup>-/-</sup>   | 2147 ± 132.9<br>2498 ± 119.1<br>2303 ± 105.2                   | 3(28)<br>4(51)<br>4(54)          | ns, p > 0.05  | One-way ANOVA   |
| Synapse number<br>per μm dendrite<br>Figure S2G             | (1) Wild-type<br>(2) RAB3A <sup>+/+</sup> , BCD <sup>-/-</sup><br>(3) RAB3ABCD <sup>-/-</sup>   | 0.32 ± 0.01<br>0.257 ± 0.01<br>0.30 ± 0.01                     | 3(28)<br>4(51)<br>4(54)          | ns, p > 0.05: 1 versus 3<br>* p < 0.05: 2 versus 3<br>** p < 0.01: 1 versus 2   | One-way ANOVA   |
| VGLUT1 intensity (F)<br>Figure S2H                          | (1) Wild-type<br>(2) RAB3A <sup>+/+</sup> , BCD <sup>-/-</sup><br>(3) RAB3ABCD <sup>-/-</sup>   | 2883 ± 123.5<br>2607 ± 99.7<br>2423 ± 114.9                    | 3(28)<br>4(51)<br>4(54)          | ns, p > 0.05  | Kruskal-Wallis with<br>Dunn's correction                  |
| CHGB puncta (#)<br>Figure S2J                               | (1) Wild-type<br>(2) RAB3A <sup>+/+</sup> , BCD <sup>-/-</sup><br>(3) RAB3ABCD <sup>-/-</sup>   | 6358 ± 558.9<br>4286 ± 316.4<br>5909 ± 450.5                   | 3(20)<br>4(53)<br>4(56)          | ns, p > 0.05: 1 versus 3<br>* p < 0.05: 2 versus 3<br>** p < 0.01: 1 versus 2   | Kruskal-Wallis with<br>Dunn's correction                  |

(Continued on next page)



**Continued**

| Dataset  | Condition                                     | Value<br>(mean ± SEMs) | n <sup>a</sup> | p value  | Statistical test                         |
|--|---|------------------------|----------------|--|--|
| Neurite length (mm)<br>Figure S2K                | (1) Wild-type                                 | 12598 ± 1328           | 3(20)          | ns, p > 0.05: 1 versus 2,<br>1 versus 3<br>* p < 0.05: 2 versus 3  | Kruskal-Wallis with<br>Dunn's correction |
|  | (2) RAB3A <sup>+/-</sup> , BCD <sup>-/-</sup> | 9919 ± 705.1           | 4(53)          |  |  |
|  | (3) RAB3ABCD <sup>-/-</sup>                   | 13012 ± 841.4          | 4(56)          |  |  |
| CHGB puncta per μm<br>neurite<br>Figure S2L      | (1) Wild-type                                 | 0.54 ± 0.03            | 3(20)          | ns, p > 0.05: 1 versus 3,<br>2 versus 3<br>* p < 0.05: 1 versus 2  | One-way ANOVA                            |
|  | (2) RAB3A <sup>+/-</sup> , BCD <sup>-/-</sup> | 0.46 ± 0.02            | 4(53)          |  |  |
|  | (3) RAB3ABCD <sup>-/-</sup>                   | 0.46 ± 0.02            | 4(56)          |  |  |
| CHGB intensity (F)<br>Figure S2M                 | (1) Wild-type                                 | 2172 ± 162.2           | 3(20)          | ns, p > 0.05: 1 versus 2<br>*** p < 0.001: 1 versus 3,<br>2 versus 3   | One-way ANOVA                            |
|  | (2) RAB3A <sup>+/-</sup> , BCD <sup>-/-</sup> | 2043 ± 112.0           | 4(53)          |  |  |
|  | (3) RAB3ABCD <sup>-/-</sup>                   | 947.6 ± 42.83          | 4(56)          |  |  |
| ChgB levels<br>(westernblot)<br>Figure S2N       | (1) Wild-type                                 | 1.0 ± 0.0              | 5              | ns, p = 0.5231   | Kruskal-Wallis with<br>Dunn's correction |
|  | (2) RAB3A <sup>+/-</sup> , BCD <sup>-/-</sup> | 1.74 ± 0.6             | 5              |  |  |
|  | (3) RAB3A <sup>+/-</sup> , BCD <sup>-/-</sup> | 1.42 ± 0.4             | 5              |  |  |
|  | (4) RAB3ABCD <sup>-/-</sup>                   | 1.01 ± 0.2             | 5              |  |  |
| RIM 1/2: DCV fusion experiments                  |   |                        |                |  |  |
| DCV fusion events (#) –<br>NPY<br>Figure 2E      | Control                                       | 25.8 ± 6.2             | 4(14)          | ***p < 0.0002  | Mann-Whitney<br>U test                   |
|  | RIM cDKO                                      | 0.9 ± 0.3              | 4(17)          |  |  |
| NPY-pHluorin DCV<br>fusion events<br>Figure S3G  | Control                                       | 13.9 ± 4.4             | 4(14)          | **** p = < 0.0001  | Mann-Whitney<br>U test                   |
|  | RIM cDKO                                      | 0.06 ± 0.06            | 4(17)          |  |  |
| Total DCV pool (#)<br>Figure S3H                 | Control                                       | 1300 ± 138.6           | 4(14)          | ns, p = 0.9551   | Student's t test                         |
|  | RIM cDKO                                      | 1309 ± 92.12           | 4(17)          |  |  |
| Spontaneous DCV<br>fusion (#/30 s)<br>Figure S3I | Control                                       | 0.50 ± 0.17            | 4(14)          | ns, p = 0.0508   | Mann-Whitney<br>U test                   |
|  | RIM cDKO                                      | 0.12 ± 0.08            | 4(17)          |  |  |
| DCV fusion events (#) –<br>BDNF<br>Figure S3L    | Control                                       | 75.68 ± 12.68          | 3(31)          | ****p < 0.0001   | Mann-Whitney<br>U test                   |
|  | RIM cDKO                                      | 4.39 ± 1.30            | 3(28)          |  |  |
| DCV fusion events (#)<br>Figure 3D               | (1) Control                                   | 99.6 ± 31.1            | 4(19)          | ns, p > 0.05: 1 versus 3,<br>1 versus 4, 1 versus 5,<br>2 versus 6, 3 versus 4,<br>3 versus 5, 4 versus 5,<br>4 versus 6, 5 versus 6<br>*p < 0.05: 1 versus 6,<br>3 versus 6<br>**p < 0.01: 2 versus 4,<br>2 versus 5<br>***p < 0.001: 1 versus 2,<br>2 versus 3 | Kruskal-Wallis with<br>Dunn's correction |
|  | (2) DKO                                       | 0.4 ± 0.2              | 4(25)          |  |  |
|  | (3) cDKO+RIM1α                                | 83.3 ± 22.8            | 4(14)          |  |  |
|  | (4) cDKO + RIM1β                              | 26.4 ± 9.4             | 3(17)          |  |  |
|  | (5) cDKO + RIM1α-<br>ΔPDZ                     | 56.2 ± 28.8            | 3(13)          |  |  |
|  | (6) cDKO + RIM1α-<br>K144/6E                  | 9.6 ± 4.6              | 3(16)          |  |  |
| Total DCV pool (#)<br>Figure S6J                 | (1) Control                                   | 778.7 ± 66.63          | 4(19)          | ns, p > 0.05   | Kruskal-Wallis with<br>Dunn's correction |
|  | (2) cDKO                                      | 754.3 ± 76.81          | 4(25)          |  |  |
|  | (3) cDKO+RIM1α                                | 917.6 ± 104.6          | 4(14)          |  |  |
|  | (4) cDKO + RIM1β                              | 1045 ± 92.52           | 3(17)          |  |  |
|  | (5) cDKO + RIM1α-<br>ΔPDZ                     | 1031 ± 98.1            | 3(13)          |  |  |
|  | (6) cDKO + RIM1α-<br>K144/6E                  | 819.5 ± 66.57          | 3(16)          |  |  |

(Continued on next page)

## Continued

| Dataset  | Condition  | Value<br>(mean ± SEMs) | n <sup>a</sup> | p value   | Statistical test                                 |
|--|--|------------------------|----------------|---|--|
| Fluorescent intensity<br>RIM constructs<br>Figure S6H      | (1) cDKO+RIM1 $\alpha$ :<br>synaptic, extra-synaptic                 | 2.65 ± 0.14            | 24             | 1: synaptic versus extra-synaptic: **** p < 0.0001<br>2: synaptic versus extra-synaptic:<br>**** p < 0.0001<br>3: synaptic versus extra-synaptic:<br>**** p < 0.0001<br>4: synaptic versus extra-synaptic:<br>**** p < 0.0001   | Mann-Whitney<br>U test                           |
|  | (2) cDKO + RIM1 $\beta$ :<br>synaptic, extra-synaptic                | 1.72 ± 0.10            | 21             |   |  |
|  | (3) cDKO + RIM1 $\alpha$ - $\Delta$ PDZ:<br>synaptic, extra-synaptic | 0.16 ± 0.06            | 21             |   |  |
|  | (4) cDKO + RIM1 $\alpha$ -<br>K144/6E:<br>synaptic, extra-synaptic   | 2.32 ± 0.20            | 18             |   |  |
|  |  | 0.16 ± 0.06            | 18             |   |  |
| DCV fusion events (#)<br>Figure 3I                         | Control (5 $\mu$ M Ionomycin)  | 60.0 ± 18.6            | 4(8)           | *** p = < 0.0007  | Mann-Whitney<br>U test                           |
|  | RIM cDKO (5 $\mu$ M Ionomycin)                                       | 2.13 ± 1.63            | 4(8)           |   |  |
| Total DCV pool (#)<br>Figure S6M                           | Control (5 $\mu$ M Ionomycin)  | 611.9 ± 74.72          | 4(8)           | ns, p = 0.3229  | Student's t test                                 |
|  | RIM cDKO (5 $\mu$ M Ionomycin)                                       | 696.5 ± 35.2           | 4(8)           |   |  |
| DCV fusion events (#)<br>Figure 4E                         | (1) Control  | 65.3 ± 18.4            | 3(12)          | ns, p > 0.05: 1 versus 3,<br>1 versus 4, 1 versus 5,<br>2 versus 5, 3 versus 4,<br>3 versus 5, 4 versus 5<br>*p < 0.05: 2 versus 4<br>** p < 0.01: 2 versus 3<br>*** p < 0.001: 1 versus 2  | Kruskal-Wallis with<br>Dunn's correction         |
|  | (2) cDKO   | 0.13 ± 0.1             | 3(15)          |   |  |
|  | (3) cDKO + RIM1 $\alpha$   | 35 ± 11.2              | 3(8)           |   |  |
|  | (4) cDKO+ Munc13-2 (WT)  | 26.7 ± 12.6            | 3(7)           |   |  |
|  | (5) cDKO + Munc13-2-( $\Delta$ N)                                    | 12.9 ± 7.6             | 3(10)          |   |  |
| Total DCV pool (#)<br>Figure S7C                           | (1) Control  | 842.3 ± 118.0          | 3(12)          | ns, p > 0.05  | Kruskal-Wallis with<br>Dunn's correction         |
|  | (2) cDKO   | 658.5 ± 65.44          | 3(15)          |   |  |
|  | (3) cDKO + RIM1 $\alpha$   | 690.0 ± 93.0           | 3(8)           |   |  |
|  | (4) cDKO+ Munc13-2 (WT)  | 846.6 ± 160.3          | 3(7)           |   |  |
|  | (5) cDKO + Munc13-2-( $\Delta$ N)                                    | 617.1 ± 88.0           | 3(10)          |   |  |
| Fluorescent intensity<br>MUNC13-2 constructs<br>Figure S7A | (1) cDKO+ Munc13-2 (WT):<br>Synaptic,                                | 2.50 ± 0.42            | 18             | 1: ns, p = 0.0556<br>2: ns, p = 0.1060  | 1: Mann-Whitney<br>U test<br>2: Student's t test |
|  | Extra-synaptic (2) cDKO +<br>Munc13-2-( $\Delta$ N)                  | 1.59 ± 0.31            | 18             |   |  |
|  | Synaptic,<br>Extra-synaptic  | 1.40 ± 0.18            | 21             |   |  |
|  |  | 1.07 ± 0.09            | 21             |   |  |
| DCV fusion events (#)<br>Figure 5D                         | (1) Control  | 92.1 ± 34.4            | 3(12)          | ns, p > 0.05: 1 versus 3,<br>1 versus 4, 2 versus 4,<br>2 versus 5, 2 versus 6,<br>2 versus 7, 3 versus 4,<br>3 versus 7, 4 versus 5,<br>4 versus 6, 4 versus 7,<br>5 versus 6, 5 versus 7,<br>6 versus 7<br>*p < 0.05: 1 versus 7<br>** p < 0.01: 1 versus 5,<br>3 versus 5<br>*** p < 0.001: 1 versus 2,<br>1 versus 6, 2 versus 3,<br>3 versus 6 | Kruskal-Wallis with<br>Dunn's correction         |
|  | (2) cDKO   | 0.8 ± 0.2              | 3(17)          |   |  |
|  | (3) cDKO+ RIM1 $\alpha$  | 96.9 ± 30.8            | 3(17)          |   |  |
|  | (4) cDKO+ RIM1 $\alpha$ -RZ  | 57.7 ± 20.1            | 3(15)          |   |  |
|  | (5) cDKO+ RIM1 $\beta$ -Z  | 15.3 ± 8.6             | 3(12)          |   |  |
|  | (6) cDKO+ RIM1 $\alpha$ -<br>RZ-K144/6E                              | 0.7 ± 0.4              | 3(10)          |   |  |
|  | (7) cDKO + RIM1 $\beta$ -<br>Z-K144/6E                               | 7.8 ± 4.0              | 3(11)          |   |  |

(Continued on next page)

## Continued

| Dataset  | Condition  | Value<br>(mean ± SEMs)   | n <sup>a</sup>  | p value   | Statistical test  |
|--|--|--|---|---|---|
| Total DCV pool (#)<br>Figure S7H                             | (1) Control<br>(2) cDKO<br>(3) cDKO+ RIM1 $\alpha$<br>(4) cDKO+ RIM1 $\alpha$ -RZ<br>(5) cDKO+ RIM1 $\beta$ -Z<br>(6) cDKO+ RIM1 $\alpha$ -RZ-K144/6E<br>(7) cDKO + RIM1 $\beta$ -Z-K144/6E  | 741.5 ± 108.7<br>483.9 ± 31.96<br>940.6 ± 78.39<br>695.1 ± 82.00<br>766.3 ± 72.39<br>774.3 ± 79.76<br>738.5 ± 68.68                                | 3(12)<br>3(17)<br>3(17)<br>3(15)<br>3(12)<br>3(10)<br>3(11) | ns, p > 0.05: 1 versus 2,<br>1 versus 3, 1 versus 4,<br>1 versus 5, 1 versus 6,<br>1 versus 7, 2 versus 4,<br>2 versus 5, 2 versus 6,<br>2 versus 7, 3 versus 4,<br>3 versus 6, 3 versus 7,<br>4 versus 5, 4 versus 6,<br>4 versus 7, 5 versus 6,<br>5 versus 7, 6 versus 7<br>*p < 0.05: 3 versus 5<br>*** p < 0.001: 2 versus 3 | Kruskal-Wallis with<br>Dunn's correction                      |
| Fluorescent intensity<br>RIM constructs<br>Figure S7F        | (1) cDKO+ RIM1 $\alpha$ : synaptic,<br>extra-synaptic<br>(2) cDKO+ RIM1 $\alpha$ -RZ:<br>synaptic, extra-synaptic<br>(3) cDKO+ RIM1 $\alpha$ -RZ-<br>K144/6E:<br>synaptic, extra-synaptic<br>(4) cDKO+ RIM1 $\beta$ -Z:<br>synaptic, extra-synaptic<br>(5) cDKO + RIM1 $\beta$ -Z-<br>K144/6E: synaptic,<br>extra-synaptic | 1.20 ± 0.23<br>0.32 ± 0.12<br>2.00 ± 0.25<br>0.37 ± 0.12<br>1.05 ± 0.11<br>0.44 ± 0.09<br>1.81 ± 0.42<br>0.44 ± 0.08<br>1.09 ± 0.21<br>0.61 ± 0.13 | 18<br>18<br>18<br>18<br>18<br>6<br>6<br>15<br>15            | 1: synaptic versus extra-<br>synaptic: *** p < 0.0002<br>2: synaptic versus extra-<br>synaptic:<br>**** p < 0.0001<br>3: synaptic versus extra-<br>synaptic:<br>*** p < 0.0001<br>4: synaptic versus extra-<br>synaptic:<br>** p = 0.0043<br>5: synaptic versus extra-<br>synaptic: ns, p = 0.060                                 | 1, 2, 4: Mann-<br>Whitney U test<br>3, 5: Student's<br>t test |
| DCV fusion events (#)<br>Figure S6D                          | (1) Control<br>(2) RIM1 <sup>+/+</sup> RIM2 <sup>-/-</sup><br>(3) RIM1 <sup>+/-</sup> RIM2 <sup>-/-</sup><br>(4) RIM1 <sup>-/-</sup> RIM2 <sup>+/+</sup><br>(5) RIM1 <sup>-/-</sup> RIM2 <sup>+/-</sup>  | 63.67 ± 14.84<br>63.33 ± 16.34<br>10.60 ± 5.57<br>15.67 ± 9.17<br>18.11 ± 8.25   | 3(15)<br>3(18)<br>1(5)<br>1(3)<br>3(18)                     | ns, p > 0.05: 1 versus 2,<br>1 versus 3, 1 versus 4,<br>2 versus 3, 2 versus 4,<br>3 versus 4, 3 versus 5,<br>4 versus 5<br>*p < 0.05: 2 versus 5<br>**p < 0.01: 1 versus 5   | Kruskal-Wallis with<br>Dunn's correction                      |
| Total DCV pool (#)<br>Figure S6E                             | (1) Control<br>(2) RIM1 <sup>+/+</sup> RIM2 <sup>-/-</sup><br>(3) RIM1 <sup>+/-</sup> RIM2 <sup>-/-</sup><br>(4) RIM1 <sup>-/-</sup> RIM2 <sup>+/+</sup><br>(5) RIM1 <sup>-/-</sup> RIM2 <sup>+/-</sup>  | 577.9 ± 62.12<br>662.4 ± 69.94<br>671.4 ± 95.21<br>864.0 ± 185.3<br>716.1 ± 68.71  | 3(15)<br>3(18)<br>1(5)<br>1(3)<br>3(18)                     | ns, p > 0.05  | Kruskal-Wallis with<br>Dunn's correction                      |
| Spontaneous DCV<br>fusion (#/30 s)<br>Figure S6F             | (1) Control<br>(2) RIM1 <sup>+/+</sup> RIM2 <sup>-/-</sup><br>(3) RIM1 <sup>+/-</sup> RIM2 <sup>-/-</sup><br>(4) RIM1 <sup>-/-</sup> RIM2 <sup>+/+</sup><br>(5) RIM1 <sup>-/-</sup> RIM2 <sup>+/-</sup>  | 0.53 ± 0.24<br>0.61 ± 0.23<br>0.0 ± 0.0<br>0.0 ± 0.0<br>1.17 ± 0.69  | 3(15)<br>3(18)<br>1(5)<br>1(3)<br>3(18)                     | ns, p > 0.5027  | Kruskal-Wallis with<br>Dunn's correction                      |
| DCV fusion events (#) -<br>Cre at DIV 5<br>Figure S5O        | Control<br>RIM cDKO  | 58.6 ± 20.91<br>1.92 ± 0.50  | 2(5)<br>3(12)   | ** p < 0.01   | Mann-Whitney<br>U test  |
| DCV fusion events (#)<br>Wild-type Cre/control<br>Figure S5R | Wild-type + control<br>Wild-type + Cre   | 17.83 ± 3.71<br>31.14 ± 17.85  | 1(6)<br>1(7)  | ns, p = 0.667   | Mann-Whitney<br>U test  |
| RIM 1/2: DCV transport                                       |  |  |   |   |   |
| Co-trafficking NPY +<br>RIM1 $\alpha$ -RZ (%)<br>Figure 6D   | RIM cDKO<br>RAB3ABCD <sup>-/-</sup>  | 32.92 ± 4.40<br>11.53 ± 2.88   | 1(14)<br>1(15)  | ** p = 0.0011   | Mann-Whitney<br>U test  |
| Average velocity ( $\mu$ m/s)<br>Figure S5D                  | Control<br>RIM cDKO  | 0.343 ± 0.03<br>0.38 ± 0.03  | 6(18)<br>6(19)  | ns, p = 0.438   | Mann-Whitney<br>U test  |

(Continued on next page)

**Continued**

| Dataset   | Condition                         | Value<br>(mean $\pm$ SEMs) | n <sup>a</sup> | p value  | Statistical test       |  |
|---|-----------------------------------|----------------------------|----------------|--|------------------------|--|
| Velocity ( $\mu\text{m/s}$ )<br>Figure S5E              | (1) Control – before stimulation  | 0.397 $\pm$ 0.039          | 6(18)          | ns, p = 0.2424 (1 versus 2)<br>ns, p = 0.1991 (3 versus 4) | Mann-Whitney<br>U test |  |
|   | (2) RIM cDKO – before stimulation | 0.466 $\pm$ 0.042          | 6(19)          |  |                        |  |
|   | (3) Control – during stimulation  | 0.302 $\pm$ 0.035          | 6(18)          | ns, p = 0.6050 (5 versus 6)                                |                        |  |
|   | (4) RIM cDKO – during stimulation | 0.375 $\pm$ 0.039          | 6(19)          |  |                        |  |
|   | (5) Control – after stimulation   | 0.329 $\pm$ 0.037          | 6(18)          |  |                        |  |
|   | (6) RIM cDKO – after stimulation  | 0.298 $\pm$ 0.034          | 6(19)          |  |                        |  |
| Distance ( $\mu\text{m}$ )<br>Figure S5G                | Control                           | 2.55 $\pm$ 0.34            | 6(18)          | ns, p = 0.502  | Mann-Whitney<br>U test |  |
|   | RIM cDKO                          | 2.28 $\pm$ 0.28            | 6(19)          |  |                        |  |
| RIM 1/2: morphology, protein level and EM analysis      |                                   |                            |                |  |                        |  |
| Synapse number<br>Figure S4B                            | Control                           | 670.1 $\pm$ 47.37          | 5(59)          | ** p = 0.0015  | Mann-Whitney<br>U test |  |
|   | RIM cDKO                          | 486.9 $\pm$ 24.78          | 5(93)          |  |                        |  |
| Dendritic length (mm)<br>Figure S4C                     | Control                           | 2.343 $\pm$ 0.129          | 5(59)          | ** p = 0.0024  | Student's t test       |  |
|   | RIM cDKO                          | 1.905 $\pm$ 0.078          | 5(93)          |  |                        |  |
| Synapse number per $\mu\text{m}$ dendrite<br>Figure S4D | Control                           | 0.278 $\pm$ 0.01           | 5(59)          | * p = 0.0172   | Student's t test       |  |
|   | RIM cDKO                          | 0.25 $\pm$ 0.01            | 5(93)          |  |                        |  |
| Synapse area ( $\mu\text{m}^2$ )<br>Figure S4E          | Control                           | 1.470 $\pm$ 0.05           | 5(59)          | ns, p = 0.46   | Mann-Whitney<br>U test |  |
|   | RIM cDKO                          | 1.392 $\pm$ 0.02           | 5(93)          |  |                        |  |
| VGLUT1 intensity (F)<br>Figure S4F                      | Control                           | 2.955 $\pm$ 0.087          | 5(59)          | * p = 0.233  | Mann-Whitney<br>U test |  |
|   | RIM cDKO                          | 2.758 $\pm$ 0.067          | 5(93)          |  |                        |  |
| MUNC13 intensity (F)<br>Figure S4G                      | Control                           | 1.921 $\pm$ 0.170          | 2(20)          | ** p = 0.007   | Student's t test       |  |
|   | RIM cDKO                          | 1.266 $\pm$ 0.150          | 2(19)          |  |                        |  |
| CHGB puncta (#)<br>Figure S4H                           | Control                           | 2442 $\pm$ 184.6           | 4(50)          | ns, p = 0.50   | Mann-Whitney<br>U test |  |
|   | RIM cDKO                          | 2322 $\pm$ 175.8           | 4(47)          |  |                        |  |
| Neurite length (mm)<br>Figure S4I                       | Control                           | 5.80 $\pm$ 0.34            | 4(50)          | ns, p = 0.25   | Mann-Whitney<br>U test |  |
|   | RIM cDKO                          | 5.28 $\pm$ 0.34            | 4(47)          |  |                        |  |
| CHGB puncta per $\mu\text{m}$ neurite<br>Figure S4J     | Control                           | 0.422 $\pm$ 0.02           | 4(50)          | ns, p = 0.23   | Student's t test       |  |
|   | RIM cDKO                          | 0.453 $\pm$ 0.02           | 4(47)          |  |                        |  |
| CHGB intensity (F)<br>Figure S4K                        | Control                           | 1.329 $\pm$ 0.105          | 4(50)          | ns, p = 0.44   | Student's t test       |  |
|   | RIM cDKO                          | 1.221 $\pm$ 0.092          | 4(47)          |  |                        |  |
| Pearson's correlation VGLUT1::CHGB<br>Figure S4M        | Control                           | 0.631 $\pm$ 0.02           | 3(28)          | * p < 0.025  | Mann-Whitney<br>U test |  |
|   | RIM cDKO                          | 0.694 $\pm$ 0.02           | 3(27)          |  |                        |  |
| Manders' coefficients<br>Figure S4N                     | Control (M1: VGLUT1::CHGB)        | 0.678 $\pm$ 0.03           | 3(28)          | ns, p > 0.05   | Student's t test       |  |
|   | RIM cDKO (M1: VGLUT1::CHGB)       | 0.731 $\pm$ 0.03           | 3(27)          |  |                        |  |
|   | Control (M2: CHGB::VGLUT1)        | 0.516 $\pm$ 0.03           | 3(28)          |  |                        |  |
|   | RIM cDKO (M2: CHGB::VGLUT1)       | 0.571 $\pm$ 0.03           | 3(27)          |  |                        |  |
|   |                                   |                            |                |  |                        |  |
|   |                                   |                            |                |  |                        |  |
| DCVs per synapse section<br>Figure S4P                  | Control                           | 1.58 $\pm$ 0.19            | 3(60 synapses) | ns, p = 0.0571   | Mann-Whitney<br>U test |  |
|   | RIM cDKO                          | 2.38 $\pm$ 0.32            | 3(42 synapses) |  |                        |  |

(Continued on next page)

**Continued**

| Dataset  | Condition          | Value<br>(mean ± SEMs) | n <sup>a</sup> | p value   | Statistical test                         |
|--|--------------------|------------------------|----------------|---|--|
| Synapse number -<br>Cre at DIV 5<br><a href="#">Figure S5I</a>                 | Control            | 386.3 ± 60.56          | 3(25)          | ns, p = 0.67  | Mann-Whitney<br>U test                   |
|  | RIM cDKO           | 370.8 ± 62.24          | 3(23)          |   |  |
| Dendritic length (mm) -<br>Cre at DIV 5<br><a href="#">Figure S5J</a>          | Control            | 1718 ± 167.0           | 3(25)          | ns, p = 0.92  | Mann-Whitney<br>U test                   |
|  | RIM cDKO           | 1788 ± 191.9           | 3(23)          |   |  |
| Synapse number per μm<br>dendrite - Cre at DIV 5<br><a href="#">Figure S5K</a> | Control            | 0.204 ± 0.02           | 3(25)          | ns, p = 0.457   | Student's t test                         |
|  | RIM cDKO           | 0.187 ± 0.02           | 3(23)          |   |  |
| VGLUT1 intensity (F)-<br>Cre at DIV 5<br><a href="#">Figure S5L</a>            | Control            | 2.08 ± 0.185           | 3(25)          | ns, p = 0.7432  | Student's t test                         |
|  | RIM cDKO           | 2.00 ± 0.14            | 3(23)          |   |  |
| Manders' coefficients<br><a href="#">Figure S8D</a>                            | (1) MUNC13::VGLUT1 | 0.803 ± 0.03           | 8              | * p < 0.05: 1 versus<br>2 ns, p > 0.05: 1<br>versus 3, 2 versus 3 | Kruskal-Wallis with<br>Dunn's correction |
|  | (2) CHGB::MUNC13   | 0.657 ± 0.04           | 8              |   |  |
|  | (3) CHGB::VGLUT1   | 0.688 ± 0.04           | 8              |   |  |

<sup>a</sup>n = number of experiments (cells); unless otherwise indicated

<sup>b</sup>ns = non-significant

**DATA AND CODE AVAILABILITY**

The data that support the findings of this study are available from the Lead Contact upon reasonable request.

**Neuron, Volume 104**

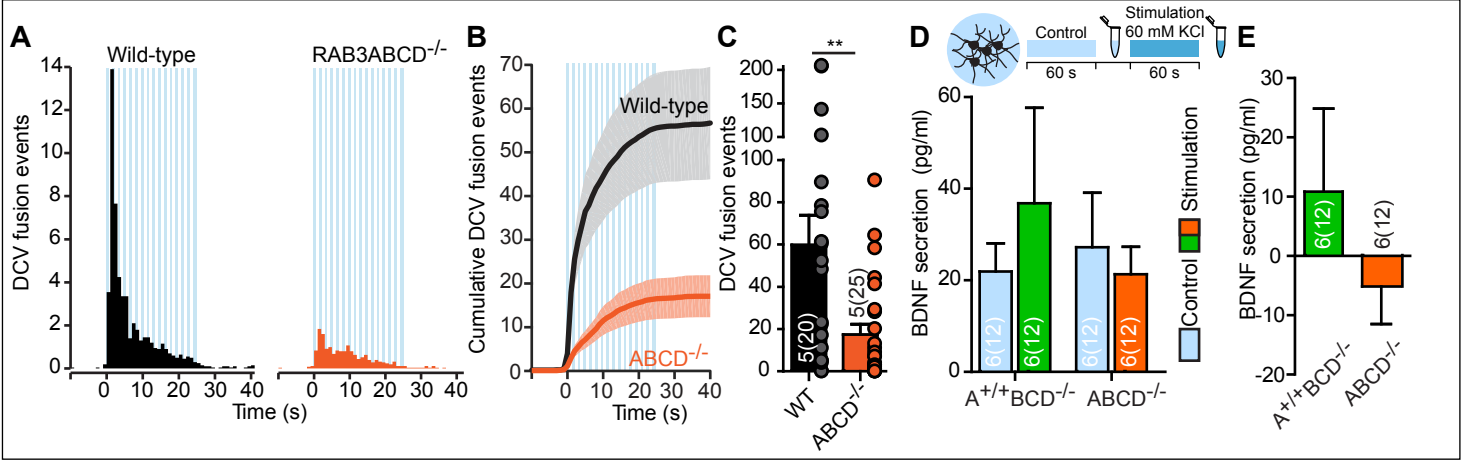
**Supplemental Information**

**The RAB3-RIM Pathway Is Essential  
for the Release of Neuromodulators**

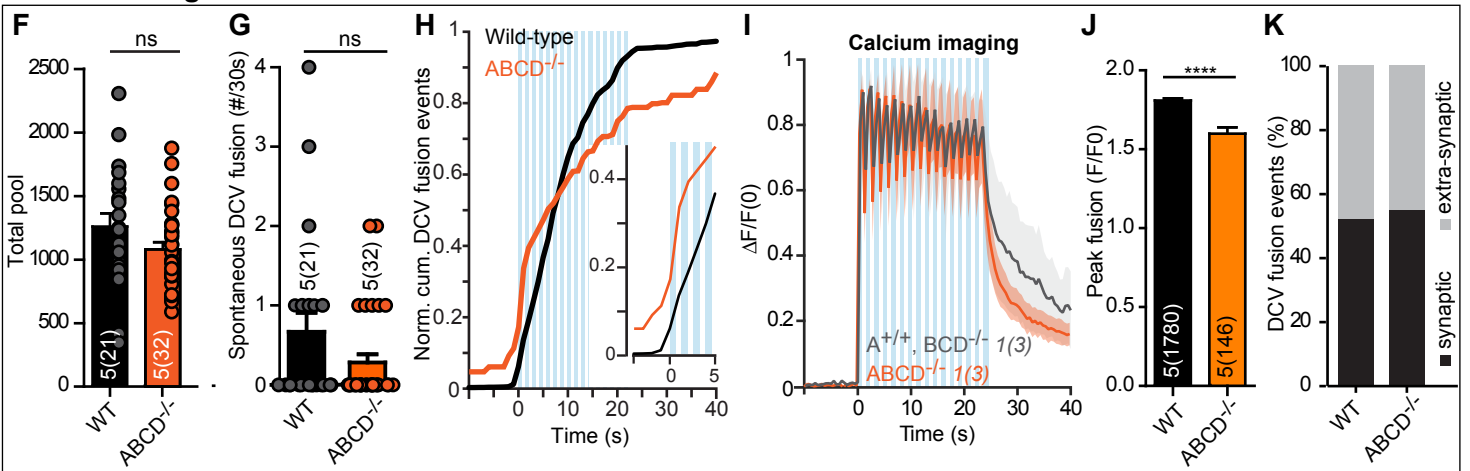
**Claudia M. Persoon, Rein I. Hoogstraaten, Joris P. Nassal, Jan R.T. van Weering, Pascal S. Kaeser, Ruud F. Toonen, and Matthijs Verhage**

**Figure S1 - Related to Figure 1**

**BDNF-pHluorin**



**Related to Figure 1 C-E**



**Related to Figure 1 F-H**

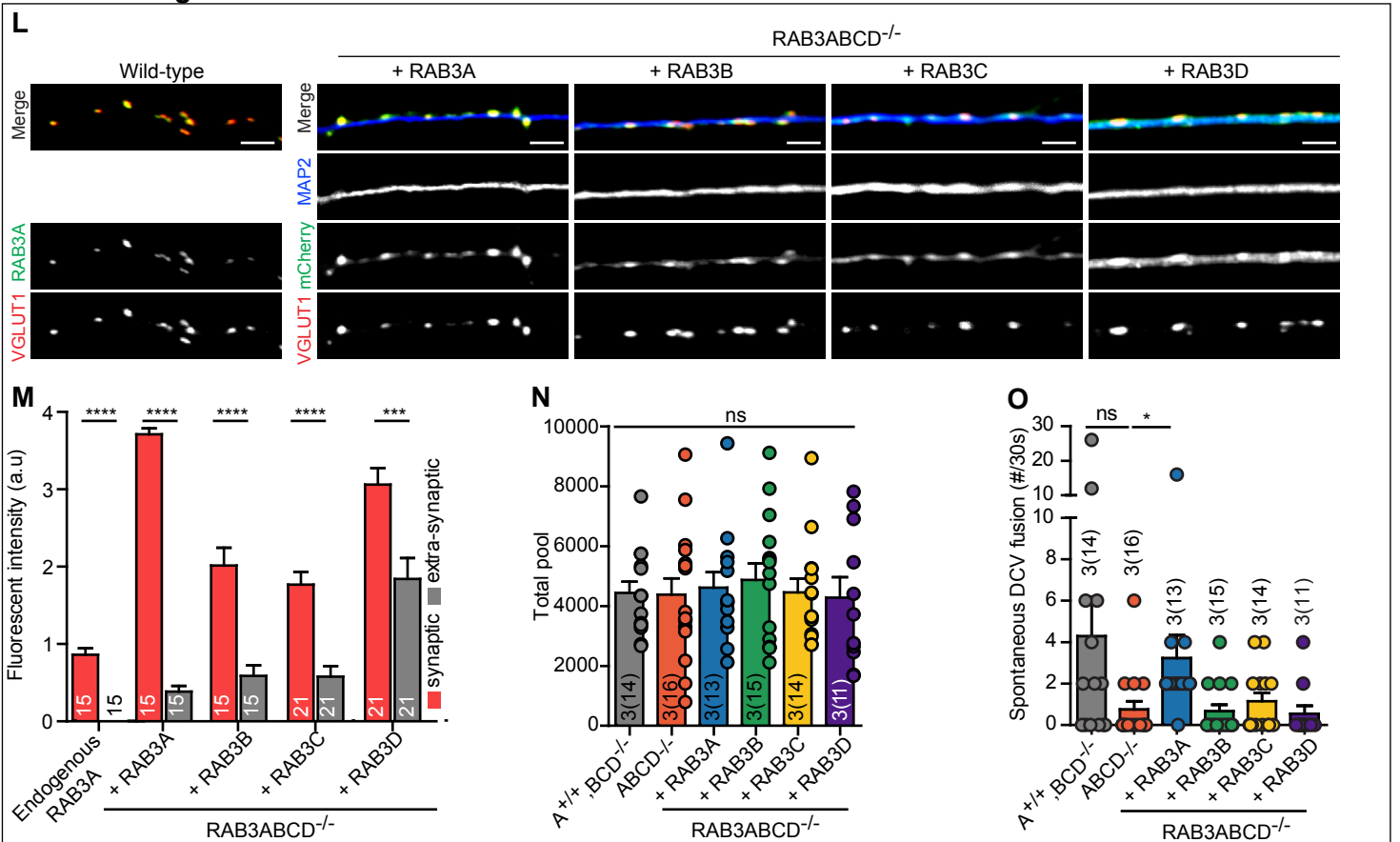


## Figure S1 (related to Figure 1) RAB3 deletion impairs secretion of neuropeptides

(A-C) DCV fusion analysis using BDNF-pHluorin in single isolated hippocampal neurons derived from Wild-type or RAB3ABCD<sup>-/-</sup> mice.

(A) Histograms of DCV fusion events per cell for wild-type or RAB3ABCD<sup>-/-</sup> neurons.

(B) Cumulative plot of DCV fusion events per cell.

(C) Summary graph of DCV fusion events per cell. Mann-Whitney U test: \*\*  $p < 0.005$ .

(D-E) Endogenous BDNF secretion upon stimulation with 60 mM KCl containing Tyrode's buffer from mass cultures of RAB3A<sup>+/+</sup>BCD<sup>-/-</sup> (Control) or RAB3ABCD<sup>-/-</sup> mice measured by ELISA. *Evoked BDNF release was detected in control neurons, but not in RAB3ABCD<sup>-/-</sup> neurons. Please note, this assay shows poor resolution, poor sensitivity and high background. Only 3-5% binding was obtained under our experimental conditions. ELISAs do not have the resolution that our pHluorin-based assays have.*

(D) Schematic representation of experimental design (above). Mass cultured neurons (DIV 8), derived from cortex of RAB3A<sup>+/+</sup>BCD<sup>-/-</sup> or RAB3ABCD<sup>-/-</sup> mice, were incubated for 60 seconds with normal Tyrode's solution and supernatant was collected (Control). 60 seconds incubation with Tyrode's buffer containing 60 mM KCl followed to stimulate DCV fusion and supernatant was collected (60 mM KCl). BDNF levels (pg/ml) were measured in supernatant samples (below). Kruskal-Wallis with Dunn's correction, non-significant,  $p > 0.05$ .

(E) BDNF secretion (pg/ml) from RAB3A<sup>+/+</sup>BCD<sup>-/-</sup> or RAB3ABCD<sup>-/-</sup> mass cultures normalized for control levels of BDNF (D). Mann-Whitney U test, non-significant,  $p > 0.05$ .

### (F-K) Related to Figure 1 C-E

(F) Total number of DCVs (total pool) of neurons, measured as number of NPY-pHluorin puncta upon application of 50 mM NH<sub>4</sub>Cl containing Tyrode's solution to visualize the total number of DCVs. Student's t-test: ns = non-significant,  $p = 0.1049$ .

(G) Summary plot of spontaneous DCV fusion events during 30 seconds baseline recording of neurons in figure 1F. Mann-Whitney U test: ns = non-significant,  $p = 0.1783$ .

(H) Normalized cumulative plot of DCV fusion events per cell. Inset shows normalized cumulative plot of DCV fusion events per cell in first 5 seconds of stimulation.

(I)  $\Delta F/F_0$  trace of rise in intracellular calcium (Fluo5-AM) upon repetitive electrical stimulation in RAB3 TKO (A<sup>+/+</sup>, BCD<sup>-/-</sup>) and RAB3 QKO (ABCD<sup>-/-</sup>) neurons. Traces are corrected for baseline (first 10 frames) and normalized.

(J) Fluorescence intensity (F/F<sub>0</sub>) of single DCV fusion events in WT and ABCD<sup>-/-</sup> neurons. Mann-Whitney U test: \*\*\*\*  $p < 0.0001$ .

(K) Percentage of DCV fusion events at synaptic (black) or extra-synaptic (grey) regions.

### (L-O) Related to Figure 1 F-H

(L) Left panels show WT neurite immunostained for RAB3A (green) and VGLUT1 (red). Right panels show MAP2 labeled dendrites with VGLUT1 marked synapses and mCherry signal of the RAB rescue constructs in RAB3ABCD<sup>-/-</sup> neurons. Scale bars: 5  $\mu$ m.

(M) Summary data of fluorescence intensity of endogenous RAB3A and mCherry-labeled RAB3 rescue constructs at VGLUT1 positive synapses (red bars, synaptic) or at extra-synaptic sites (grey bars, extra-synaptic) along MAP2 labeled dendrites. Mann-Whitney U test \*\*\*  $p < 0.001$ , \*\*\*\*  $p < 0.0001$ .



(N) Total number of DCVs (total pool) of neurons analyzed in Figure 1 F-H, measured as number of NPY-pHluorin puncta upon application of 50 mM NH<sub>4</sub>Cl containing Tyrode's solution to visualize the total number of DCVs. One-way ANOVA: ns = non-significant,  $p > 0.05$ .

(O) Summary plot of spontaneous DCV fusion events during 30 seconds baseline recording of neurons analyzed in Figure 1 F-H. One-way ANOVA: ns = non-significant,  $p > 0.05$ ; \*  $p < 0.05$ .

Repetitive electrical stimulation (16 trains of 50APs at 50 Hz) is represented by blue bars. All data shown as mean  $\pm$  SEM. N represents number of experiments and number of single neuron observations/samples in brackets. Individual neurons are represented as dots. Detailed information (average, SEM, n and detailed statistics) is shown in STAR Methods.

**Figure S2 - Related to Figure 1**

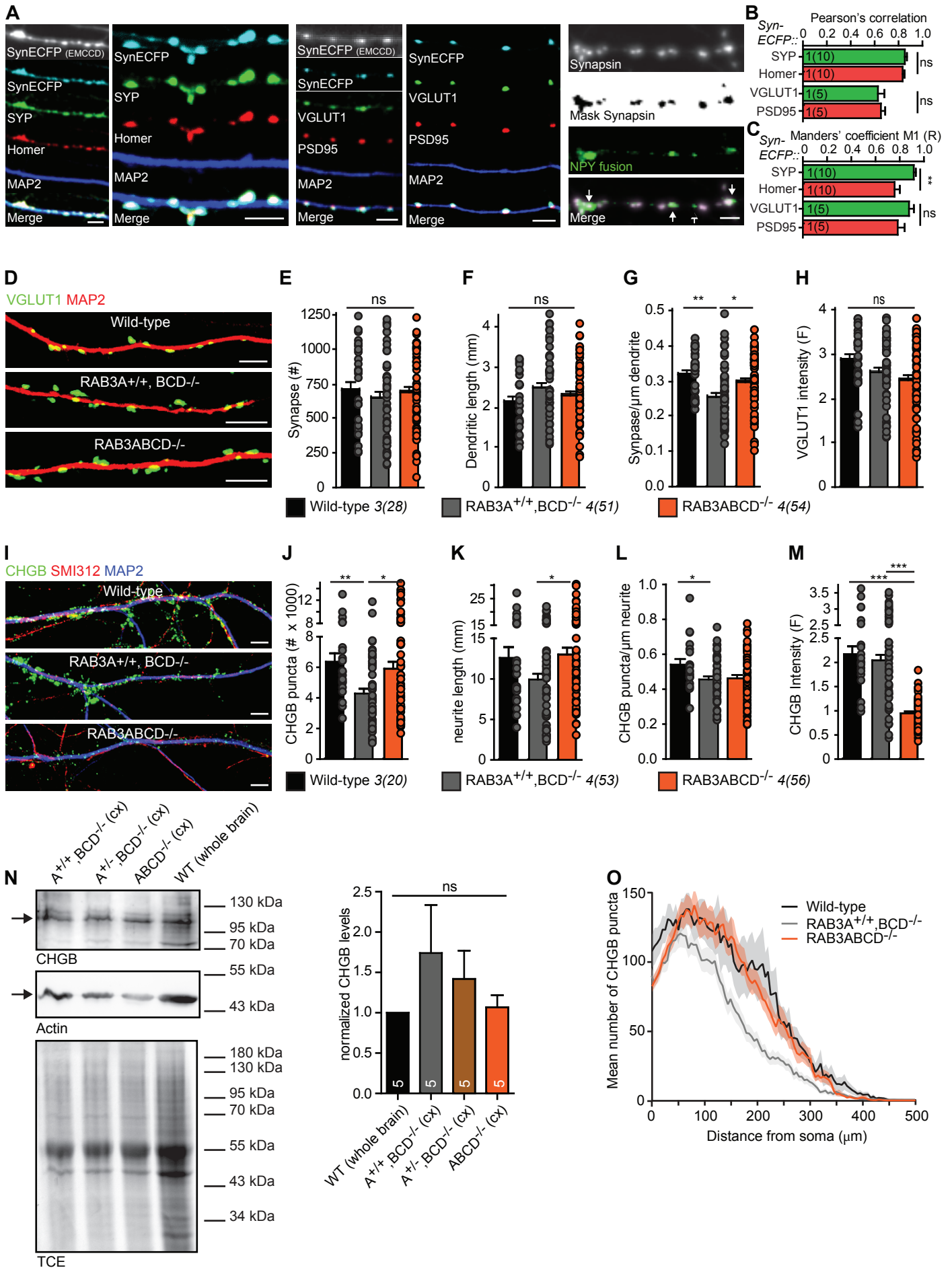


## Figure S2 (related to Figure 1)

### (A-C) Characterization of Synapsin-ECFP as marker for synapses

(A) Representative composite confocal images of MAP2-positive dendrites from single cultured hippocampal neurons expressing Synapsin-ECFP immunostained for the presynaptic marker Synaptophysin (SYP, green) and post synaptic marker Homer (red) or the presynaptic marker VGLUT1 (green) and postsynaptic PSD95 (red). Top panels show the same area with Synapsin-ECFP signal during live cell imaging experiments to quantify synaptic and extra-synaptic events (SynECFP EMCCD). Right panels, Synapsin-ECFP signal (Synapsin) with binary mask (Mask Synapsin) used to quantify synaptic (filled arrows in Merge) and extra-synaptic (open arrow in Merge) NPY fusion events. Scale bars: 5  $\mu\text{m}$ .

(B) Summary data of Pearson's correlation of Synapsin-ECFP co-localization with presynaptic Synaptophysin (SYP) or VGLUT1 (green bars) and post-synaptic Homer and PSD95 (red bars). Mann-Whitney U test: ns non-significant  $p > 0.05$ .

(C) Summary data of Manders' M1 coefficient of expression of Synapsin-ECFP in Synaptophysin, VGLUT1, Homer or PSD95 labeled synapses. Mann-Whitney U test: \*\*  $p < 0.01$ , ns non-significant  $p > 0.05$ .

### (D-O) Analysis of number of synapses, DCVs and neuronal length in RAB3 KO neurons.

(D-H) Morphological analysis of single isolated hippocampal neurons (DIV 14) cultured from wild-type (black), RAB3A<sup>+/+</sup>, BCD<sup>-/-</sup> (grey) or RAB3ABCD<sup>-/-</sup> (orange) littermates. Neurons were immunostained for dendritic marker MAP2 and pre-synaptic marker VGLUT1 and analyzed using automated analysis software (SynD).

(D) Representative zooms of dendritic region (MAP2, red) containing synapses (VGLUT1, green) in wild-type, RAB3A<sup>+/+</sup>, BCD<sup>-/-</sup> and RAB3ABCD<sup>-/-</sup> neurons. Scale bar: 5  $\mu\text{m}$ .

(E) Number of synapses per neuron. Kruskal-Wallis with Dunn's correction: ns = non-significant,  $p > 0.05$ .

(F) Dendritic length (mm) per neuron. One-way ANOVA: ns = non-significant,  $p > 0.05$ .

(G) Synapses per  $\mu\text{m}$  dendrite length. One-way ANOVA: \*  $p < 0.05$ , \*\*  $p < 0.01$ .

(H) Synaptic VGLUT1 intensity. Kruskal-Wallis with Dunn's correction: ns = non-significant,  $p > 0.05$ .

(I-M, O) Analysis of DCV numbers in single isolated hippocampal neurons (DIV 14) cultured from wild-type (black), RAB3A<sup>+/+</sup>, BCD<sup>-/-</sup> (grey) or RAB3ABCD<sup>-/-</sup> (orange) littermates. Neurons were immunostained for the endogenous DCV protein CHGB, dendritic marker MAP2 and axonal marker SMI312. CHGB puncta were analyzed in the total neuron (dendrites + axons) with the automated analysis software SynD.

(I) Representative zooms of axons (SMI312, red) and dendrites (MAP2, blue) containing DCVs (CHGB, green) in wild-type, RAB3A<sup>+/+</sup>, BCD<sup>-/-</sup> and RAB3ABCD<sup>-/-</sup> neurons. Scale bar: 5  $\mu\text{m}$ .

(J) Number of CHGB puncta per neuron. Kruskal-Wallis with Dunn's correction: \*  $p < 0.05$ , \*\*  $p < 0.01$ .

(K) Total neurite length (mm; dendrites + axons) per neuron. Kruskal-Wallis with Dunn's correction: \*  $p < 0.05$ .

(L) CHGB puncta per  $\mu\text{m}$  neurite length. One-way ANOVA: \*  $p < 0.05$ .

(M) CHGB intensity per puncta (F). One-way ANOVA: \*\*\*  $p < 0.001$ .

(N) Immunoblot analysis of CHGB levels (upper blot; arrow) with Actin as loading control (middle blot; arrow) in cortex tissue of RAB3A<sup>+/+</sup> BCD<sup>-/-</sup>, RAB3A<sup>+/-</sup> BCD<sup>-/-</sup>, RAB3ABCD<sup>-/-</sup> littermates (E18.5) and wild-type whole brain tissue (E18.5). Lower blot shows TCE staining of total protein content used to normalize CHGB levels. Right panel: quantification of CHGB levels normalized to WT whole brain lysate. Average of 5 independent experiments. Kruskal-Wallis with Dunn's correction: ns: non-significant, p=0.5231.

(O) Sholl analysis showing mean number of CHGB puncta per distance from soma ( $\mu\text{m}$ ).

Bars show mean  $\pm$  SEM. N represents number of experiments and number of single neuron observations in brackets. Individual neurons are represented as dots. Detailed information (average, SEM, n and detailed statistics) is shown in STAR Methods.

**Figure S3 - Related to Figure 2**

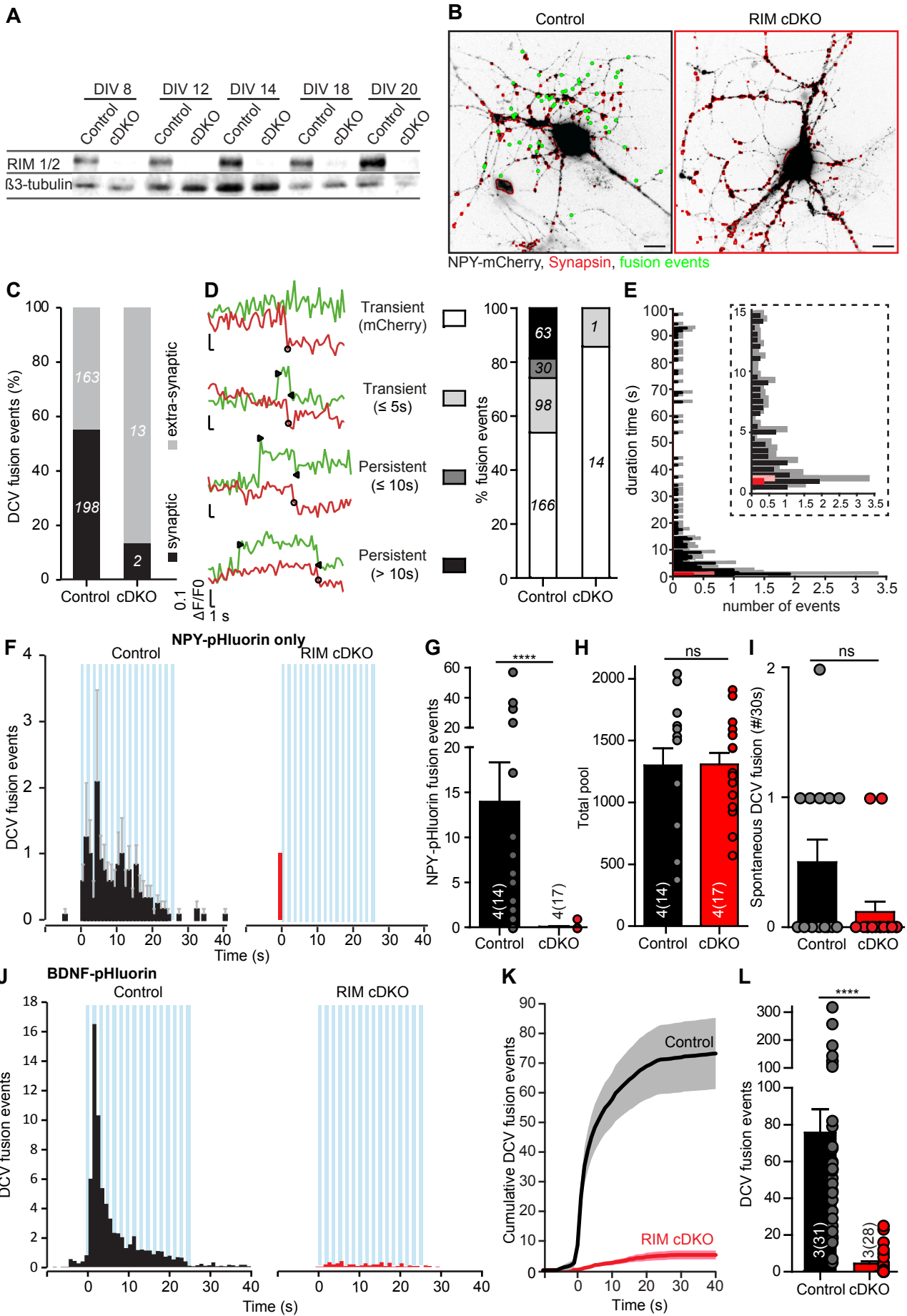


**Figure S3 (related to Figure 2) DCV fusion properties, synaptic fusion and total pool in RIM-deficient neurons.**

(A) Immunoblot of cultured RIM cDKO neurons expressing lentiviral constructs containing active (cDKO) or inactive (control) Cre-recombinase. Neurons were infected at DIV 0 and RIM1/2 protein levels were measured at indicated time-points.  $\beta$ 3-tubulin was used as loading control.

(B) Representative control (left) or RIM cDKO (right) single cultured hippocampal neuron (DIV 14) used for live imaging and labeled with NPY-mCherry (black), synapsin-ECFP (red) and NPY-pHluorin. Fusion events are plotted in green. Scale bars: 20  $\mu$ m.

(C) Percentage of DCV fusion events at synaptic or extra-synaptic regions in control or RIM cDKO neurons. Total number of events are indicated in bars.

(D) Quantification of types of fusion events of dual-color labeled DCVs. Representative traces (left) of NPY-pHluorin signal (green) and NPY-mCherry signal (red) upon fusion. Transient (mCherry) events show predominant decrease in NPY-mCherry, Transient ( $\leq 5$  s) events show an increase of pHluorin fluorescence and decrease within 5 seconds, Persistent ( $\leq 10$  s) events show an increase of pHluorin fluorescence and decrease between 5 and 10 seconds, Persistent ( $> 10$  s) events show an increase of pHluorin fluorescence and decrease after minimal 10 seconds. Quantification of percentage of types of fusion events in control and RIM cDKO neurons (right). Total number of events are indicated in bars.

(E) Histogram of duration of events (s) for control (black) and RIM cDKO (red) neurons. Inset shows zoom of event durations between 0 and 15 s.

(F) Histograms of DCV fusion events per cell detected by NPY-pHluorin for RIM cDKO neurons and controls (figure 2C-E) evoked by electrical stimulation consisting of 16 trains of 50APs at 50 Hz (represented by blue bars).

(G) DCV fusion events per cell detected by NPY-pHluorin for RIM cDKO neurons and controls (subset of data from figure 2C-E). Mann-Whitney U test: \*\*\*\*  $p = < 0.0001$ .

(H) Total number of DCVs (total pool) of neurons analyzed in figure 2C-E, measured as number of NPY-mCherry puncta.

(I) Summary plot of spontaneous DCV fusion events during 30 seconds baseline recording of neurons analyzed in Figure 2C-E. Mann-Whitney U test: ns = non-significant,  $p > 0.05$ .

(J-L) DCV fusion analysis using BDNF-pHluorin in single isolated hippocampal control (black) or RIM1/2 cDKO (red) neurons.

(J) Histograms of DCV fusion events per cell for RIM cDKO neurons and controls evoked by electrical stimulation consisting of 16 trains of 50APs at 50 Hz (represented by blue bars).

(K) Cumulative plot of DCV fusion events per cell.

(L) Summary graph of DCV fusion events per cell. Mann-Whitney U test: \*\*\*\*  $p = < 0.0001$ .

Repetitive electrical stimulation (16 trains of 50APs at 50 Hz) is represented by blue bars above graphs. Bars show mean  $\pm$  SEM. N represents number of experiments and number of single neuron observations in brackets. Individual neurons are represented as dots. Detailed information (average, SEM, n and detailed statistics) is shown in STAR Methods.

**Figure S4 - Related to Figure 2**

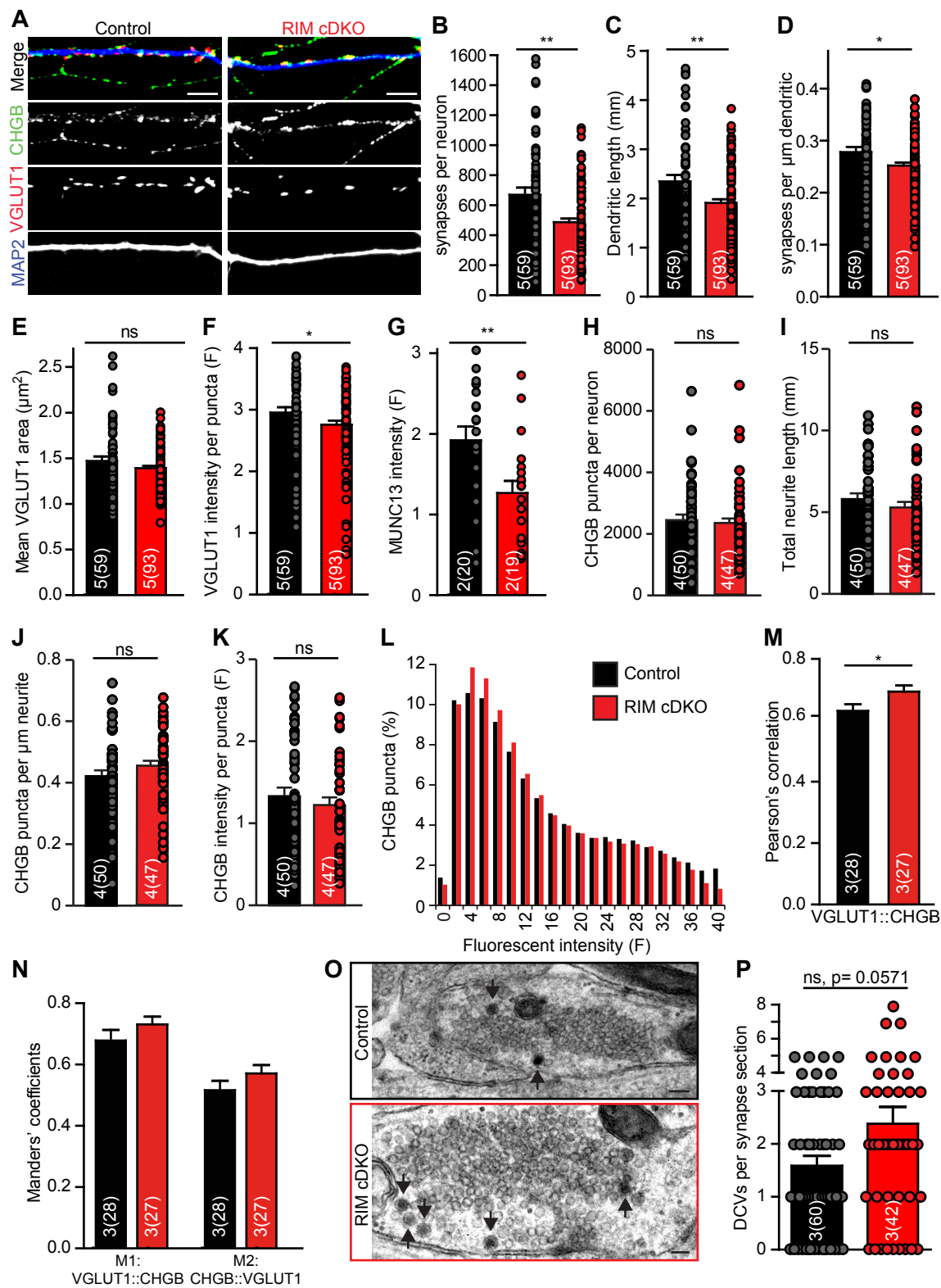


**Figure S4 (related to Figure 2) Analysis of number of synapses, DCVs and neuronal length in RIM cDKO neurons.**

(A) Representative zooms of control or RIM cDKO neurons containing synapses (VGLUT1, red) and DCVs (CHGB, green) at dendrites (MAP2, blue) and axons (MAP2 negative). Scale bar: 5  $\mu$ m.

(B-F) Analysis of synapses in control (black) or RIM cDKO (red) single isolated hippocampal neurons (DIV 14). Neurons were immunostained for dendritic marker MAP2 and pre-synaptic marker VGLUT1 and analyzed using automated analysis software SynD.

(B) Number of synapses per neuron. Mann–Whitney U test, \*\*  $p < 0.0015$ .

(C) Dendritic length (mm) per neuron. Student's t-test \*\*  $p < 0.0024$ .

(D) Synapses per  $\mu$ m dendrite length. Student's t-test \*  $p < 0.0172$ .

(E) VGLUT1 area ( $\mu$ m<sup>2</sup>) per neuron. Mann–Whitney U test, ns= non–significant,  $p > 0.05$ .

(F) VGLUT1 intensity per puncta (F) per neuron. Mann–Whitney U test \*  $p < 0.05$ .

(G) MUNC13 intensity (F) at VGLUT1-positive synapses per neuron. Student's t-test \*\* $p < 0.01$ .

(H-L) Analysis of total DCV number in control (black) or RIM cDKO (red) single isolated hippocampal neurons (DIV 14). Neurons were immunostained for the endogenous DCV protein CHGB, dendritic marker MAP2 and axonal marker SMI312. CHGB puncta were analyzed in the total neuron (dendrites + axons) with automated analysis software SynD.

(H) Number of CHGB puncta per neuron. Mann–Whitney U test, ns = non-significant,  $p = 0.50$ .

(I) Total neurite length (mm; dendrites + axons) per neuron. Mann–Whitney U test, ns = non-significant,  $p = 0.25$ .

(J) CHGB puncta per  $\mu$ m neurite length. Student's t-test, ns = non-significant,  $p = 0.23$ .

(K) CHGB intensity per puncta (F). Student's t-test, ns = non-significant,  $p = 0.44$ .

(L) Distribution of fluorescent intensity per CHGB puncta (%).

(M) Pearson's correlation of VGLUT1 and CHGB. Student's t-test, \*  $p < 0.015$

(N) Manders' co-localization coefficients of VGLUT1 and CHGB.

(O) Representative electron micrographs of synaptic sections of control or RIM cDKO neurons containing DCVs (arrows). Scale bars: 100 nm.

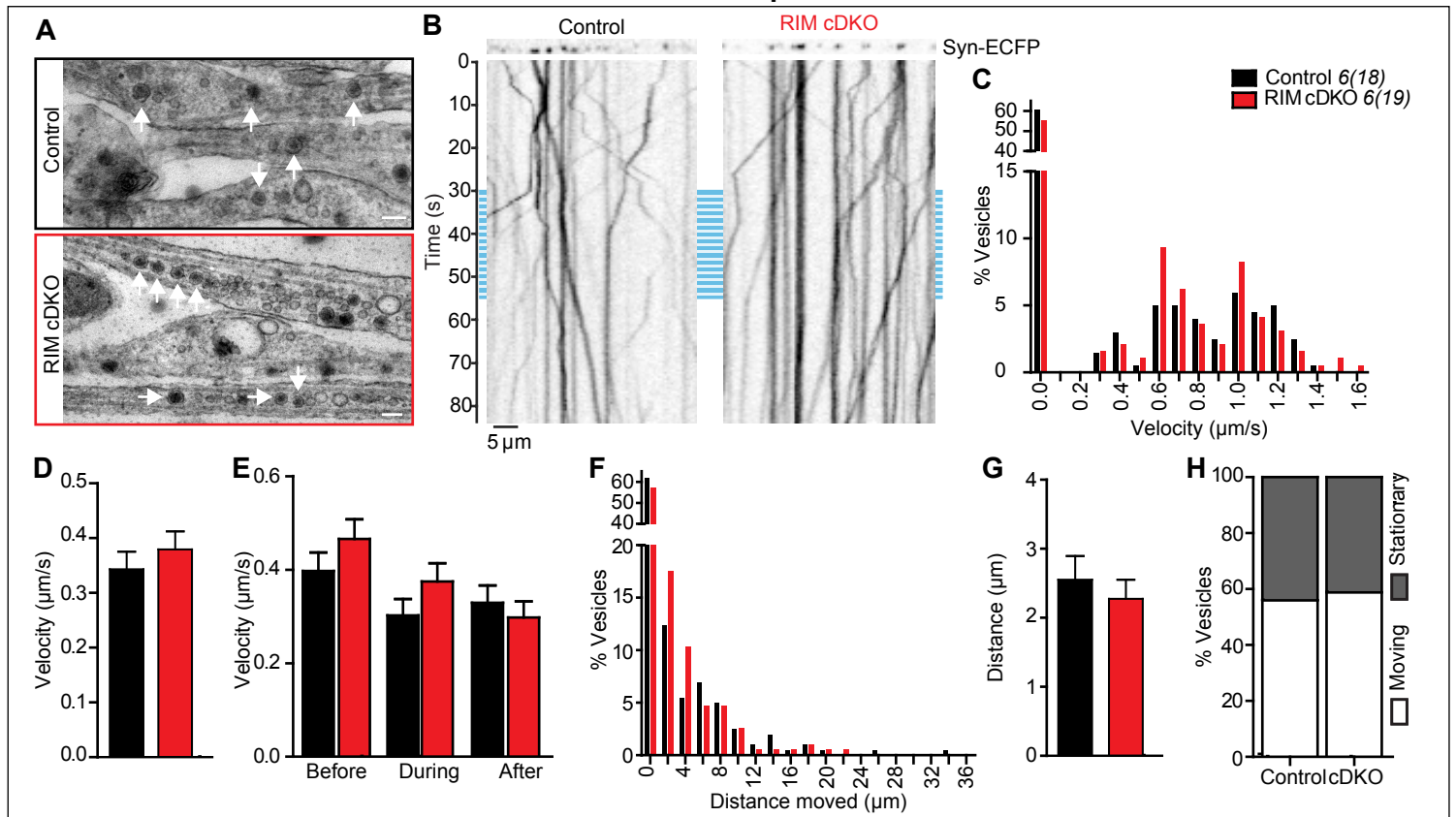
(P) Number of DCVs per synapse section in control (black) or RIM cDKO neurons (red). Mann–Whitney U test, ns = non-significant,  $p = 0.0571$ .

Bars show mean  $\pm$  SEM. N represent numbers of experiments and number of single neuron observations in brackets. Individual neurons are represented as dots. Detailed information (average, SEM, n and detailed statistics) is shown in STAR Methods.

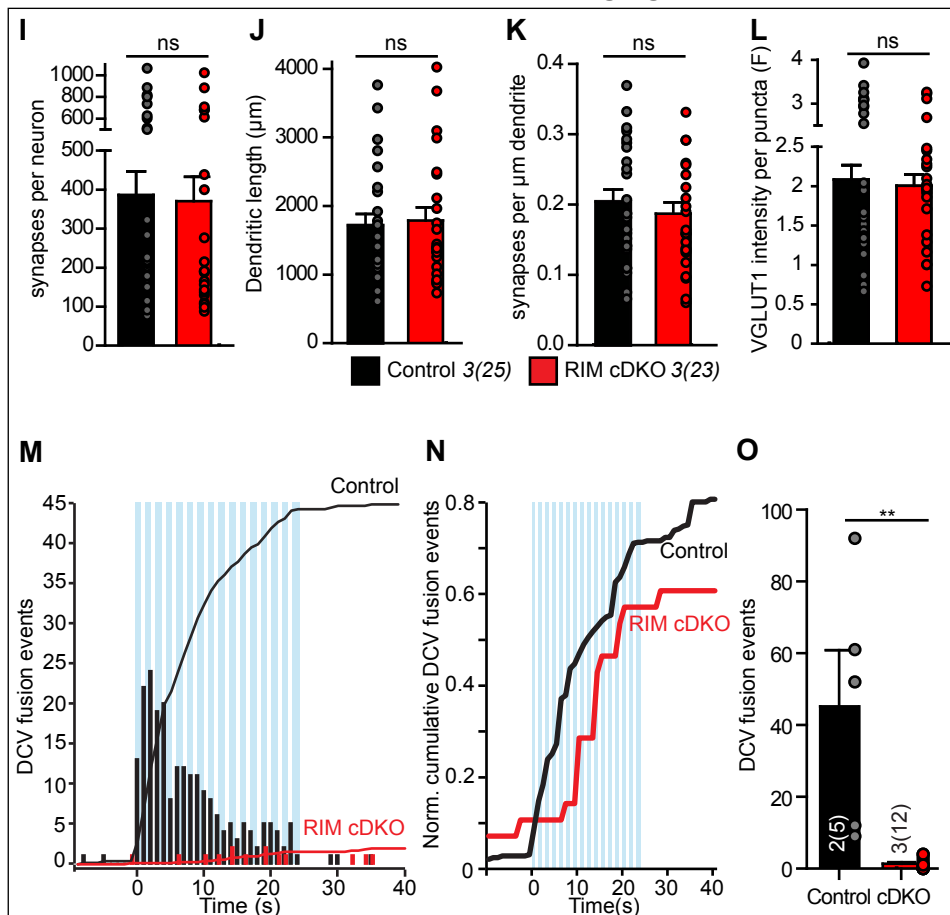


Figure S5 - Related to Figure 2

DCV transport



DIV 5 Cre / DIV18 imaging



Wild-type

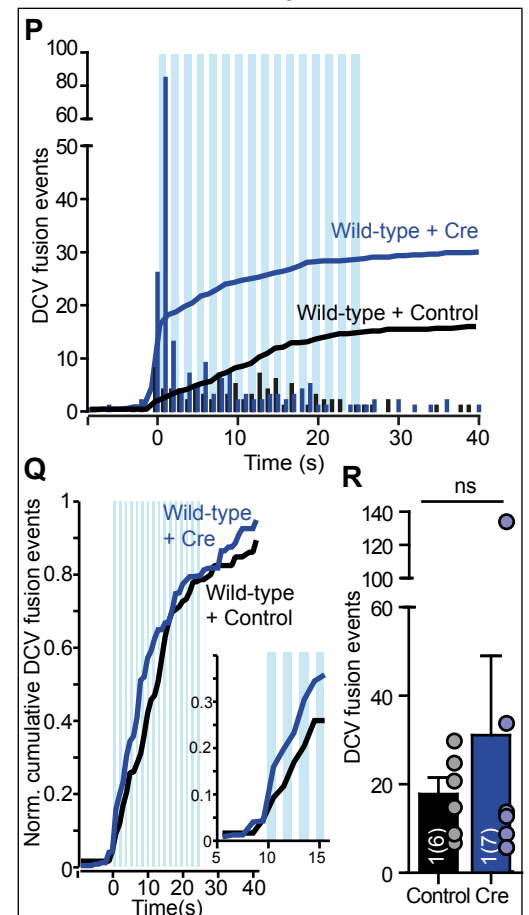


## Figure S5 (related to Figure 2)

### (A-H) Transport of DCVs is not affected in RIM-deficient cDKO neurons.

(A) Representative electron micrographs of neurites of control or RIM cDKO neurons containing DCVs in close proximity to microtubules (arrows). Scale bars: 100 nm.

(B-H) DCV transport was measured in timelapse recordings (2 Hz) of single cultured RIM cDKO and control hippocampal neurons (DIV14) labeled with NPY-mCherry by manual tracking in ImageJ. Repetitive electrical stimulation (16 trains of 50APs at 50 Hz) was applied after 30 seconds of recording. Control: N = 6 (18 cells, 202 vesicles); RIM cDKO: N = 6 (19 cells, 194 vesicles).

(B) Representative kymographs illustrating the behavior of NPY-mCherry labeled DCVs in control and RIM cDKO neurons. Synapses are labeled with Synapsin-ECFP (Syn-ECFP) plotted above kymographs. Repetitive electrical stimulation (16 trains of 50APs at 50 Hz) is represented by blue bars.

(C-D) Histogram (C) and bar graph (D) of average velocity ( $\mu\text{m/s}$ ) of control (black) and RIM cDKO (red) neurons.

(E) Average velocity ( $\mu\text{m/s}$ ) before, during and after repetitive electrical stimulation of 16 bursts of 50 AP at 50 Hz for control (black) and RIM cDKO (red) neurons.

(F-G) Histogram (F) and bar graph (G) of average distance moved from start ( $\mu\text{m}$ ) of control (black) and RIM cDKO (red) neurons.

(H) Percentage of moving and stationary vesicles.

### (I-O) Cre-recombinase expression at DIV 5 blocks DCV fusion but does not affect number of synapses in RIM cDKO neurons.

(I-L) Analysis of synapses in single isolated hippocampal neurons (DIV 18) control (black) or Cre-recombinase virus (RIM cDKO, red) infected at DIV 5. Neurons were immunostained for dendritic marker MAP2 and pre-synaptic marker VGLUT1 and analyzed using automated analysis software SynD.

(I) Number of synapses per neuron. Mann-Whitney U test, ns = non-significant,  $p = 0.67$ .

(J) Dendritic length ( $\mu\text{m}$ ) per neuron. Mann-Whitney U test, ns = non-significant,  $p = 0.92$ .

(K) Synapses per  $\mu\text{m}$  dendrite length. Student's t-test, ns = non-significant,  $p = 0.47$ .

(L) VGLUT1 intensity per puncta (F) per neuron. Student's t-test, ns = non-significant,  $p = 0.743$

(M-O) Single isolated hippocampal neurons (DIV 18) from conditional RIM1/2 DKO neurons expressing inactive (Control, black) or active Cre-recombinase virus (cDKO, red) infected at DIV 5. Neurons were labeled with NPY-pHluorin and NPY-mCherry and DCV fusion events were quantified per neuron upon repetitive electrical stimulation (16 trains of 50APs at 50 Hz).

(M) Histogram of DCV fusion events per cell per time point for RIM cDKO neurons and controls. Line graph represents cumulative plot of DCV fusion events per cell.

(N) Normalized cumulative plot of DCV fusion events per cell.

(O) Summary graph of DCV fusion events per cell. Mann-Whitney U test: \*\*  $p < 0.01$ .

(P-R) Single isolated wild-type hippocampal neurons (DIV14) expressing control (black) or Cre-recombinase virus (blue) infected at DIV 0 were labeled with NPY-pHluorin and NPY-

mCherry. DCV fusion events were quantified per neuron upon repetitive electrical stimulation (16 trains of 50APs at 50 Hz).

(P) Histogram of DCV fusion events per cell per time point for wild-type neurons expressing Cre (blue) or control (black) virus. Line graph represents cumulative plot of DCV fusion events per cell.

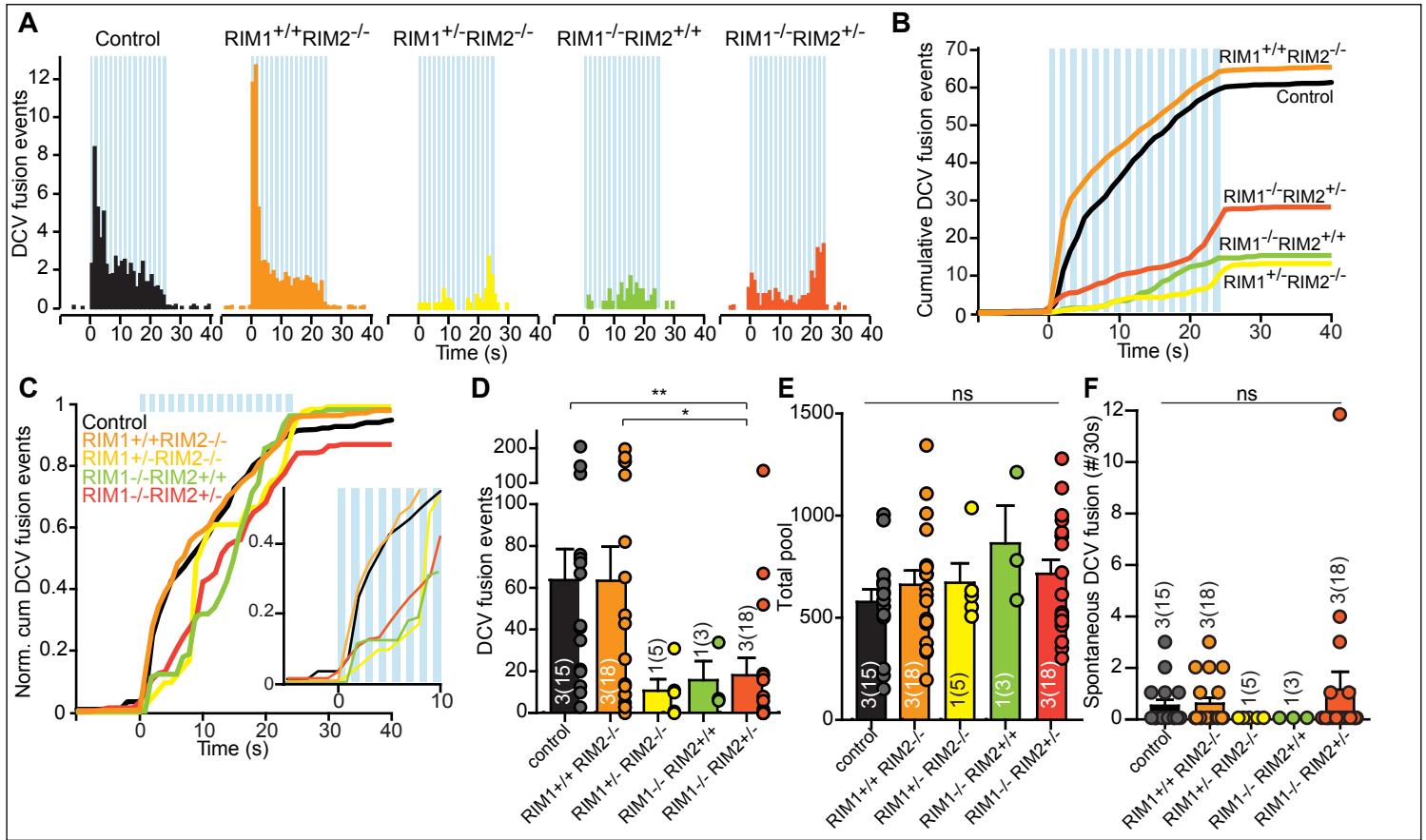
(Q) Normalized cumulative plot of DCV fusion events per cell. Inset shows normalized cumulative plot of DCV fusion events per cell in first 5 seconds of stimulation.

(R) Summary graph of DCV fusion events per cell.

Repetitive electrical stimulation (16 trains of 50APs at 50 Hz) is represented by blue bars above graphs. Bars show mean  $\pm$  SEM. N represents number of experiments and number of single neuron observations in brackets. Individual neurons are represented as dots. Detailed information (average, SEM, n and detailed statistics) is shown in STAR Methods.

**Figure S6**

**Related to Figure 2**



**Related to Figure 3**

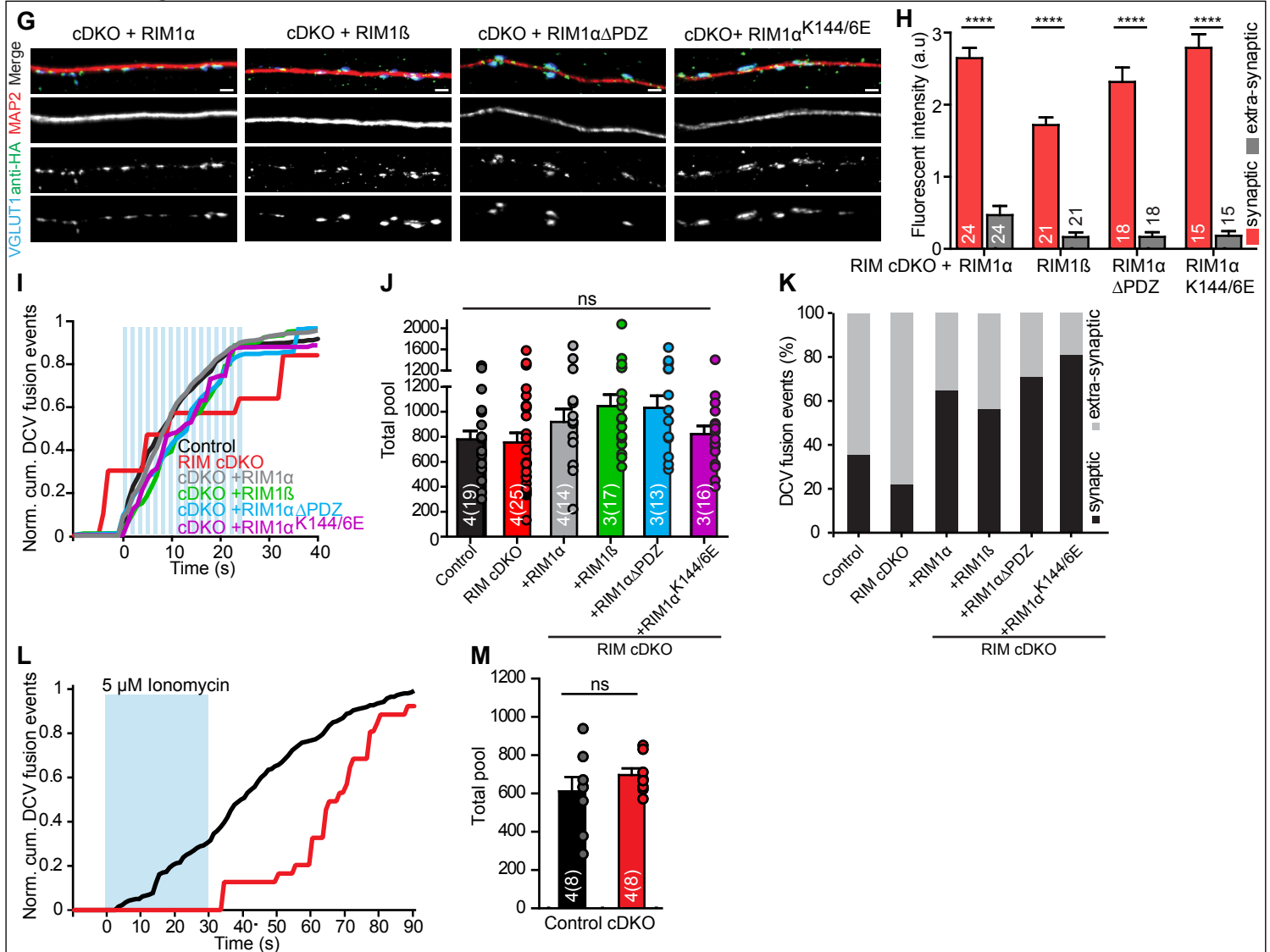


## Figure S6

### (A-F) Related to Figure 2: RIM1 is required for efficient DCV fusion.

DCV fusion analysis using NPY-pHluorin in single isolated hippocampal heterozygous/homozygous RIM1/2 cKO or control neurons.

(A) Histograms of DCV fusion events per cell per time point for different conditions.

(B) Cumulative plot of DCV fusion events per cell for different conditions.

(C) Normalized cumulative plot of DCV fusion events per cell for different conditions. Inset shows cumulative fusion in first 10 seconds of stimulation.

(D) Summary graph of DCV fusion events per cell for different conditions. Kruskal-Wallis with Dunn's correction: \*  $p < 0.05$ , \*\*  $p < 0.01$ .

(E) Total number of DCVs (total pool) measured as number of NPY-pHluorin puncta upon application of 50 mM NH<sub>4</sub>Cl containing Tyrode's solution to visualize the total pool.

(F) Summary plot of spontaneous DCV fusion events during 30 seconds baseline recording for different conditions. Kruskal-Wallis with Dunn's correction: ns = non-significant,  $p > 0.05$ .

### (G-M) Related to Figure 3: DCV total pool and synaptic fusion in RIM-deficient neurons rescued with RIM-mutant constructs

(G) Example zooms of RIM cDKO neurons expressing HA-tagged RIM-rescue constructs. Neurons were immunostained for dendritic marker MAP2 (red), pre-synapse marker VGLUT1 (blue) and RIM-rescue constructs were visualized by anti-HA (green).

(H) Summary data of fluorescence intensity of HA-tagged RIM-rescue constructs at VGLUT1 positive synapses (red bars, synaptic) or at extra-synaptic sites (black bars, extra-synaptic) along MAP2 labeled dendrites. Mann-Whitney U test, \*\*\*\*  $p < 0.0001$ .

(I) Normalized cumulative plot of DCV fusion events per cell for different conditions.

(J) Total number of DCVs (total pool) of neurons analyzed in figure 3 B-D, measured as number of NPY-pHluorin puncta upon application of 50 mM NH<sub>4</sub>Cl containing Tyrode's solution to visualize the total pool. Kruskal-Wallis with Dunn's correction: ns = non-significant,  $p > 0.05$ .

(K) Percentage of DCV fusion events at synaptic (black) or extra-synaptic (grey) regions of neurons analyzed in figure 3 B-D for different conditions.

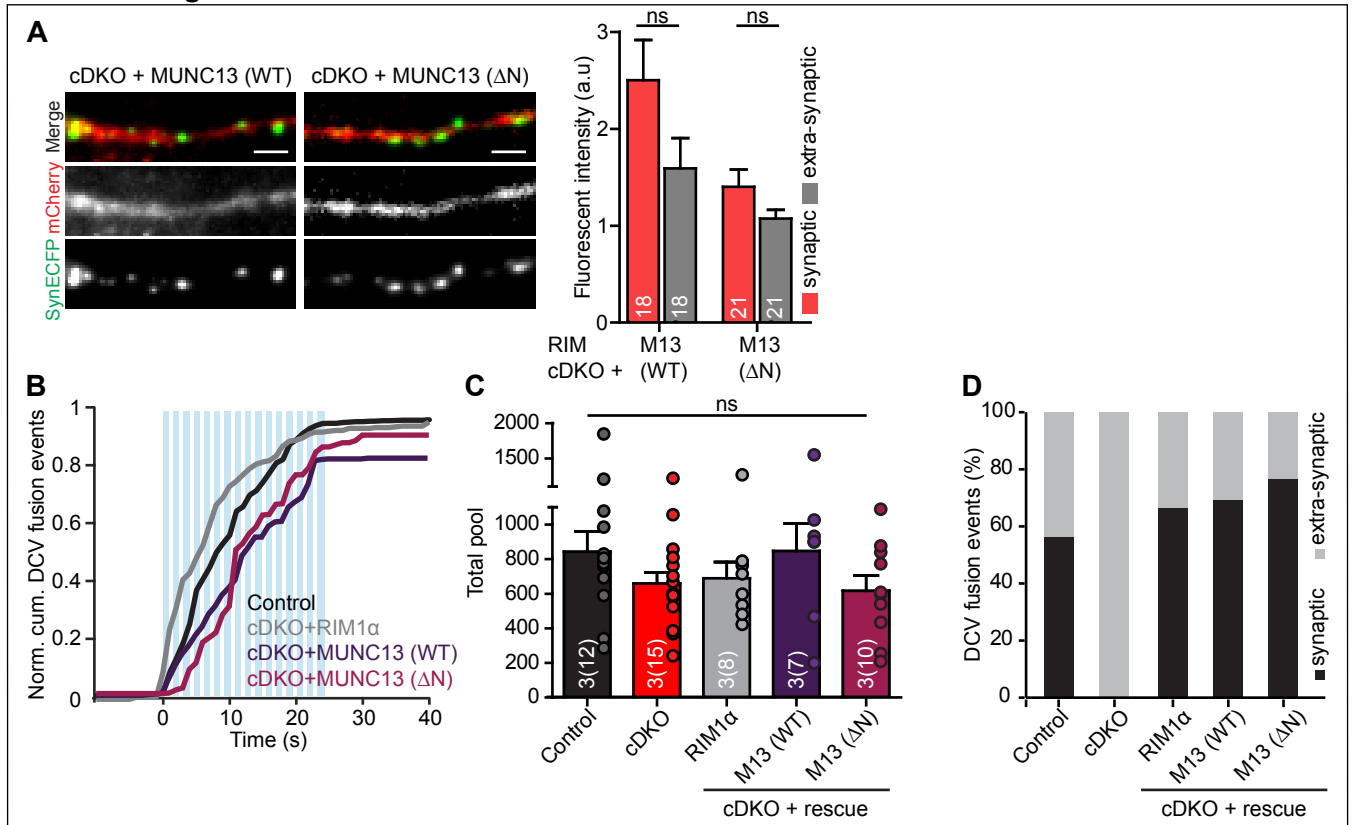
(L) Normalized cumulative plot of DCV fusion events per cell of neurons analyzed in figure 3 G-I.

(M) Total pool size of neurons analyzed in figure 3 G-I, measured as number of NPY-pHluorin puncta upon application of 50 mM NH<sub>4</sub>Cl containing Tyrode's solution to visualize the total pool. Student's t-test ns,  $p = 0.3229$ .

Repetitive electrical stimulation (16 trains of 50APs at 50 Hz) is represented by blue bars, application of 5  $\mu$ M Ionomycin is represented by blue bar. Bars show mean  $\pm$  SEM. N represents number of experiments and number of single neuron observations in brackets. Individual neurons are represented as dots. Detailed information (average, SEM, n and detailed statistics) is shown in STAR Methods.

**Figure S7**

Related to Figure 4



Related to Figure 5

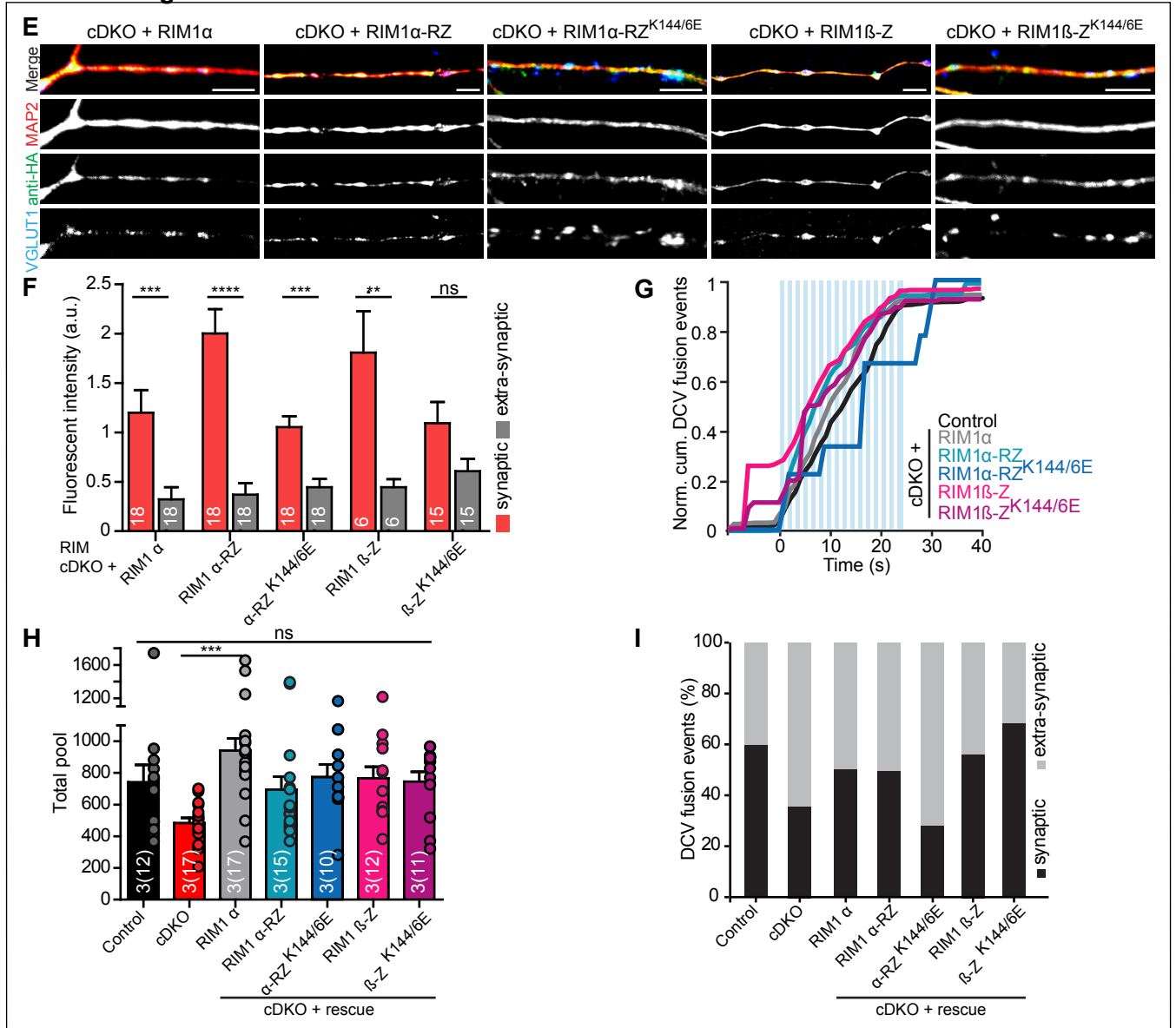


## Figure S7 DCV total pool and synaptic fusion in RIM-deficient neurons rescued with MUNC13-2 or N-terminal RIM-mutant constructs

### (A-D) Related to Figure 4

(A) Example zooms of RIM cDKO neurons expressing mCherry-tagged MUNC13 WT or  $\Delta$ N constructs (red) and Synapsin-ECFP (green). Right panel, summary data of fluorescence intensity of HA-tagged MUNC13 constructs at Synapsin-ECFP positive synapses (red bars, synaptic) or at extra-synaptic sites (grey bars, extra-synaptic). Mann-Whitney U test: ns=non-significant  $p > 0.05$ .

(B) Normalized cumulative plot of DCV fusion events per cell for neurons analyzed in figure 4.

(C) Total number of DCVs (Total pool) of neurons analyzed in figure 4, measured as number of NPY-pHluorin puncta upon application of 50 mM NH<sub>4</sub>Cl containing Tyrode's solution to visualize the total pool. Kruskal-Wallis with Dunn's correction: ns = non-significant,  $p > 0.05$ .

(D) Percentage of DCV fusion events at synaptic (black) or extra-synaptic (grey) regions for different conditions.

### (E-I) Related to Figure 5

(E) Example zooms of RIM cDKO neurons expressing HA-tagged RIM-rescue constructs. Neurons were immunostained for dendritic marker MAP2 (red), pre-synapse marker VGLUT1 (blue) and RIM-rescue constructs were visualized by anti-HA (green).

(F) Summary data of fluorescence intensity of HA-tagged RIM-rescue constructs at VGLUT1 positive synapses (red bars, synaptic) or at extra-synaptic sites (grey bars, extra-synaptic) along MAP2 labeled dendrites. Mann-Whitney U test, \*\*\*\*  $p < 0.0001$ ; \*\*\*  $p < 0.001$ ; \*\*  $p < 0.01$ ; ns=non-significant  $p > 0.05$ .

(G) Normalized cumulative plot of DCV fusion events per cell for neurons analyzed in figure 5.

(H) Total number of DCVs (Total pool) of neurons analyzed in figure 5, measured as number of NPY-pHluorin puncta upon application of 50 mM NH<sub>4</sub>Cl containing Tyrode's solution to visualize the total pool. Kruskal-Wallis with Dunn's correction: \*\*\*  $p < 0.001$ , ns= non-significant,  $p > 0.05$ .

(I) Percentage of DCV fusion events at synaptic (black) or extra-synaptic (grey) regions for different conditions.

Repetitive electrical stimulation (16 trains of 50APs at 50 Hz) is represented by blue bars. Bars show mean  $\pm$  SEM. N represents number of experiments and number of single neuron observations in brackets. Individual neurons are represented as dots. Detailed information (average, SEM, n and detailed statistics) is shown in STAR Methods.

**Figure S8 - Related to Figure 6**

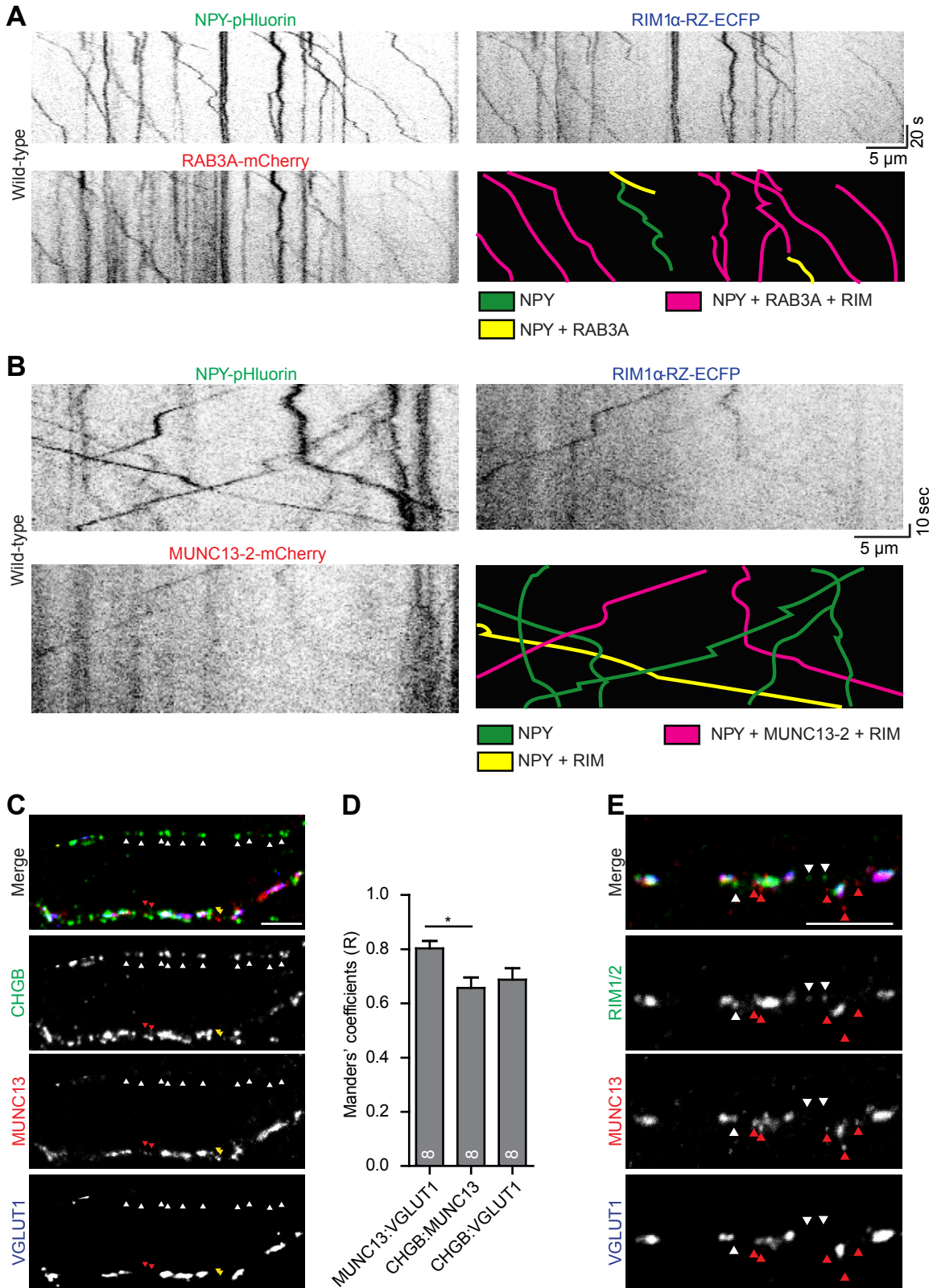




### Figure S8 (related to Figure 6)

(A) Representative kymographs showing trajectories of DCVs (NPY-pHluorin), RAB3A-mCherry and RIM1 $\alpha$ -RZ-ECFP in wild-type neurons. Green overlay indicates examples of NPY only transport, co-transport of NPY and RAB3A is indicated by yellow and co-transport of NPY, RAB3A and RIM in magenta.

(B) Example kymographs of co-transport of NPY-pHluorin with RIM1 $\alpha$ -RZ-ECFP and MUNC13-2-mCherry in WT neurons. Graphical overlay (bottom right) indicates transport of NPY (green), co-transport of NPY with RIM1 $\alpha$ -RZ (yellow) or NPY with MUNC13-2 and RIM1 $\alpha$ -RZ (magenta).

(C) Representative confocal zooms of neurites immunostained for the DCV marker CHGB (green), MUNC13 (red) and synapse marker VGLUT1 (blue). White arrow heads indicate CHGB puncta without MUNC13 or VGLUT1, red arrow heads show CHGB puncta overlapping with MUNC13 but not VGLUT1, and yellow arrow heads show MUNC13 clusters non-overlapping with the synaptic marker VGLUT1.

(D) Manders' co-localization coefficients of MUNC13 and VGLUT1, CHGB and MUNC13 and CHGB and VGLUT1. Kruskal-Wallis with Dunn's correction: \* $p < 0.05$ , ns=non-significant,  $p > 0.05$

(E) Representative confocal zooms of neurites immunostained for RIM1/2 (green), MUNC13 (red) and the synapse marker VGLUT1 (blue) showing the predominantly synaptic localization of RIM1/2 and MUNC13 with some extra-synaptic RIM1/2 puncta (white arrow heads) and MUNC13 puncta (red arrow heads).

Bars show mean  $\pm$  SEM. N represents number of single neuron observations. Detailed information (average, SEM, n and detailed statistics) is shown in STAR Methods.